Agenzia nazionale per le nuove tecnologie, l'energia
e lo sviluppo economico sostenibile

Ministero dello Sviluppo Economico

RICERCA DI SISTEMA ELETTRICO

Pre-test analysis of thermal-hydraulic behaviour of the NACIE facility for the characterization of a fuel pin bundle

G. Barone, N. Forgione, D. Martelli, A. Del Nevo

Report RdS/2012/058

PRE-TEST ANALYSIS OF THERMAL-HYDRAULIC BEHAVIOUR OF THE NACIE FACILITY FOR THE CHARACTERIZATION OF A FUEL PIN BUNDLE

G. Barone, N. Forgione, D. Martelli – CIRTEN Università di Pisa, A. Del Nevo - ENEA

Settembre 2012

Report Ricerca di Sistema Elettrico
Accordo di Programma Ministero dello Sviluppo Economico - ENEA
Area: Governo, gestione e sviluppo del sistema elettrico nazionale
Progetto: Nuovo nucleare da fissione: collaborazioni internazionali e sviluppo competenze in materia nucleare

Responsabile del Progetto: Mariano Tarantino, ENEA

RICERCA DI SISTEMA ELETTRICO

CIRTEN

Pre-test analysis of thermal-hydraulic behaviour of the NACIE facility for the characterization of a fuel pin bundle

(Analisi numerica di pre-test del comportamento termoidraulico dell'impianto NACIE per la caratterizzazione di un fuel pin bundle)

G. Barone, N. Forgione, D. Martelli
(DIMNP – Università di Pisa)

A. Del Nevo
(ENEA – Brasimone)

Pisa, August 2012

Lavoro svolto in esecuzione dell'Attività LP3-C4
AdP MSE-ENEA sulla Ricerca di Sistema Elettrico - Piano Annuale di Realizzazione 2011
Progetto 1.3.1 "Nuovo Nucleare da Fissione:
collaborazioni internazionali e sviluppo competenze in materia nucleare"

Index

Summary

This report, carried out at the DIMNP (Dipartimento di Ingegneria Meccanica, Nucleare e della Produzione) of the University of Pisa in collaboration with ENEA Brasimone Research Centre, illustrates the pre-test thermo-fluidynamic analysis of the NACIE (Natural Circulation Experiment) facility, built at ENEA, in its new configuration of the heat exchanger and of the heater system.
In particular, the first part of the work regards the study performed by RELAP5/Mod3.3 system code, modified in order to take into account LBE fluid properties and the appropriate convective heat transfer correlations. The code was employed to support the design of SEARCH experimental campaign, devoted to characterize the performance of a wire spaced fuel bundle relevant for MYRRHA facility (i.e. heat exchange and pressure drop) in shutdown conditions and providing data for code validation. For this purpose, low heat power simulations on NACIE facility have been performed to investigate the established loop natural flow rate and related parameters for increasing values of loop hydraulic resistance. The second part of the work concerns the first application, to a simplified representation of NACIE facility, of the coupling between the RELAP5 thermal-hydraulic system code and the CFD Fluent commercial code. Preliminary comparative analysis among the simulations performed by RELAP5-Fluent coupled codes and by RELAP5 stand-alone code showed very good agreement among them, giving confidence to this innovative coupling strategy.

1. The NACIE facility

NACIE [1] is a loop facility designed at ENEA-Brasimone Research Centre, to qualify and characterize components, systems and procedures relevant for HLM nuclear technologies. In particular it is possible to carry out natural circulation and mixed convection experimental tests in the field of thermal hydraulic, fluid dynamics, chemistry control, corrosion and liquid metal heat exchange allowing the investigation of essential correlation for the design and development of new generation nuclear facilities. NACIE is a rectangular loop (7.5 m height) that basically consists of two vertical pipes (O.D. 2.5", S40) (i.e. the downcomer and the riser), connected with two horizontal pipes (O.D. 2.5", S40). A heat source (*HS*) (electric pins) is placed at the lower part of the riser, whereas a heat exchanger (*HX*) is placed on the downcomer side (a different height from the *HS* midplane could be configured). NACIE loop is entirely made of austenitic stainless steel, AISI 304, and can operate with both lead-bismuth (LBE) and lead as working fluid. The experimental tests will be carried out using LBE. A gas (argon) is injected through the riser during the assisted circulation tests to promote the circulation inside the loop.

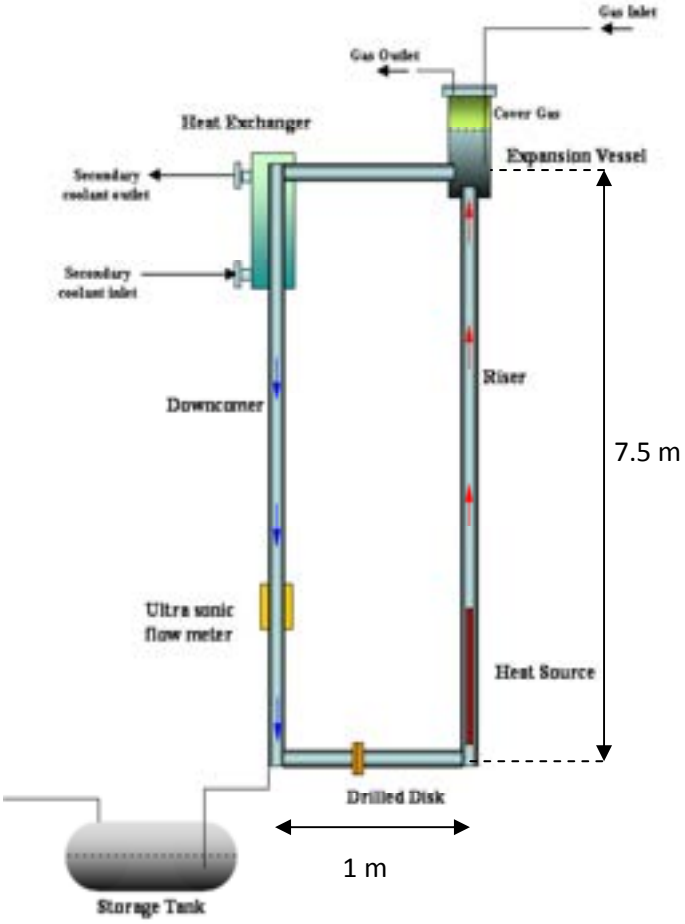

Figure 1.1: NACIE facility conceptual sketch.

An expansion vessel is installed, coaxially with the riser (on the top part), which enables the thermal expansion of the LBE during operational transient and allows the separation and recovery of the argon from the LBE to be reused in a closed loop to promote liquid metal circulation. The free level of the expansion vessel is kept at a slight overpressure (about 200 mbar) by means of a hydrogen-argon mixture. The facility internal volume is about 0.1 m^3 (100 liters), which totally corresponds to 1000 kg of liquid metal. The design temperature of the facility is 550°C even though it's generally operated at a lower temperature.

Furthermore a ball valve will be installed to regulate the hydraulic losses. A conceptual scheme of NACIE with the main dimension is depicted in Figure 1.1.

1.1 Heat source

A specifically designed new heat source (*HS*) will be installed in the NACIE facility to carry out the experimental SEARCH WP2 campaign. The heat source [2] characterized by an overall thermal power of 250 kW; consists of 19 electrically heated pin bundle arranged in a hexagonal array and closed into a hexagonal wrapper as depicted in Figure 1.2.

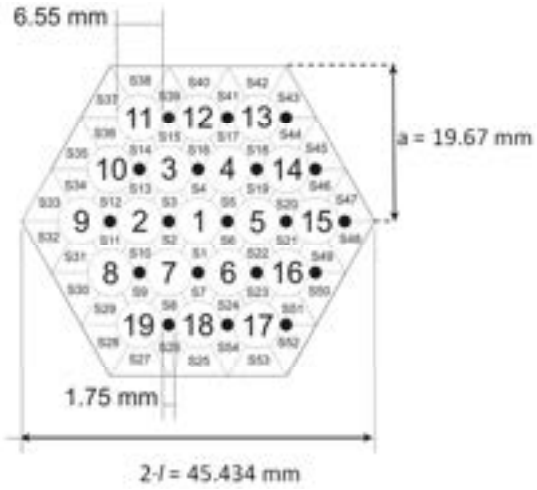

Figure 1.2: Electrical wire-spaced pin bundle cross section.

The technical specifications are summarized in Table 1.1.

Table 1.1: Electrical wire-spaced pin bundle parameters.

d	6.55 mm	Rod diameter
p/d	1.276	Pitch to diameter ratio
d_w	1.75 mm	Wire diameter
H_w	262 mm	Wire pitch
q''_{max}	1 MW/m^2	Maximum heat flux at pin wall
Q_{max}	~ 235 kW	Maximum bundle thermal power

The electric pin (total length L_{tot}=2000 mm), shown in Figure 1.3, is characterized by an active region of L_2 = 600 mm. No spacer grids are foreseen for the bundle, instead wire spacers will be installed over a pin length of approximately 1300 mm:

- L_1 ~ 500 mm (Inactive)
- L_2 = 600 mm (Active)
- L_3 = 100 mm (Inactive)

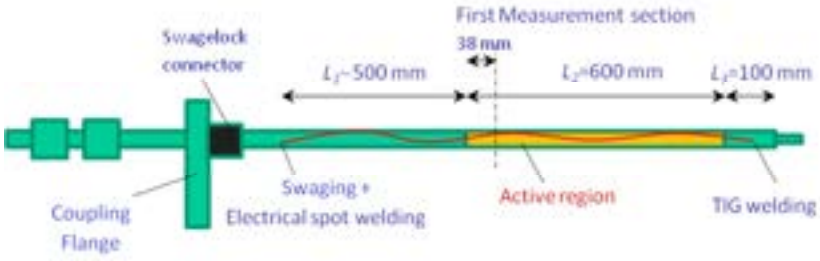

Figure 1.3: Wire installation along pin length.

Pins 2, 4, 6, 7, 9, 16, 18 and 19 will be equipped with embedded thermocouples on a generatrix parallel to the pin axis, as shown in Figure 1.4. Three different levels will be considered *z* = 38, 300 and 562 mm starting from the beginning of the active region.

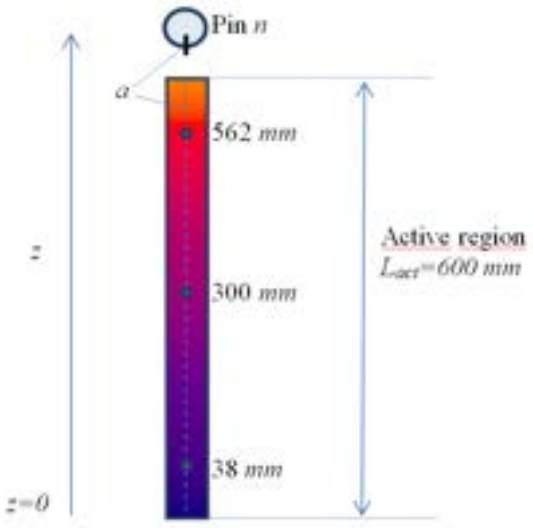

Figure1.4: Wall Embedded TCs location.

1.2 Heat exchanger

In order to remove the heat power from the new electrical bundle, a convenient “shell and tube” heat exchanger has been proposed (see Figure 1.5) [2]. Heat exchanger pipe parameters are found in Table 1.2. The tubes are arranged in a hexagonal lattice (one central and six surrounding tubes) and are double-wall type, in order to mitigate the axial thermal stresses caused by the differential thermal expansion and to avoid accidental contact of the liquid metal with water. The gap between the two walls (2.5 mm) is filled by steel powder (good thermal conductivity) to guarantee the thermal flux towards secondary water. Hot liquid metal flows downward through the inner pipes and exits from the bottom heat exchanger outlet.
The shell side (where secondary sub-cooled water flows at a pressure of 16 bar) of the heat exchanger is divided into two separate sections:

- *HX-2*: Low power section (0.3 m)
- *HX-1*: High power section (2.1 m)

Table 1.2: Heat Exchanger pipe geometrical parameters.

Component	Pipe size [in]	Sch.	d_e [mm]	d_i [mm]	t [mm]	Material
Shell	16	40	406.4	381.0	12.7	AISI 316L
Inner tube	2 ½	40	73.0	62.7	5.2	AISI 316L
Outer tube	3	40	88.9	77.9	5.5	AISI 316L

Each Section is associated with an independent secondary water loop which is activated according to the power that needs to be exchanged. Inside the high power section water flows counter-flow, while inside the low pressure section water flows cross-flow. The experimental tests discussed in this work will all be interested by the low power section *HX-2* (10-35 kW), with a water flow rate of 10 m^3/h and inlet temperature ranging from 120 to 170°C.

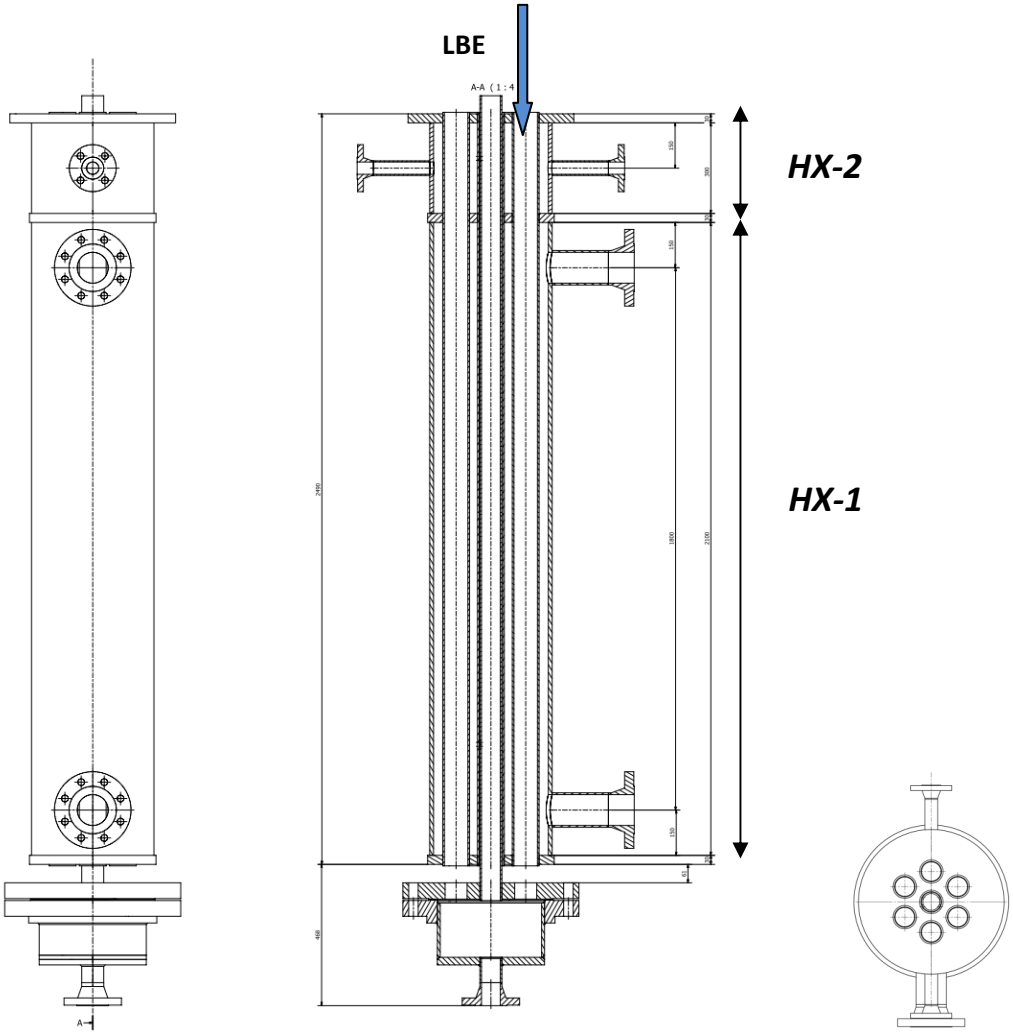

Figure 1.5: Heat Exchanger sections *HX-2* and *HX-1*.

2 Thermal-hydraulic pre-test analysis

2.1 RELAP5 NACIE model

The system code RELAP5/Mod3.3 [3], modified to take into account LBE properties [4], has been used to generate NACIE model (see Figure 2.1), according to the facility experimental setup previously described.

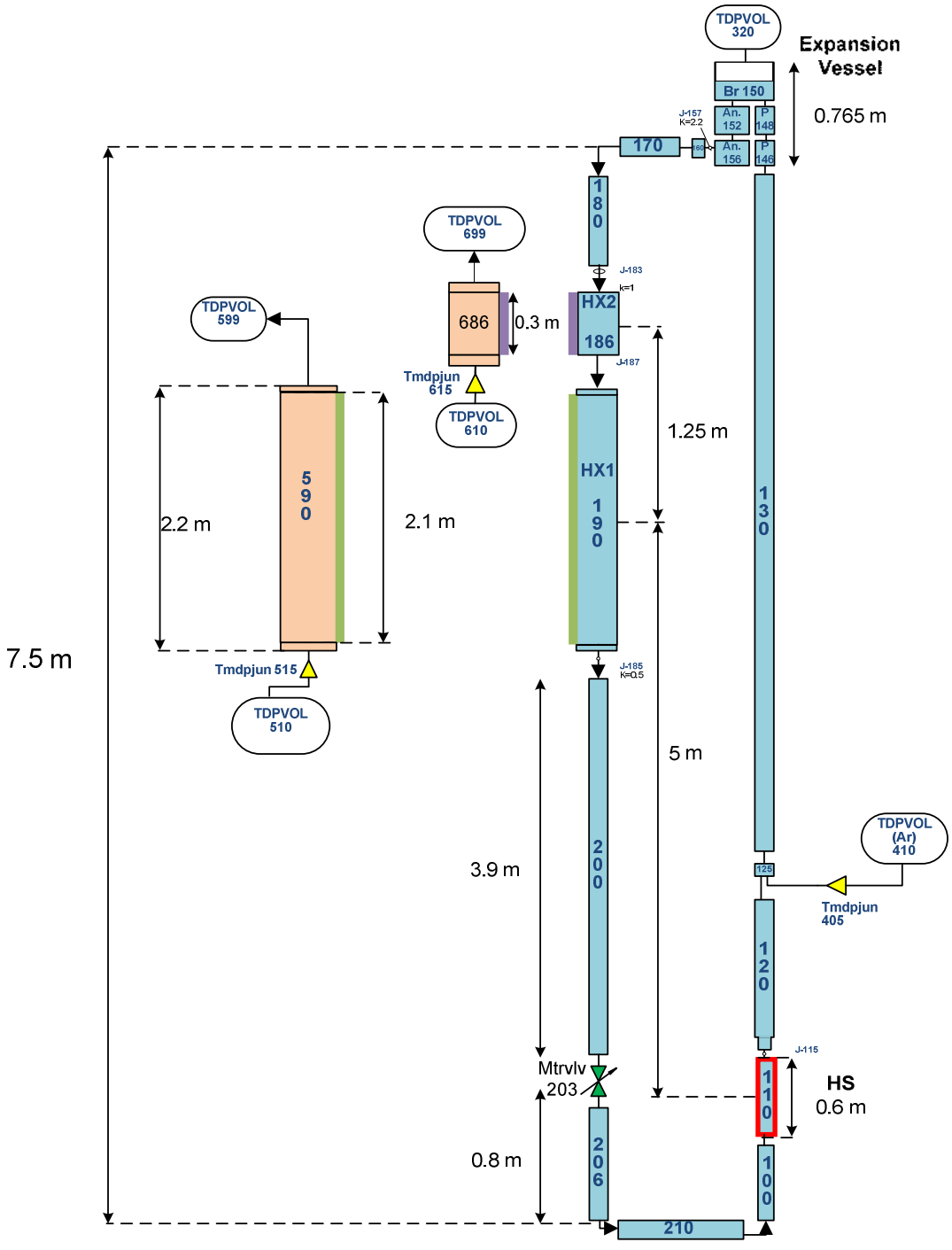

Figure 2.1: RELAP5 nodalization of NACIE.

Figure 2.1 shows the nodalizations of the primary LBE loop and of the two water secondary systems coupled with sections *HX-1* and *HX-2* respectively of the Heat Exchanger. Referring to this scheme, liquid metal circulates anticlockwise through the loop; LBE is heated in *Pipe-110* (Heat Source) positioned at the bottom of the loop and is cooled through the heat exchanger (top of loop) modelled by *Pipe-186* (*HX-2* low power section) and *Pipe-190* (*HX-1* high power section). According to the power to be exchanged, *HX-1* or *HX-2* is activated. The present report supports the design of SEARCH experimental campaign, devoted to characterizing the performance of MYRRHA fuel bundle (i.e. heat exchange and pressure drop) in shutdown conditions and to providing data for code validation. This experimental program is based on low power tests, therefore LBE exchanges power exclusively in heat section *HX-2*, water secondary loop associated to *HX-1* being deactivated. NACIE gas assisted circulation has been modelled by mean of a time dependent junction (*Tmdpjun-405*) which injects the desired Aargon flow rate (*Branch-125,* riser bottom). argon reaches the top of the expansion vessel through the riser, enhancing liquid metal circulation. From the riser prolongation inside the expansion vessel (*Pipe-146* and *Pipe-148*), LBE exits (in *Branch-150*) and is forced to pass downwards through the expansion vessel annular zone (*Annulus-152* and *Annulus-156*) promoting, therefore, gas separation and avoiding argon from reaching the upper portion of the loop (namely *Pipe-160* and *Pipe-170*). Only natural circulation tests are simulated in this work, consequently the argon injection has been deactivated. Liquid metal from the upper horizontal branch, goes downwards through *Pipe-180* to the heat exchanger sections, *HX-2* and *HX-1*. Height of *HX-2* (*Pipe-186)* and *HX-1* (*Pipe-190*) has been fixed to 0.3 m and 2.2 m respectively with a pipe cell's length of 0.05 m. The two sections are thermally coupled with two independent systems, simulating the *HX-2* and *HX-1* water secondary side (*Pipe-686* and *Pipe-590*). The two secondary systems are activated by means of time dependent junctions (*Tmdpjun-615* and *Tmdpjun-515*) regulating the water mass flow rate. Only *HX-2* secondary side water will be activated in these tests. LBE, exiting the heat exchanger sections, flows through the downcomer (*Pipe-200* and *Pipe-206*) to the lower horizontal pipe of the loop (*Pipe-210*) to reach the lower Heat Source inactive portion (*Pipe-100*). A Motor valve (*Mtrvlv-203*) is inserted in the downcomer lower section (between *Pipe-200* and *Pipe 206*) simulating the ball valve installed to regulate hydraulic losses. The nodalization is characterized by cells length of 0.1 m (mainly) for piping components and 5 cm for "heat-components" (namely Heat Source and the two Heat Exchanger sections). The value of the pipe's wall roughness has been assumed ε=32 μm .
Electrical pin bundle Heat Source, has been modelled as follows:

- Lower inactive portion (500 mm)*:* *Pipe-100;*
- Active portion (600 mm)*:* *Pipe-110;*
- Upper inactive portion (100 mm): *Pipe-120*, (first cell).

The pin bundle section is characterized by a flow area of $6.54 \cdot 10^{-4}$ m^2 and by a hydraulic diameter of $4.14\ 10^{-3}$ m. The pressure losses caused by the wire-spaced pin bundle (for a total length of ~1.3 m) are taken into account introducing a *pipe junction form loss coefficient, K,* which is a function of the Reynolds number, *Re,* and can generally be expressed as:

$$K=A+B\cdot(Re)^{-C}$$

where *A*, *B* and *C* are user-specified coefficient which have been derived from the Rehme equation [5] valid for wire spaced pin bundle (see Appendix A). Pressure losses associated with the bundle are dominant compared to the total ones; hence an accurate evaluation of the form coefficient, *K*, in this section of the loop, is an important issue for an adequate code flow prediction. Power Source, simulating the 19 fuel pins of the bundle (*d*=6.55mm, *p/d*=1.28), is modelled by an appropriate RELAP5 heat structure coupled with *Pipe-110 (HS).* Power is generated uniformly along 12 axial heat structures and released to the liquid metal, according to the convective vertical bundle option. For the Heat Exchanger (*HX-1* and *HX-2*), heat structures are introduced to simulate power transfer from LBE (flowing within tubes), to cooling water flowing within the two secondary systems. Double wall AISI 316L tubes with steel powder inside their gap have been modelled (mean value of the conductivity, *k*~3 W/(mK)). Inside *HX-1* (high power section) LBE exchange

power in counter-flow; the *vertical bundle without crossflow* option has been set for convective heat transfer water side (outside the tubes). In the low power section, *HX-2*, heat transfer occurs in crossflow mode and the value of the convective heat transfer coefficient has been fixed to 4600 W/(m^2 K) resulting from CFD simulations.

2.2 Simulation description and boundary conditions

The total amount of liquid metal filling NACIE primary loop is around 1370 kg of LBE at an initial temperature of 283°C (563.15 K). LBE initial level is set about half way of expansion vessel's height (*Branch-150*), 16 cm above the riser outlet. argon pressure inside the expansion vessel has been set to $1.2 \cdot 10^5$ Pa. Heat exchanger has been placed at the top of the downcomer to enhance LBE natural circulation with a thermal center elevation (vertical distance between *HX-2* and *HS* mid-planes) fixed to 6.25 m. Secondary side of the low power heat exchanger (*HX-2*) is characterized by a pressure of 16 bar and water flow rate is set to 10 m^3/h. The heat transfer coefficient of water flowing cross-flow through *HX-2* has been estimated from CFD simulations and fixed to the value of h_w= 4600 W/(m^{2}K). All RELAP5 simulations have been performed with the boundary conditions described above. No heat dispersion towards external environment has been considered. Simulations aim to investigate safety related parameters in case of a natural circulation condition for different values of the mass flow rate. Three power levels of the Heat Source have been investigated:

- Q_1=10.8 kW
- Q_2=21.7 kW
- Q_3=32.5 kW

The reference heat flux value at the wall of ~1 MW/m^2 is obtained for bundle nominal power of ~ 235 kW. The effect of *HX-2* water inlet temperature, in the range of 120-170°C, has been investigated as well. Heat Source power is switched on after 2000 s from the beginning of each simulation; at the same time secondary water starts flowing through *HX-2* secondary loop. Two sets of simulations have been executed:

- *Test NAT*, which is aimed at characterizing the performance of the loop and the LBE mass flow rate in natural circulation conditions, for the three reference power level.
- *Test VAL*, which is devoted to evaluating the system's performance, for different additional loop hydraulic resistances (by means of a valve, *Mtrvlv-203*), that progressively reduce natural circulation mass flow rate obtained in Test NAT.

2.3 Simulations results and discussion

2.3.1 Natural circulation (Test NAT)

The first series of simulations (Test NAT) aim at investigating the above described NACIE loop behaviour under natural circulation conditions, for three reference power levels (Q_1=10.8 kW, Q_2=21.7 kW and Q_3=32.5 kW). As described before, *HS* and *HX-2* thermal center distance has been set at 6.25 m. During these simulations it can be assumed that the NACIE loop losses of pressure are predominantly caused by the wire-spaced bundle section. Moreover, in each simulation of Test NAT, named NAT-1, NAT-2 and NAT-3 (according to the heat power level), the influence of the inlet *HX-2* secondary water temperature, T_w, has been investigated performing a stepwise increase of the secondary water, from 120 up to 170°C (step of 10°C). The time span for each water temperature level is 10000 s, (to allow the achievement of stationary conditions) for total simulation duration of 60000 s. Table 2.1 summarizes the estimated LBE mass flow rate, for each simulation, expected in NACIE loop. These values are obtained at the end of the time span when the system has reached "quasi" steady state condition.

Table 2.1: Natural circulation mass flow rate driven through NACIE loop.

Quantity	Inlet water temperature [°C]						Test name
	120	130	140	150	160	170	
$\dot{m}$ [kg/s]	1.53	1.53	1.54	1.55	1.55	1.56	NAT-1
$\dot{m}$ [kg/s]	2.05	2.05	2.06	2.06	2.07	2.07	NAT-2
$\dot{m}$ [kg/s]	2.41	2.41	2.41	2.42	2.42	2.42	NAT-3

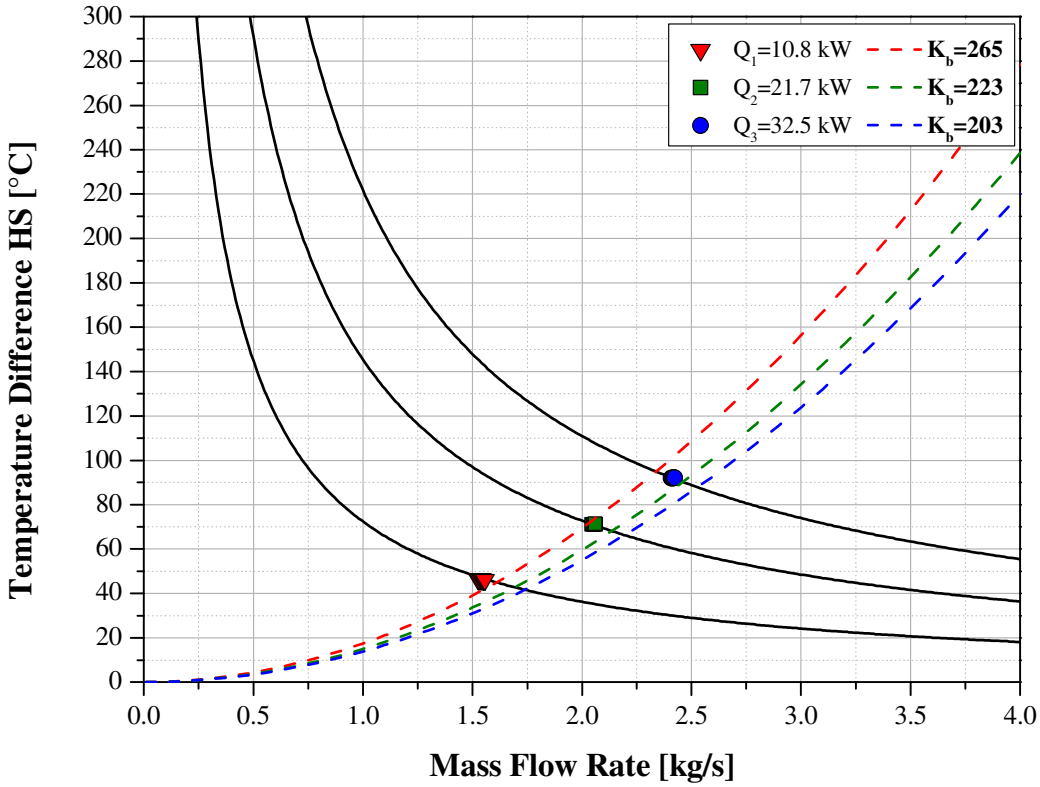

Figure 2.2: *HS* temperature difference versus LBE natural flow rate: RELAP5 simulated results and the related simplified thermal hydraulic model estimations (dash-lines).

Simulation results show that water temperature, T_w, has a negligible influence on the value of the LBE mass flow rate established in NACIE loop. These results are depicted in Figure 2.2 which plots the obtained values of natural mass flow rate, $\dot{m}$, versus the corresponding bundle temperature difference, ΔT_{HS}, for the reference power levels. According to the power level, *Q*, results stays on three curves generated from the following balance equation:

$$\Delta T_{HS} = \frac{Q}{\overline{c}_p \cdot \dot{m}} \tag{2.1}$$

The LBE specific heat capacity at constant pressure has been approximately set at $\overline{c}_p$ = 147 J/(kg K). Furthermore, by means of a simple balance between driving and resistance force, a simplified thermal-hydraulic model of NACIE loop in pure natural circulation can be written as:

$$\rho g \beta \cdot \Delta T_{HS} \cdot H = K(u) \cdot \rho \cdot \frac{u^2}{2} \tag{2.2}$$

In the simplified assumption that K is not a function of u, i.e. for sufficiently high Reynolds number, it is possible to obtain in closed form a relationship between the temperature drop and the mass flow rate in the loop:

$$\Delta T_{HS} = \frac{K u^2}{2 g \beta H} = \frac{K}{2 g \beta H \rho^2 A^2} \dot{m}^2 \tag{2.3}$$

where,

$K=K_b+K_l+K_v$	: total resistance coefficient associated to reference cross section A.
K_b	: bundle resistance coefficient.
K_l	: loop resistance coefficient (related to pipe friction, bends, contractions, enlargements and expansion vessel).
K_v	: valve resistance coefficient.
u	: LBE velocity magnitude for the reference cross section A.
A	: reference cross section.
β	: LBE volumetric thermal expansion coefficient.
H	: thermal centers elevation (H=6.25 m)
g	: gravity acceleration

A comparison of the LBE mass flow rate derived using the simplified thermal hydraulic model and results obtained by RELAP5 simulations is illustrated in Figure 2.2 as well. The three thermodynamic model parabolic trends associated with reference power levels are characterized by different bundle resistance coefficients, K_b, which are derived from RELAP5 results (for T_w=170°C). The value of the loop resistance coefficient has been approximately set to a constant value of k_l=15. Valve resistance coefficient is K_v=0, assuming the valve completely opened and the value of β and ρ have been taken for mean LBE temperature. A sufficient agreement could be observed although the thermal hydraulic model results are slightly higher compared to the ones obtained by the simulations. Detailed trend of LBE natural circulation mass flow rate and the related temperature difference through the inlet and outlet section of the *HS*, are shown, for each power level, in Figures 2.3(a,b,c).

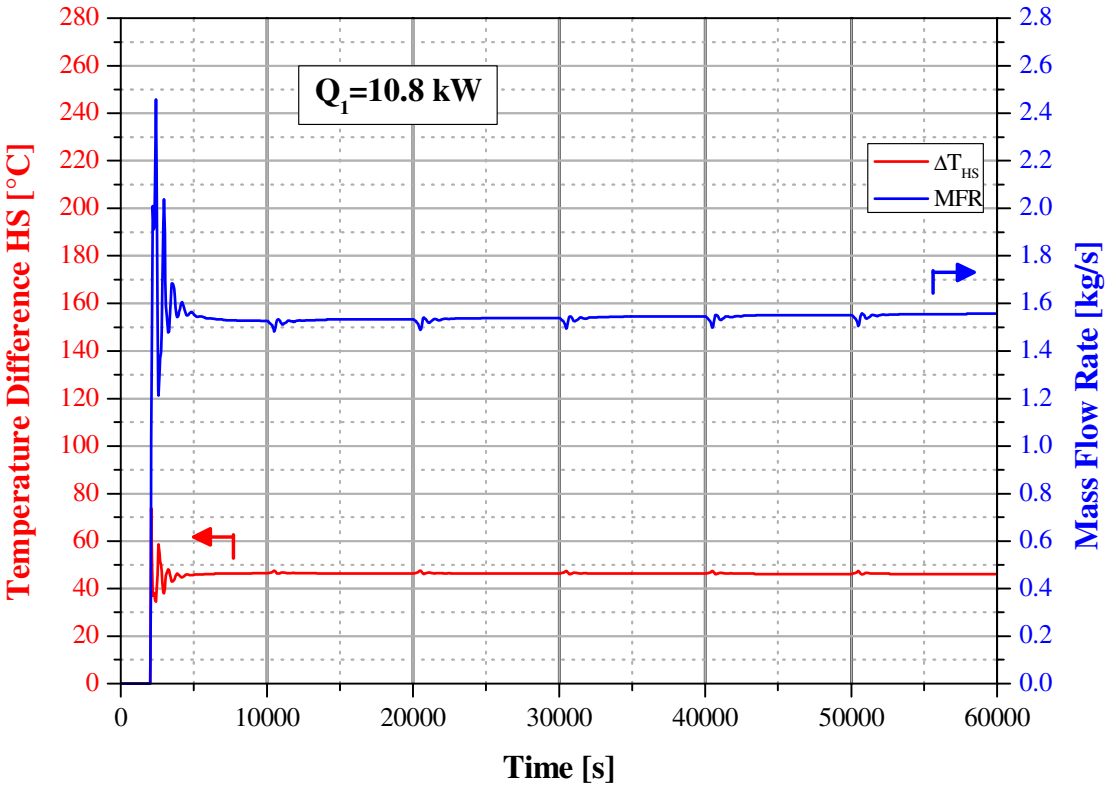

Figure 2.3.a: LBE mass flow rate along NACIE loop and the related ΔT_{HS} (Test NAT-1).

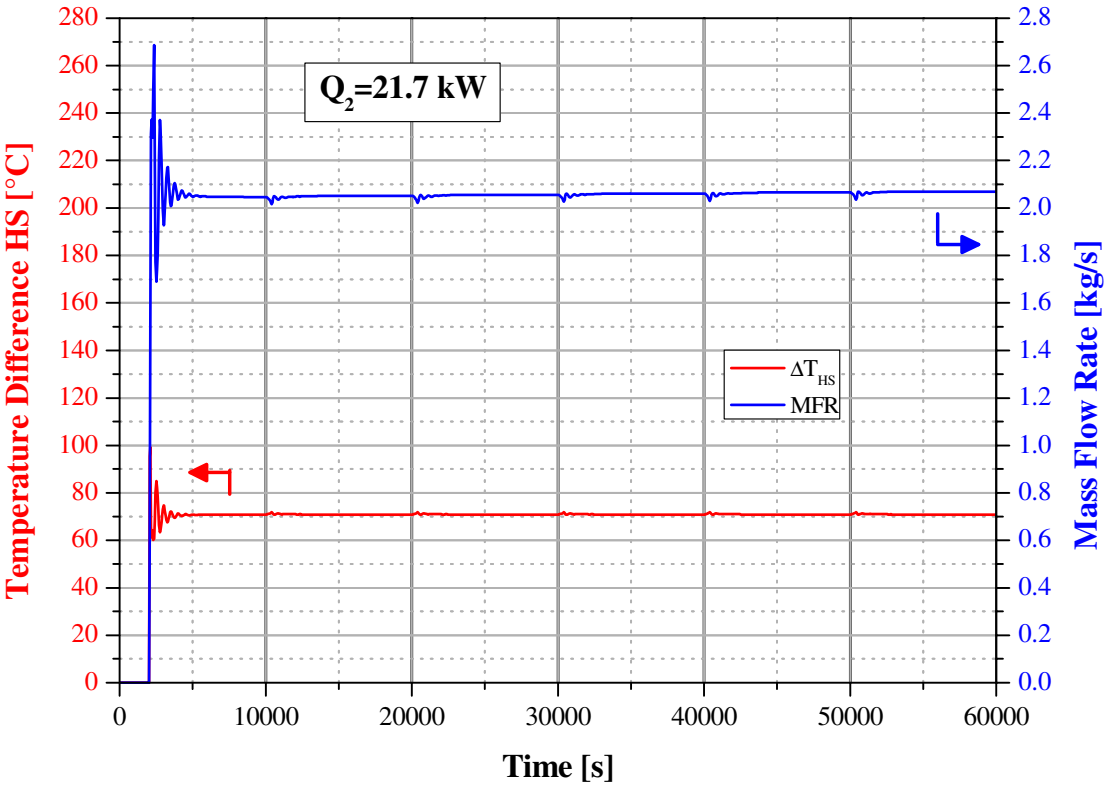

Figure 2.3.b: LBE mass flow rate along NACIE loop and the related ΔT_{HS} (Test NAT-2).

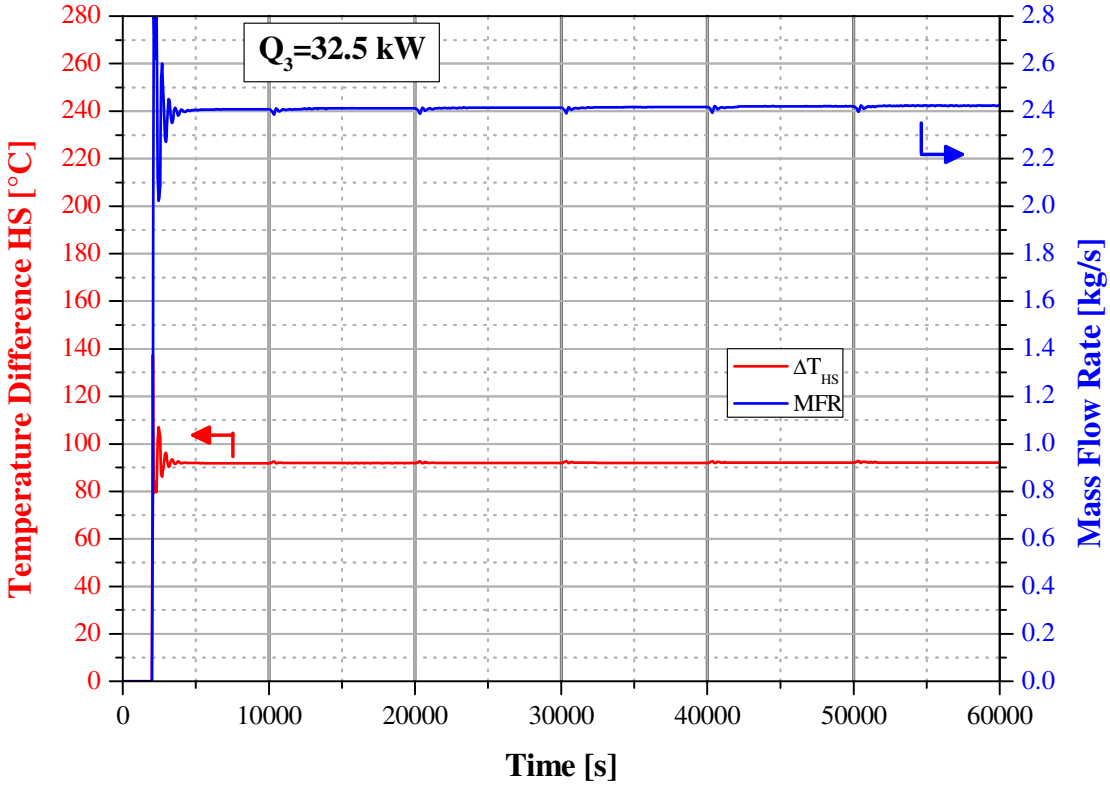

Figure 2.3.c: LBE mass flow rate along NACIE loop and the related ΔT_{HS} (Test NAT-3).

In Figures 2.4(a,b,c) the trends of the average LBE inlet and outlet Heat Source temperatures are plotted, together with pin surface temperatures estimated at the thermocouples location (see Figure 1.4). The considered heights for the TCs along the bundle active length (L_{act} = 600) are:

- z = 38 mm (TC_d)
- z = 300 mm (TC_m)
- z = 562 mm (TC_u)

Results are summarized in Table 2.2. The stepwise increasing trend of the *HX-2* water inlet temperature is depicted as well. Results show how the loop's mean temperature increases with the power level; moreover, increasing water inlet temperature causes a further increase in the loop's mean temperature trend and consequently a higher value of the maximum LBE temperature and clad surface temperature (TC_u). For Q_3=32.5 kW (Test NAT-3) and T_w=170°C, in maximum temperature conditions, the previously mentioned temperatures remain below 431°C. Furthermore, the minimum LBE temperature (176°C) is observed for Q_1=10.8 kW (Test NAT-1) and T_w=120°C, with a safety margin of about 50°C from LBE freezing point (124°C).

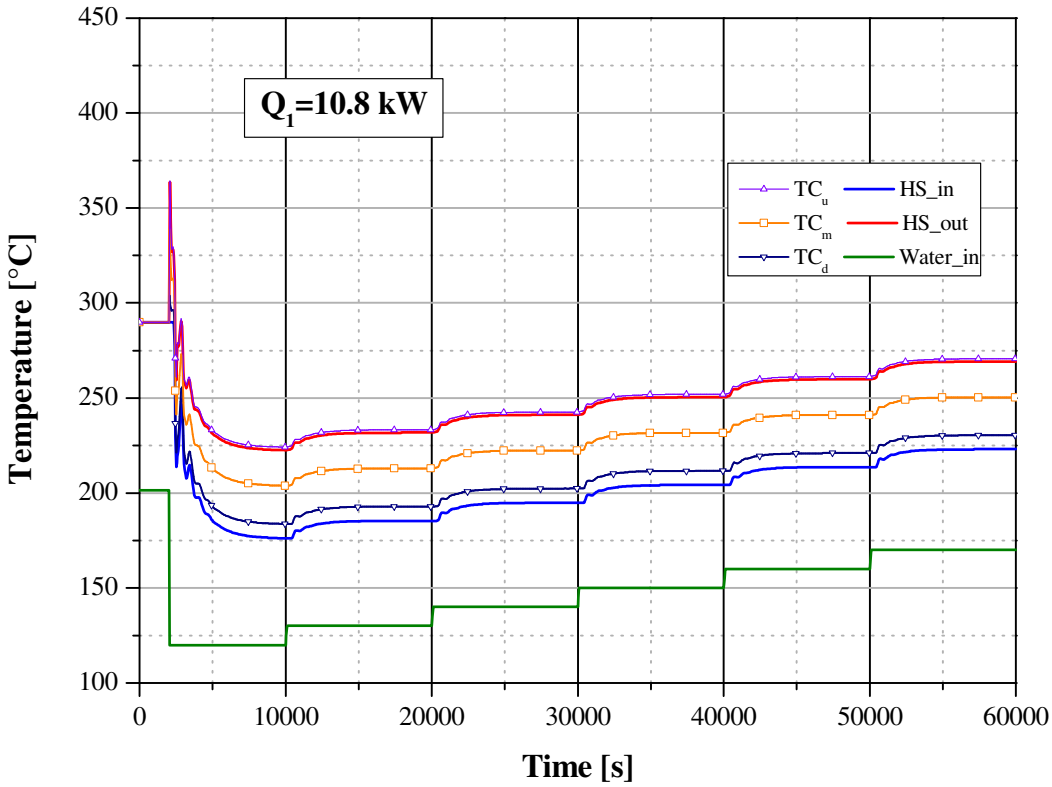

Figure 2.4.a: Inlet and outlet LBE temperatures along *HS*, clad temperature at TCs locations and trend of the *HX-2* water inlet temperature (Test NAT-1).

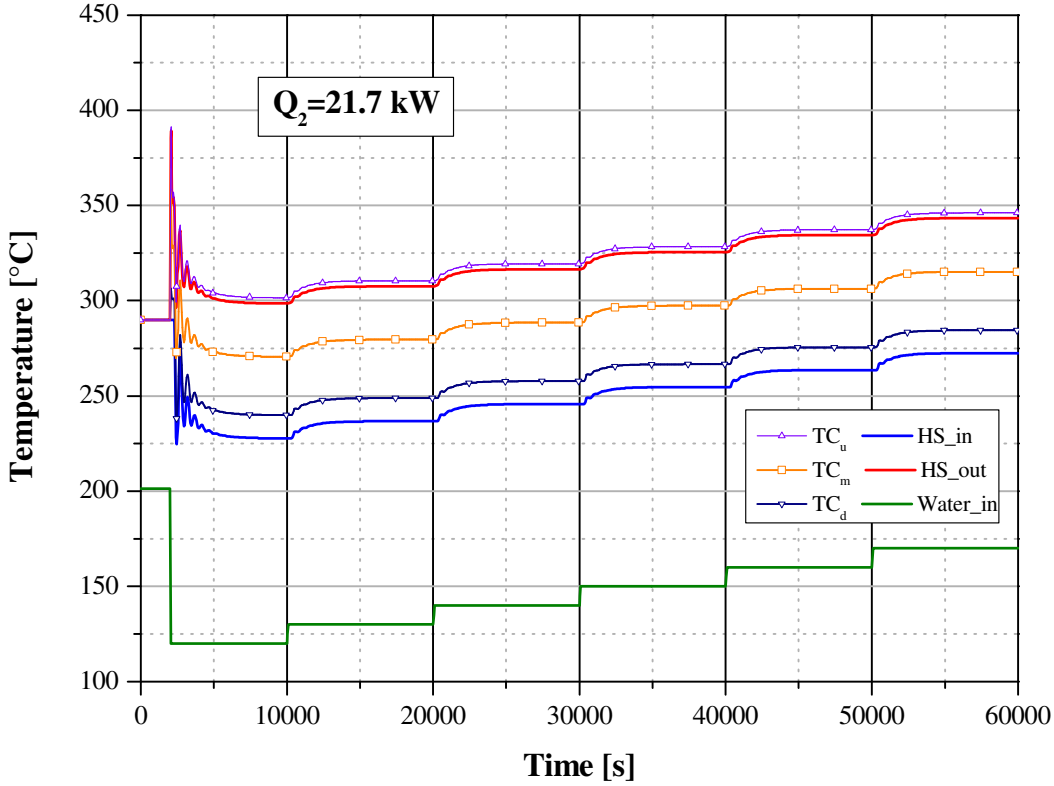

Figure 2.4.b: Inlet and outlet LBE temperatures along *HS*, clad temperature at TCs locations and trend of the *HX-2* water inlet temperature (Test NAT-2).

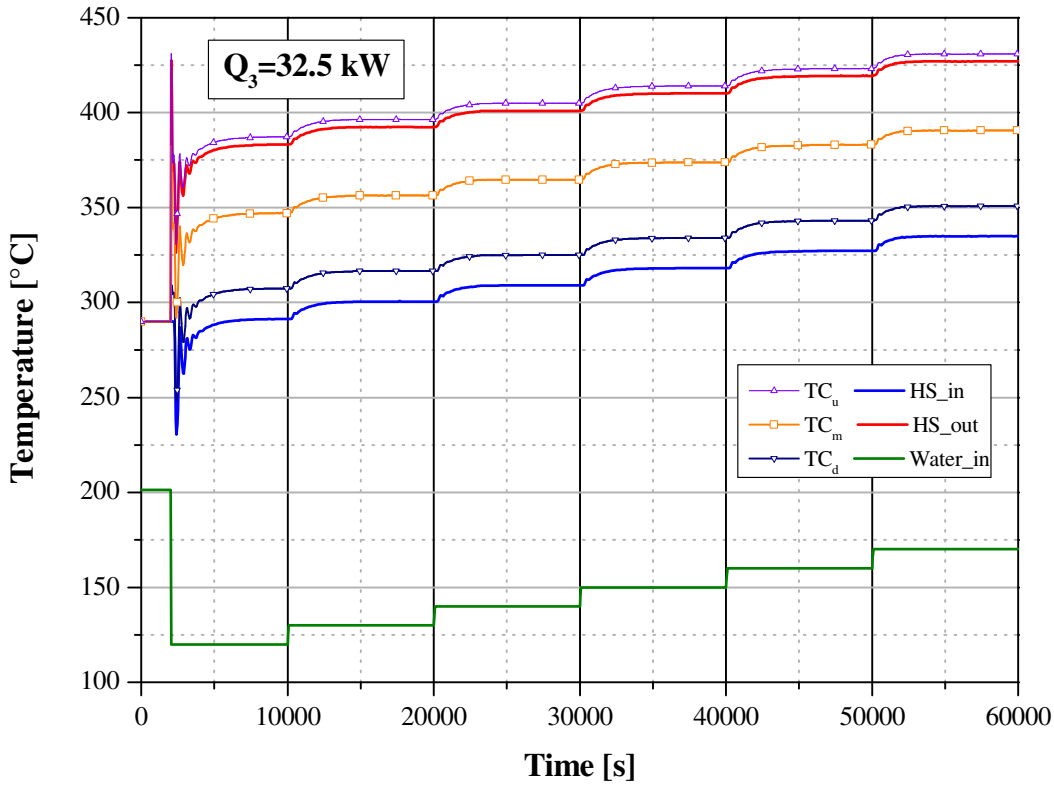

Figure 2.4.c: Inlet and outlet LBE temperatures along *HS*, clad temperature at TCs locations and trend of the *HX-2* water inlet temperature (Test NAT-3).

Table 2.2: LBE inlet/outlet *HS* temperature and clad surface temperature at thermocouple locations [°C].

Temperature [°C]	Inlet water temperature T_w [°C]						Test name
	120	*130*	*140*	*150*	*160*	*170*	
HS In	176	185	195	204	214	223	NAT-1
HS Out	223	232	241	250	260	269	
TC_d	184	193	202	212	221	230	
TC_m	204	213	222	232	241	250	
TC_u	224	233	243	252	261	271	
HS In	228	237	246	255	264	272	NAT-2
HS Out	299	308	317	325	334	343	
TC_d	240	249	258	267	276	284	
TC_m	271	280	288	297	306	315	
TC_u	302	310	319	328	337	346	
HS In	291	300	309	318	327	335	NAT-3
HS Out	383	392	401	410	419	427	
TC_d	307	317	325	334	343	351	
TC_m	347	356	365	374	383	391	
TC_u	387	396	405	414	423	431	

LBE velocity magnitude through the rod bundle Heat Source and inside the tubes of the low power Heat Exchanger (*HX-2*) are depicted in Figures 2.5(a,b,c), for the three reference power levels. An estimation of the Reynolds number trend is shown as well (right axis). Reynolds number has been evaluated for LBE mean properties (at *HS* half height). Concerning the LBE velocity magnitude through the *HS*, an analogous trend as for the mass flow rate can be observed and the velocity magnitude is not influenced by increasing water inlet temperature. *HS* velocity magnitude is about 0.23 m/s for test NAT-1, 0.30 m/s for test NAT-2 and 0.36 m/s for test NAT-3. LBE velocity magnitude inside the Heat Exchanger tubes is in the order of magnitude of some millimetres per seconds: 0.007 m/s for test NAT-1, 0.009 m/s for test NAT-2 and 0.011 m/s for test NAT-3.

Concerning the Reynolds number, it ranges (values for water temperature of 120 and 170°C):

- from 3970 to 4670 (test *NAT-1)*
- from 6430 to 7240 (test *NAT-2)*
- from 8970 to 9800 (test *NAT-3)*

Turbulent flow regime is established inside the bundle Heat Source for all the considered tests. An increase in Reynolds number is observed with the increasing inlet water temperature caused by the increase of the ratio $(\rho/\mu)_{LBE}$ with the loop mean temperature.

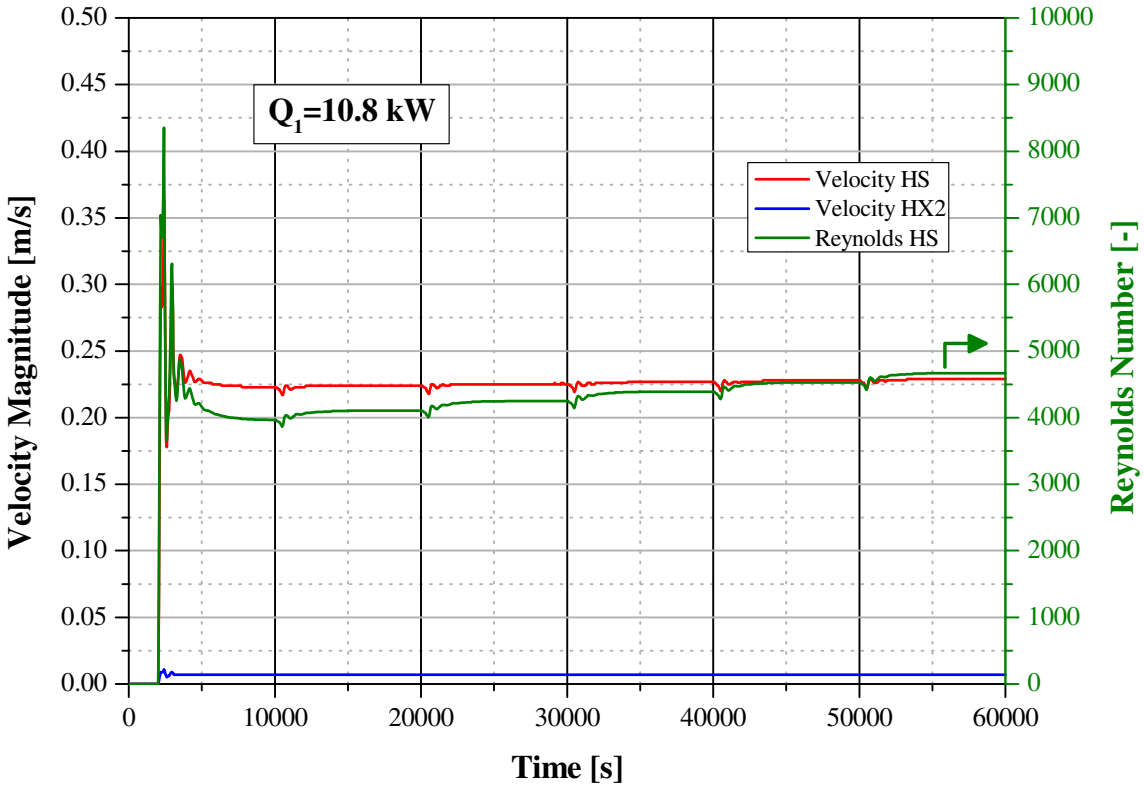

Figure 2.5.a: LBE Velocity along the *HS* bundle and inside *HX-2* tubes.
Reynolds number for *HS* (Test NAT-1).

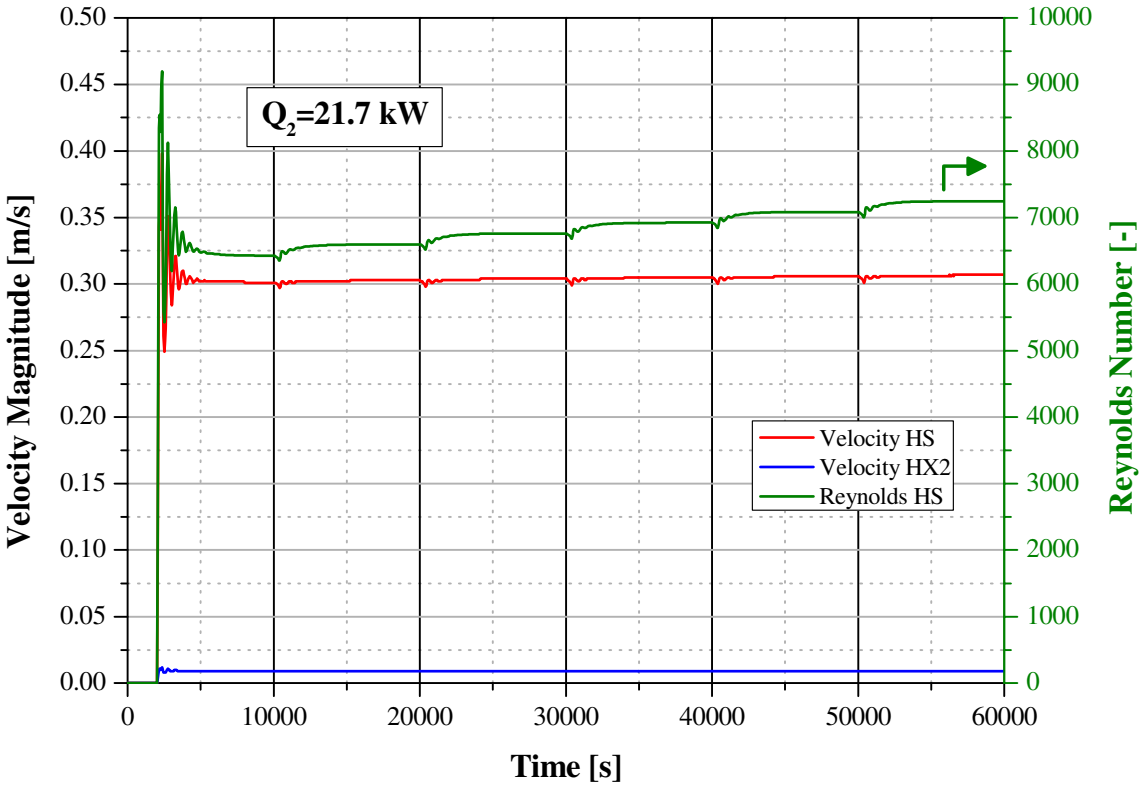

Figure 2.5.b: LBE Velocity along the *HS* bundle and inside *HX-2* tubes.
Reynolds number for *HS* (Test NAT-2)

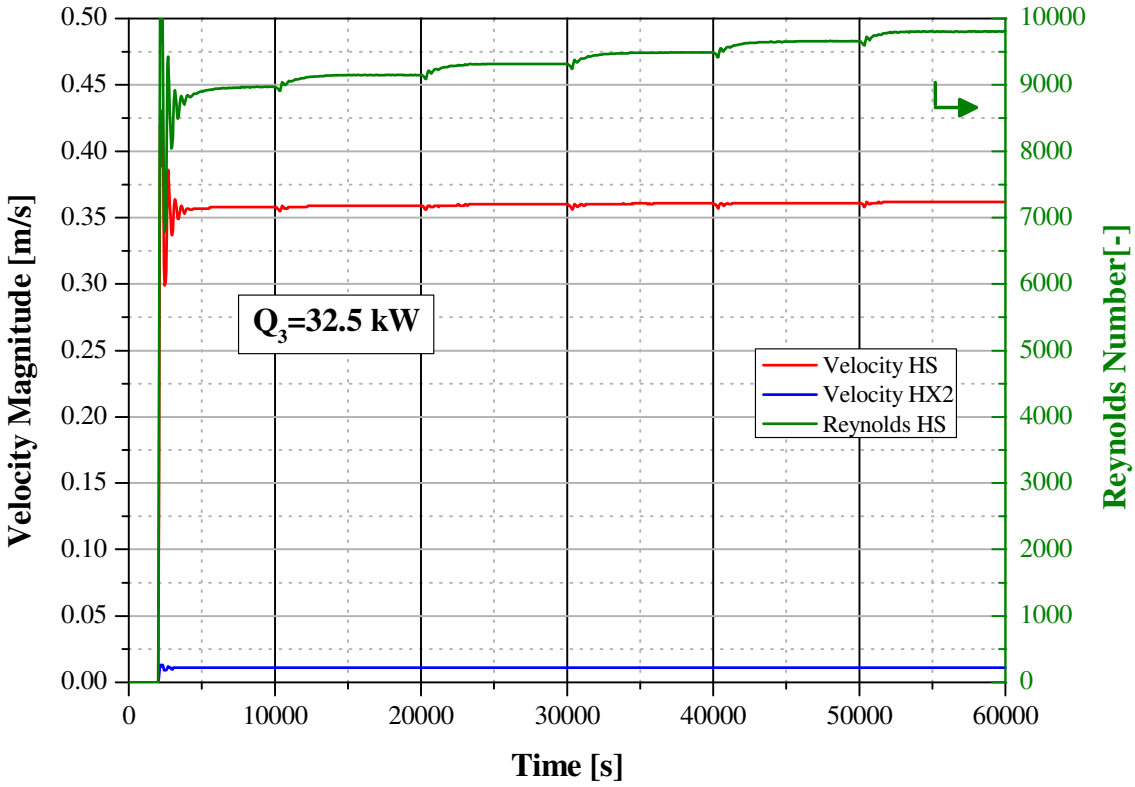

Figure 2.5.c: LBE Velocity along the *HS* bundle and inside *HX-2* tubes.
Reynolds number for *HS* (Test NAT-3).

LBE heat transfer coefficients (HTC) for *HS* (pin bundle) and for *HX-2* (tube side) are depicted in Figures 2.6(a,b,c), for the three considered tests. The heat transfer coefficient water side is plotted as well. It is set from CFD simulations to the value of 4600 W/(m^2 K). Vertical bundle heat transfer coefficient is evaluated by RELAP5, according to Ushakov correlation [6], while for LBE flowing tube side through the heat exchanger, Seban [7] relation is used. Obtained results are summarized in Table 2.3.

Table 2.3: LBE heat transfer coefficient [W/(m^{2}K)], for *HS* (bundle) and *HX-2* (tube side).

HTC [W/(m^{2}K)]	Inlet water temperature [°C]						Test name
	120	130	140	150	160	170	
HS	17458	17682	17915	18145	18373	18598	NAT-1
HX-2	949	961	975	988	1001	1014	
HS	19 756	19 966	20 174	20 380	20 584	20 786	NAT-2
HX-2	1 063	1 075	1 087	1 099	1 110	1 122	
HS	21926	22128	22312	22508	22703	22866	NAT-3
HX-2	1182	1193	1204	1215	1227	1236	

A slight heat transfer coefficient increase is observed with inlet water temperature; while from simulation NAT-1 to simulation NAT-3, HTC increases by about 20%.

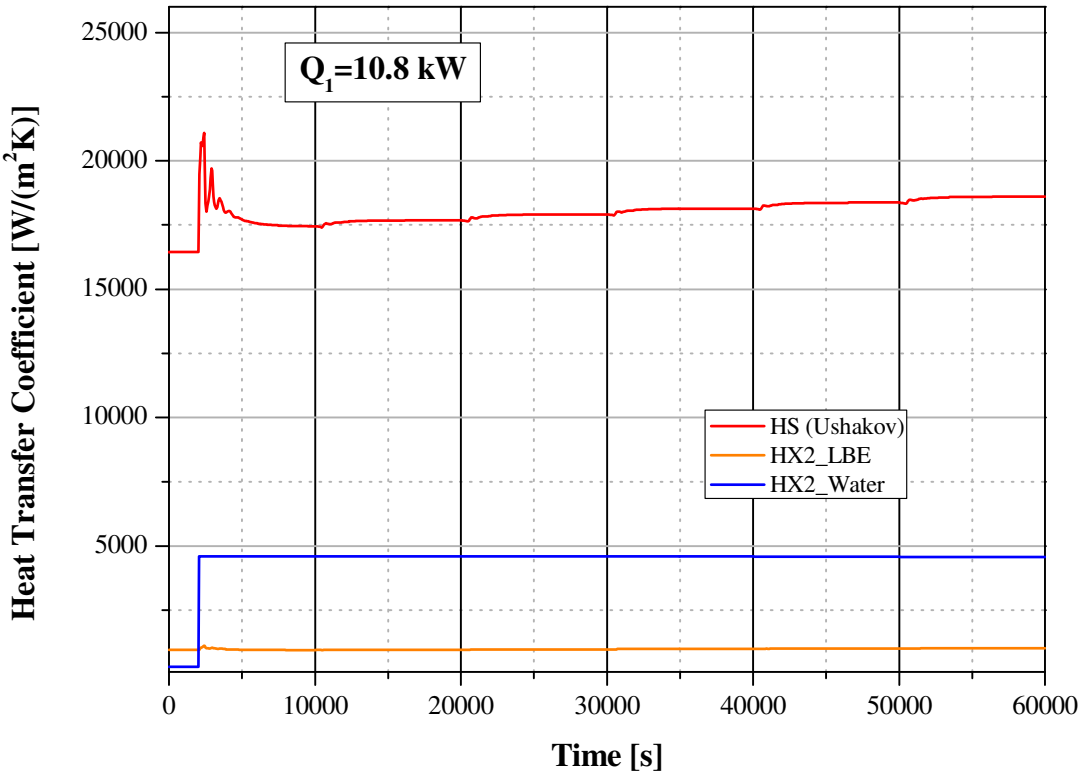

Figure 2.6.a: Heat transfer coefficient for LBE and water (Test NAT-1).

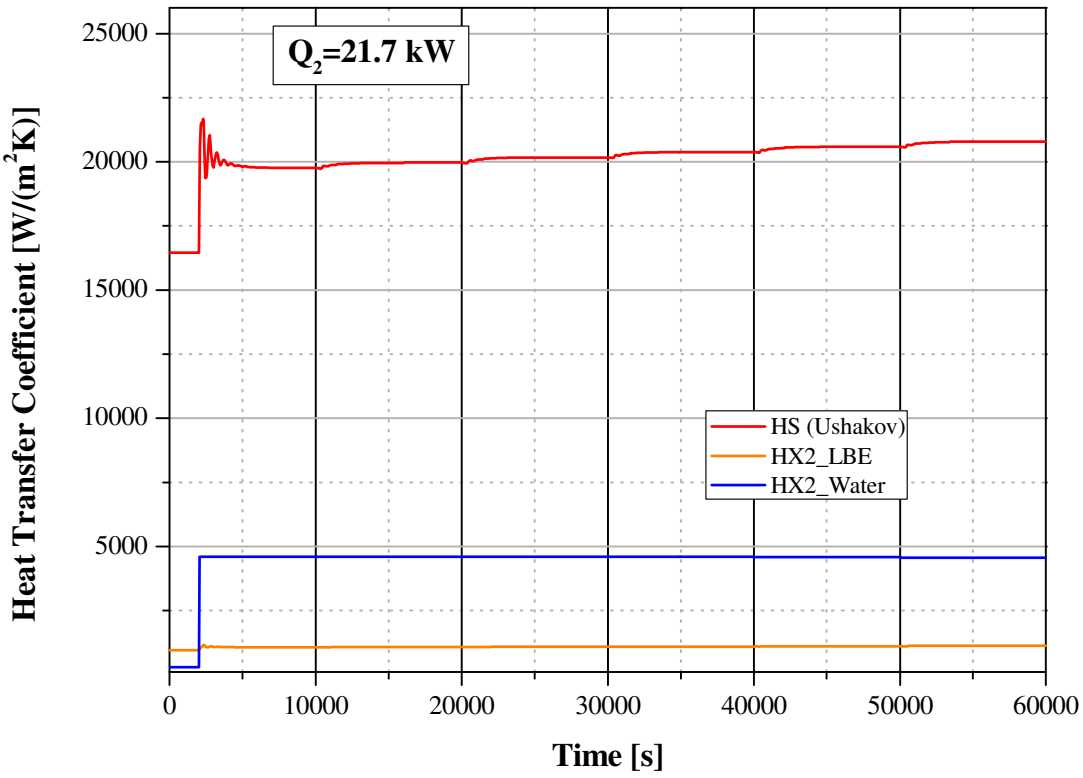

Figure 2.6.b: Heat transfer coefficient for LBE and water (Test NAT-2).

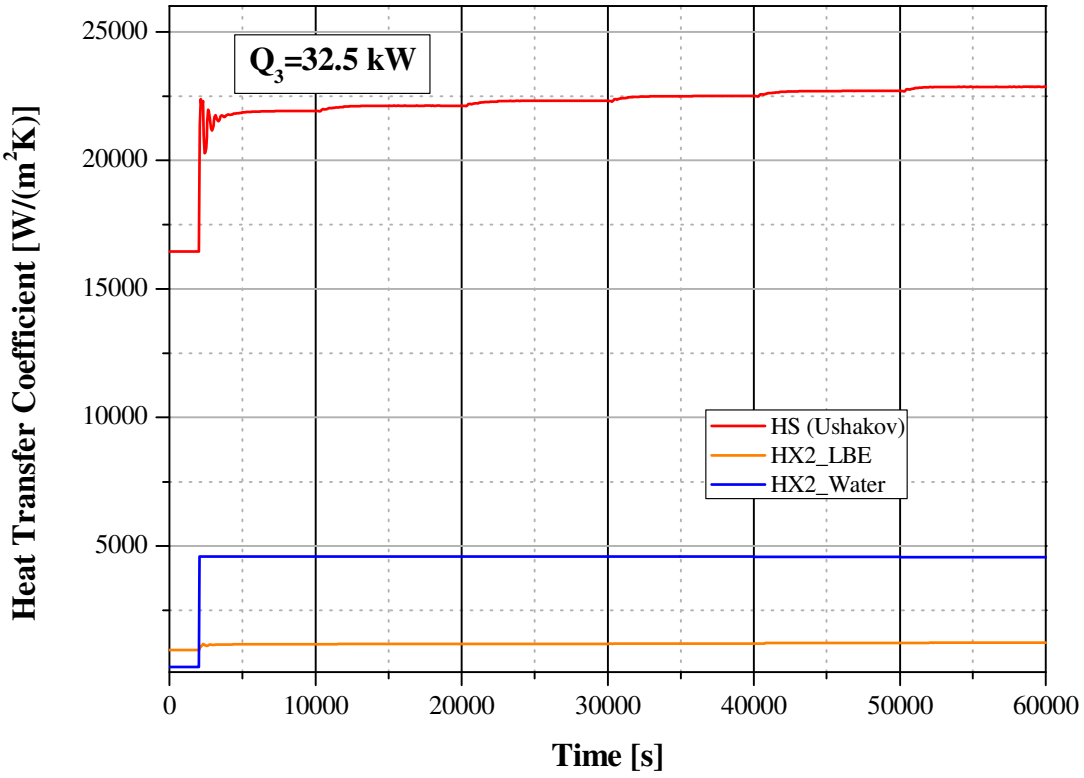

Figure 2.6.c: Heat transfer coefficient for LBE and water (Test NAT-3).

The pressure loss resistance coefficient, K_b, has been set in NACIE input, introducing coefficients in the bundle junctions form loss card, in order to obtain an equivalent loss coefficient, according to Rehme correlation (see Eq. A.4 in Appendix A). The value of K_b from RELAP5 has been compared to the theoretical value calculated with Rehme correlation, K_R, for wire spaced fuel bundle. As depicted in Figure 2.7(a,b,c) the two different evaluations are coincident. In the same figures, the value of the bundle pressure losses, ΔP_b, estimated using Eq.2.5, is compared to the theoretical pressure loss, ΔP_R, obtained using K_R value in the following correlation:

$$\Delta P_R = \frac{1}{2} \cdot K_R \rho_b u_{ref}^2 \tag{2.4}$$

Where ρ_b is the mean value of LBE density inside the fuel bundle and u_{ref} is the loop reference velocity. The ΔP_b has been estimated subtracting the pressure head to the bundle absolute pressure difference according to the following correlation:

$$\Delta P_b = (P_{in} - P_{out}) - g \cdot \sum_{i=1}^{N_b} h_i \rho_i \tag{2.5}$$

Where, P_{in} and P_{out} are the bundle absolute inlet and outlet pressure, h_i is the height of the RELAP5 bundle pipe hydrodynamic sub-volumes, N_b is the number of sub-volumes, ρ_i is the LBE density of the sub-volume and g is the gravity acceleration. Results show sufficient agreement with the theoretical estimation, being about 3 % lower for all three simulations. Table 2.4 summarizes the values of K_b and bundle pressure losses ΔP_b evaluated with Eq. 2.5. Resistance coefficient slightly decreases with temperature due to Reynolds number increase (increase of LBE ρ/μ ratio) which causes a decrease of Darcy-Weisbach friction factor, f_R, in Rehme correlation (see Eq. A.2 in Appendix A). Consequently a slight decrease of bundle pressure loss is observed.

Table 2.4: Resistance coefficient K_b and pressure drop ΔP_b [Pa] along the bundle.

Quantity	Inlet water temperature [°C]						Test name
	120	130	140	150	160	170	
K_b [-]	285	280	276	272	268	265	NAT-1
ΔP_b [Pa]	3476	3451	3430	3410	3391	3374	
K_b [-]	235	233	231	228	226	225	NAT-2
ΔP_b [Pa]	5138	5117	5097	5079	5061	5044	
K_b [-]	210	208	207	206	204	203	NAT-3
ΔP_b [Pa]	6372	6354	6337	6319	6301	6292	

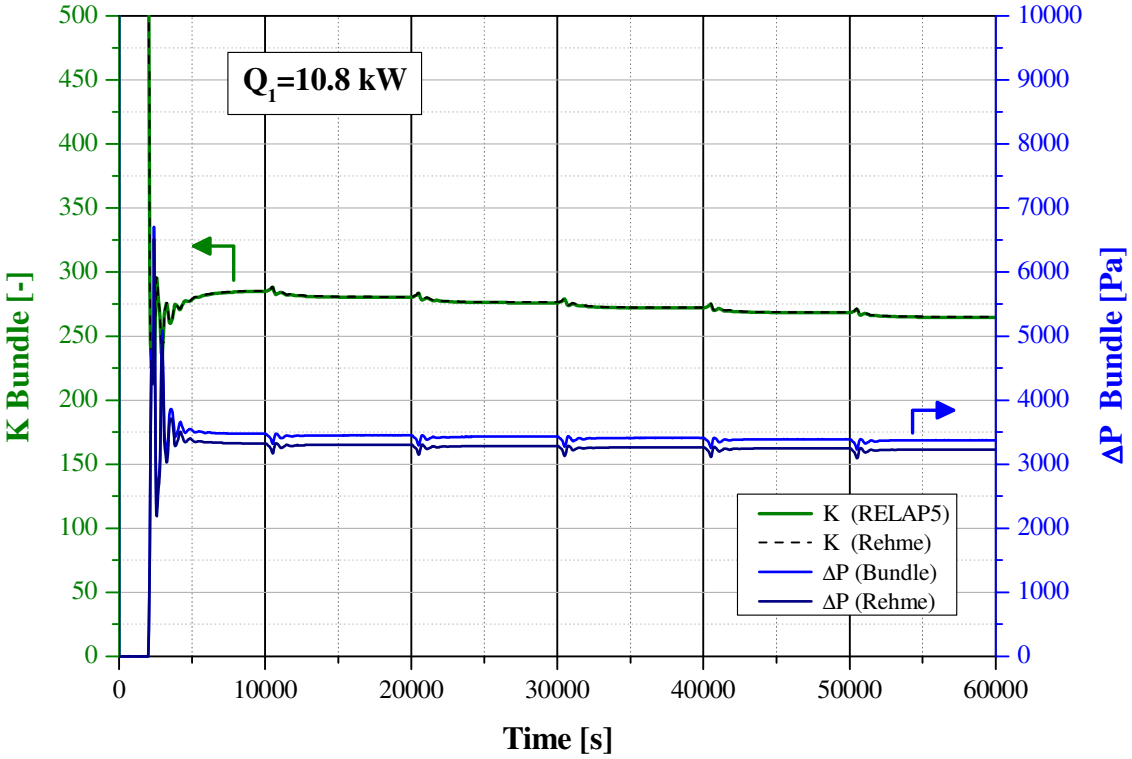

Figure 2.7.a: Bundle resistance coefficient and pressure drop (Test NAT-1).

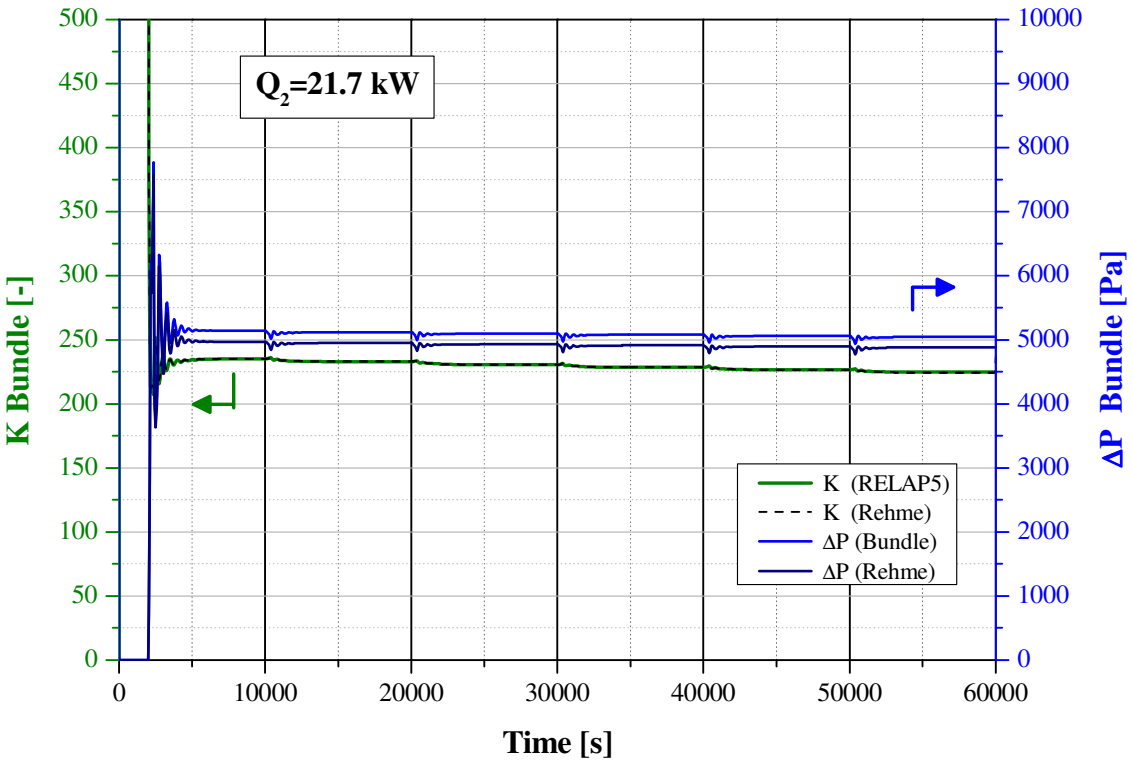

Figure 2.7.b: Bundle resistance coefficient and pressure drop (Test NAT-2).

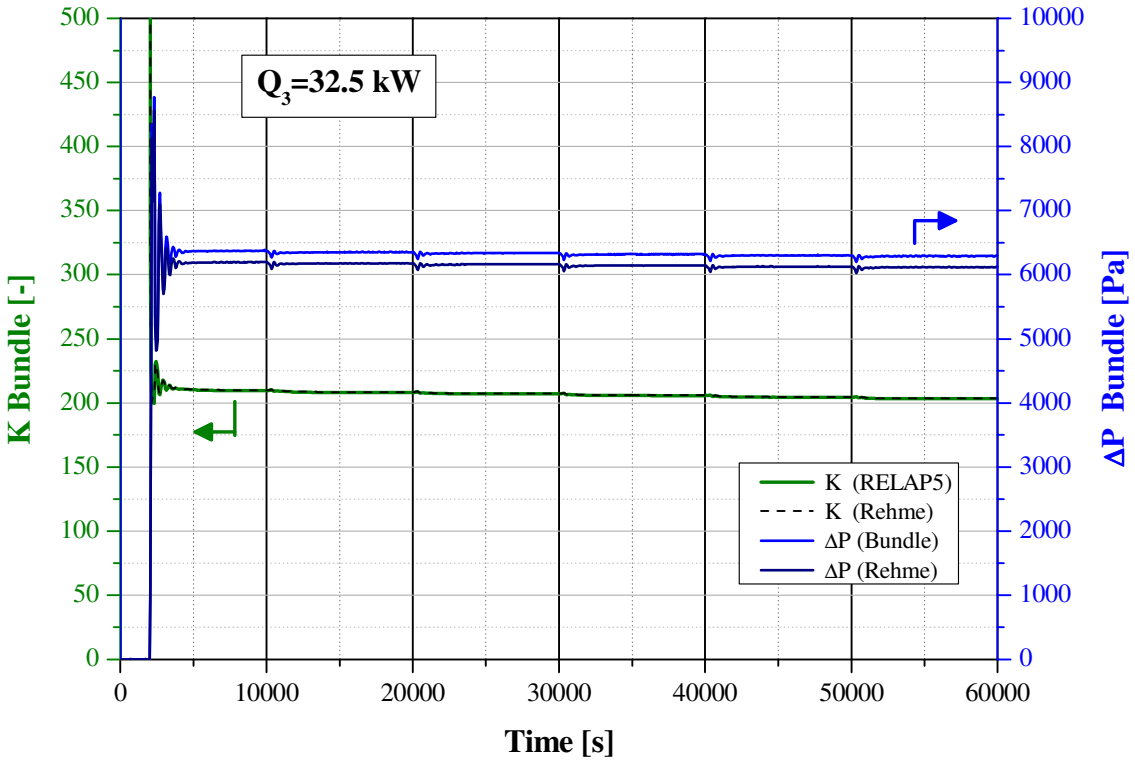

Figure 2.7.c: Bundle resistance coefficient and pressure drop (Test NAT-3).

2.3.2 Natural circulation with additional flow resistance (Test VAL)

The second series of simulations (Test VAL) aims at investigating NACIE behaviour in case of reduced natural circulation flow rate caused by an additional hydraulic resistance through the loop. Therefore, Test VAL has been performed by progressively closing the valve represented in NACIE RELAP5 model (see Figure 2.1) by the component *Mtrvlv-203*. Valve area is reduced with a stepwise trend in order to reach six progressively higher resistance coefficients: K_v=100, 500, 1300, 2800, 5000, 10000. RELAP5 dependence of K_v upon valve area is discussed in Appendix A. The time span for each value of K_v has been fixed to 10000 seconds in order for the loop parameters to reach stationary conditions. Inlet water temperature in the heat exchanger *HX-2* has been fixed to T_w=170°C. Simulation results are summarized in Figure 2.8, which show, for each power level Q_1=10.8 kW, Q_2=21.7 kW and Q_3=32.5 kW, LBE mass flow rate for progressive K_v increase (from K_v=0 of test NAT to K_v =10000) and the associated *HS* temperature difference. The curves based upon the simplified thermal hydraulic model introduced previously are depicted on the same plot. The value of resistance coefficient in Eq. 2.3 ($K=K_b+K_v+K_l$) has been evaluated considering the K_b value for the intermediate power level simulation VAL-2, K_l=15 and K_v the valve resistance coefficient.

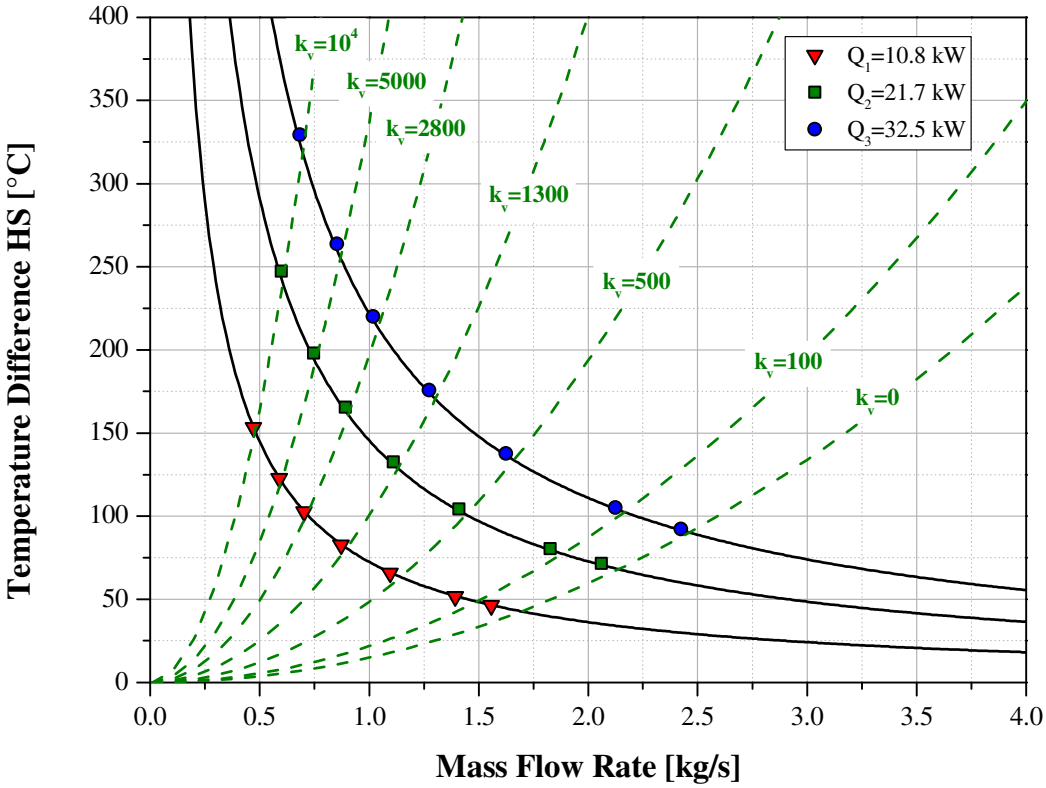

Figure 2.8: *HS* temperature difference versus LBE natural flow rate: RELAP5 simulation results for increasing values of K_v and the related simplified thermal hydraulic model estimations (dash-lines)

Outcomes show a sufficient agreement of RELAP5 results with the ones estimated by the simplified thermal hydraulic model for high values of the valve resistance coefficient, while for lower K_v the model provides slightly higher values of the LBE mass flow rate as observed for test NAT. Table 2.5 summarizes stationary LBE mass flow rate values obtained from RELAP5 simulation at increasing K_v, for the three power levels.

Table 2.5: LBE flow rate for the reference valve resistance coefficient.

Quantity	Valve resistance coefficient K_v [-]							Test name
	0	100	500	1300	2800	5000	10000	
$\dot{m}$ [kg/s]	1.56	1.39	1.10	0.87	0.70	0.59	0.47	VAL-1
$\dot{m}$ [kg/s]	2.07	1.83	1.41	1.11	0.89	0.75	0.60	VAL-2
$\dot{m}$ [kg/s]	2.42	2.12	1.62	1.27	1.02	0.85	0.68	VAL-3

In Figures 2.9(a,b,c) the trends of LBE flow rate and *HS* temperature difference are reported for each power level with the increase of K_v value (case T_w=170°C).

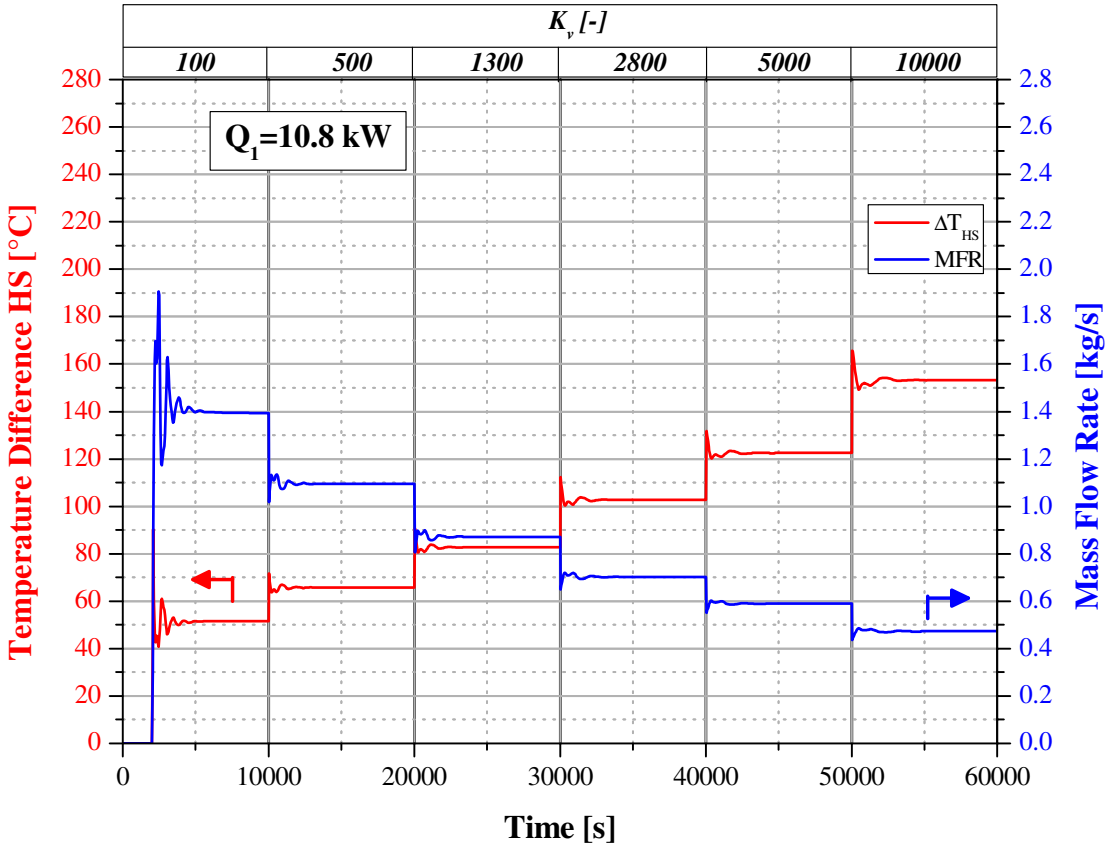

Figure 2.9.a: LBE mass flow rate along NACIE loop and the related ΔT_{HS} (Test VAL-1).

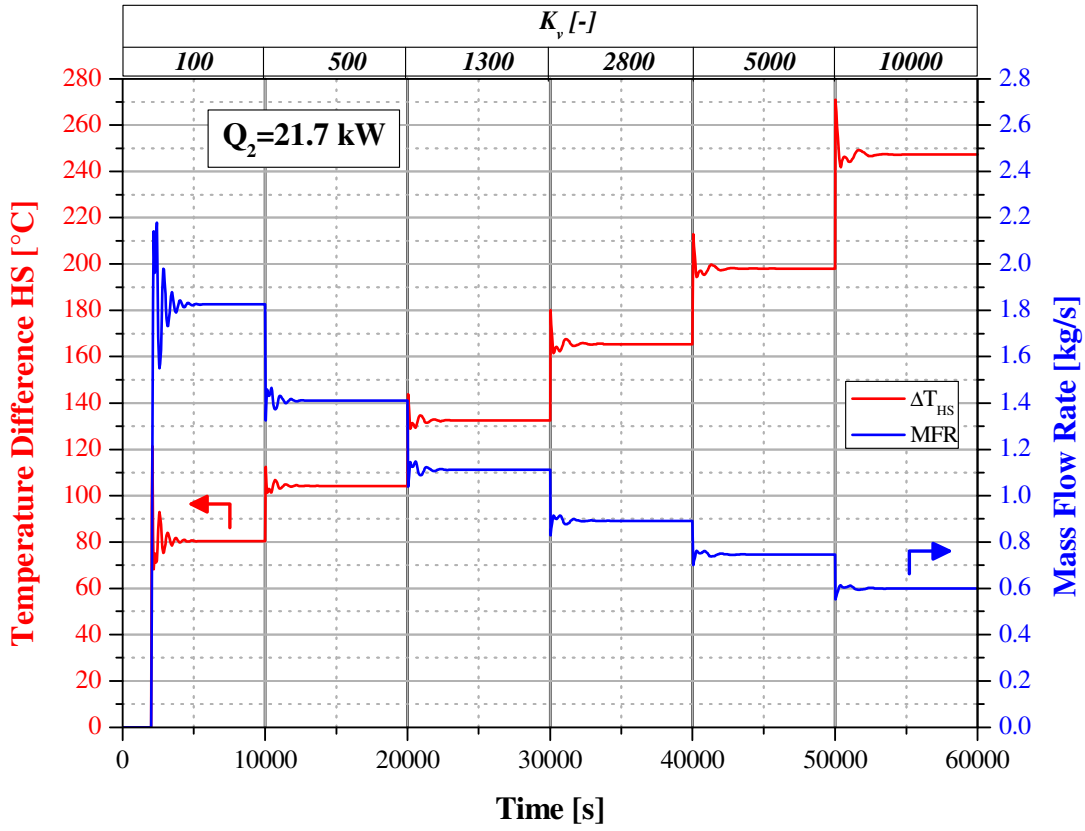

Figure 2.9.b: LBE mass flow rate along NACIE loop and the related ΔT_{HS} (Test VAL-2).

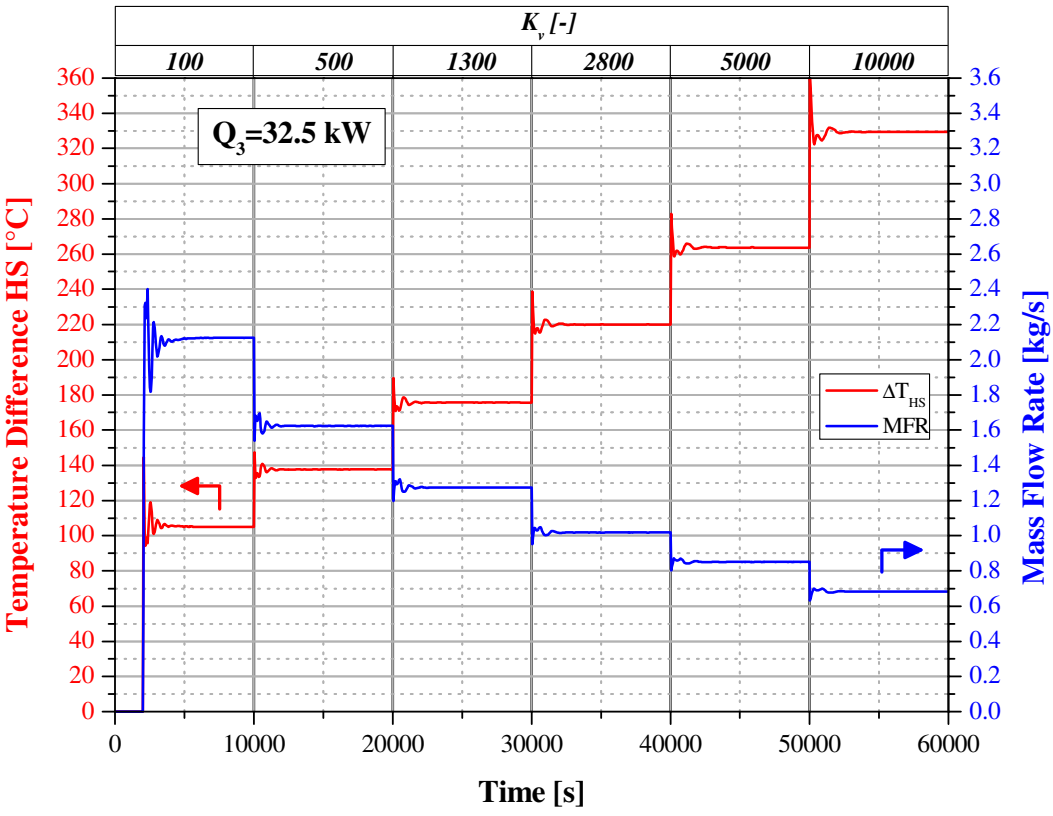

Figure 2.9.c: LBE mass flow rate along NACIE loop and the related ΔT_{HS}, (Test VAL-3).

LBE temperature for *HS* inlet/outlet and pin surface temperatures for the TCs position (see Figures 1.4) are depicted in Figure 2.10(a, b, c). Table 2.6 summarizes the obtained results.

Table 2.6: Temperature of LBE *HS* inlet/outlet and of clad surface at TCs locations [°C].

Temp. [°C]	Valve resistance coefficient K_v [-]						Test name
	100	500	1300	2800	5000	10000	
HS in	222	217	213	208	204	201	
HS out	273	283	296	311	327	355	
TC_d	230	227	224	222	220	220	VAL-1
TC_m	252	255	260	266	273	286	
TC_u	274	284	296	311	327	354	
HS in	273	266	259	251	244	234	
HS out	353	370	391	416	442	481	
TC_d	286	282	277	273	269	265	VAL-2
TC_m	320	327	334	344	355	371	
TC_u	356	372	392	417	442	480	
HS in	330	320	308	297	288	273	
HS out	435	457	483	517	551	602	
TC_d	348	341	333	327	322	314	VAL-3
TC_m	393	400	409	422	435	455	
TC_u	439	460	486	518	551	601	

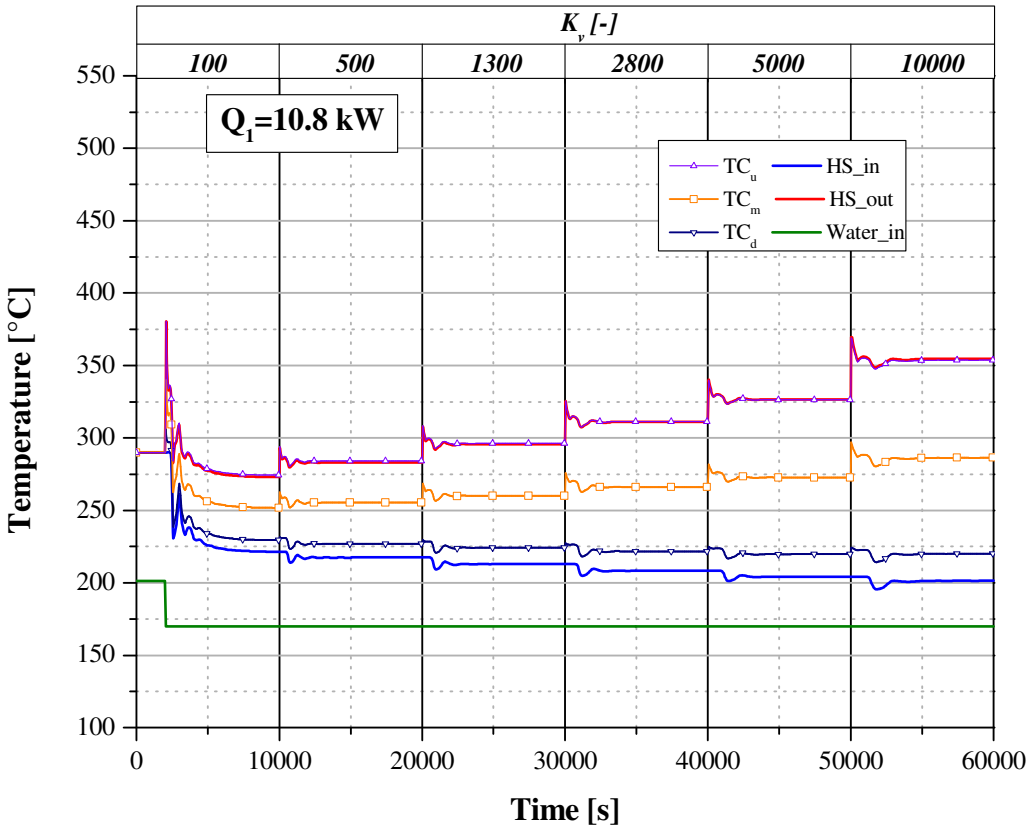

Figure 2.10.a: Inlet and outlet LBE temperatures along *HS*, clad temperature at TCs locations (Test VAL-1).

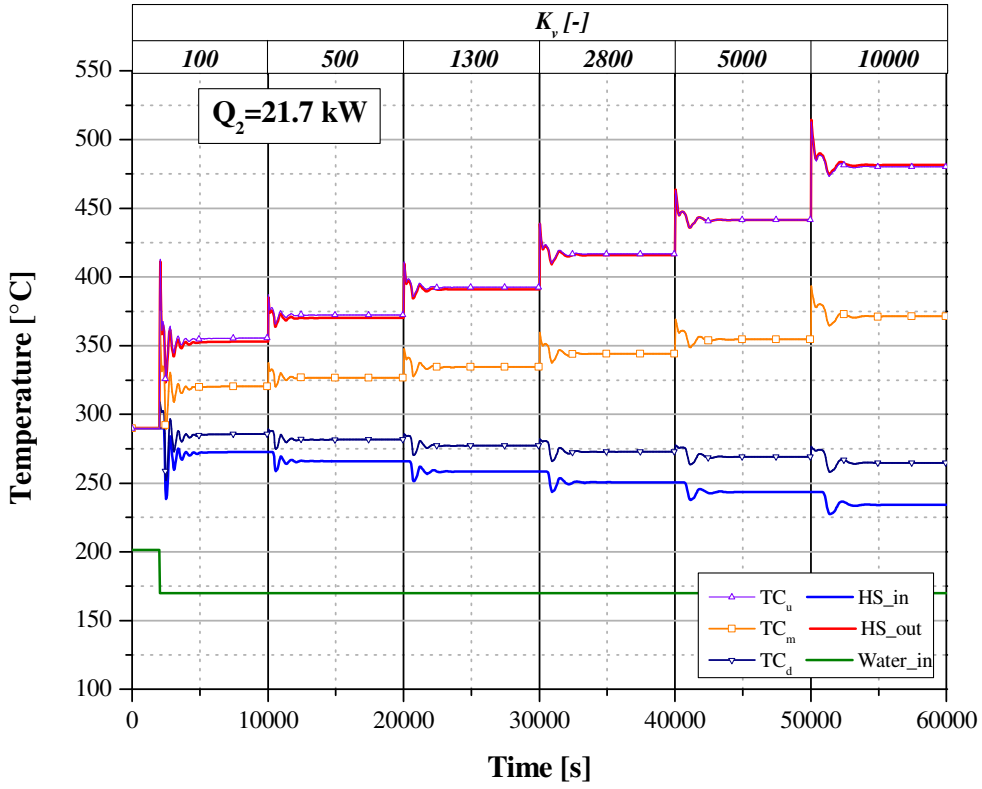

Figure 2.10.b: Inlet and outlet LBE temperatures along *HS*, clad temperature at TCs locations (Test VAL-2).

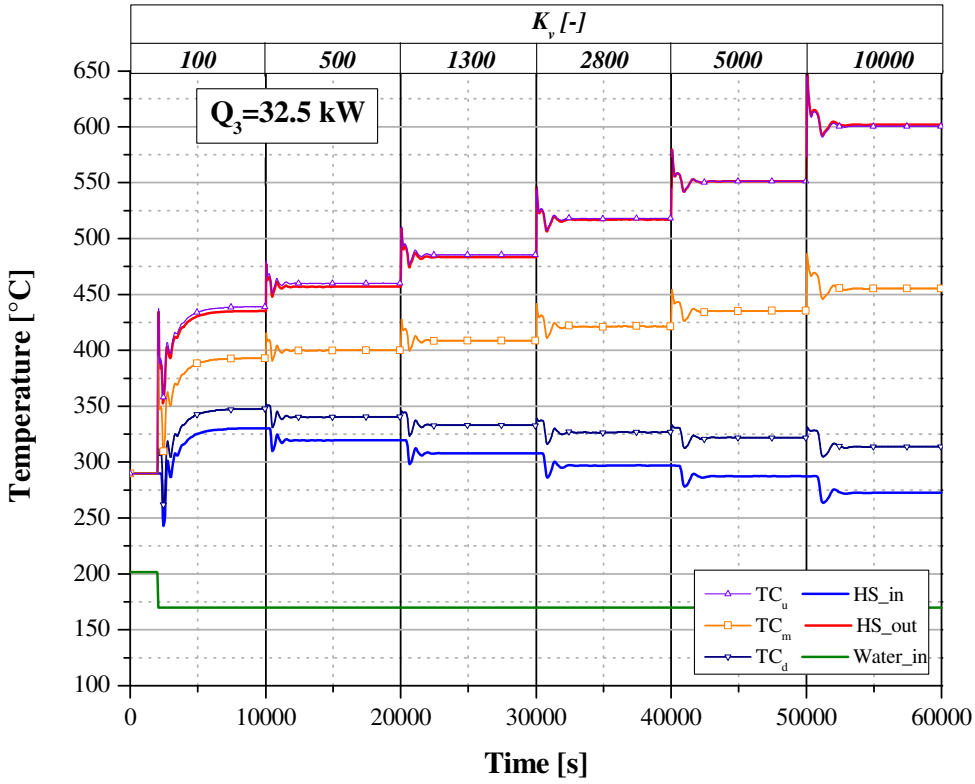

Figure 2.10.c: Inlet and outlet LBE temperatures along *HS*, clad temperature at TCs locations (Test VAL-3).

Results show (case T_w=170°C) that for Test VAL-3 and K_v greater than 1300 the predicted clad temperature at the upper thermocouple location is above 500°C reaching the value of about 600°C for K_v=10000. For the same TCs location, test VAL-1 and VAL-2, give temperatures below 480°C at the maximum K_v. LBE velocity magnitude relative to Heat Source and to *HX-2* (tube side) are summarized in Table 2.7 together with the value of the Reynolds number of the LBE flowing through the Heat Source bundle. Reynolds number has been evaluated at *HS* mid plane. Figures 2.11(a,b,c) show the trends of the above mentioned quantities for tests VAL-1, VAL2 and VAL-3.

Table 2.7: LBE Velocity magnitude [m/s] in Heat Source and *HX-2*; *HS* Reynolds number.

Quantity	Valve resistance coefficient K_v [-]						Test name
	100	500	1300	2800	5000	10000	
Vel. *HS* [m/s]	0.20	0.16	0.13	0.10	0.09	0.07	
Vel. *HX* [m/s]	0.0062	0.0049	0.0039	0.0031	0.0026	0.0021	VAL-1
Rey *HS* [-]	4194	3322	2671	2184	1861	1540	
Vel. *HS* [m/s]	0.27	0.21	0.16	0.13	0.11	0.09	
Vel. *HX* [m/s]	0.008	0.006	0.005	0.004	0.003	0.003	VAL-2
Rey *HS* [-]	6462	5047	4032	3289	2805	2317	
Vel. *HS* [m/s]	0.32	0.24	0.19	0.15	0.13	0.10	
Vel. *HX* [m/s]	0.010	0.007	0.006	0.005	0.004	0.003	VAL-3
Rey *HS* [-]	8622	6655	5283	4301	3666	3020	

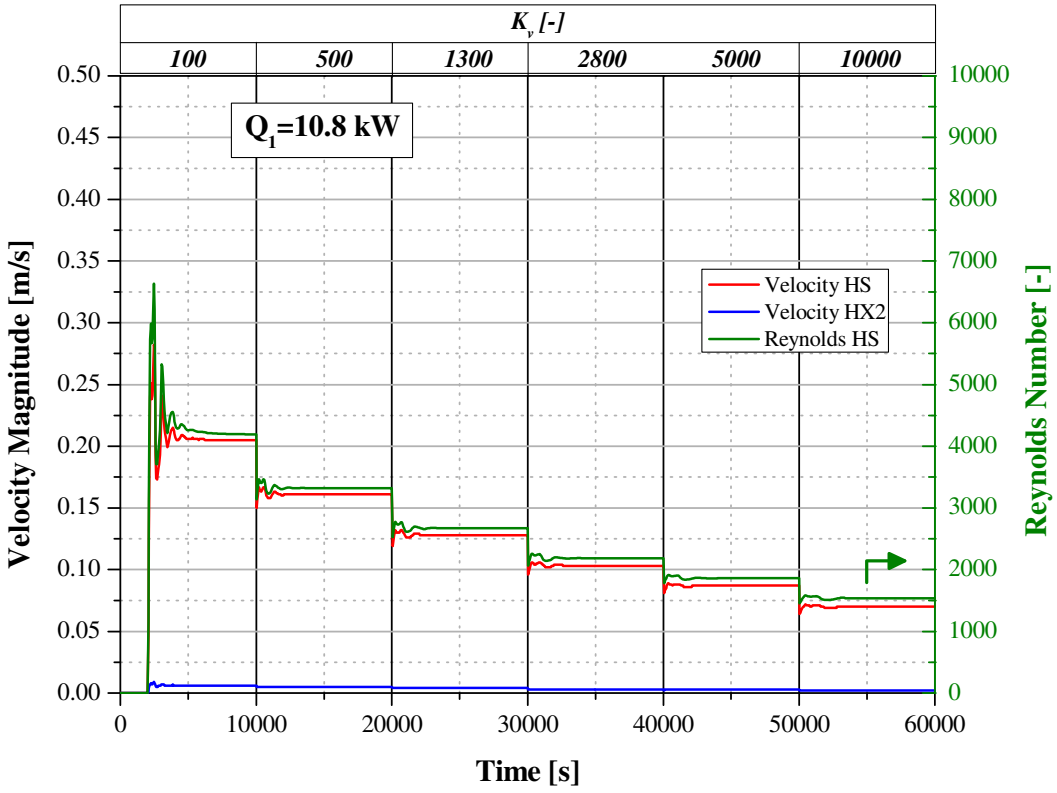

Figure 2.11.a: LBE Velocity along *HS* bundle, inside *HX-2* tubes and *HS* Reynolds number for the considered K_v (Test VAL-1).

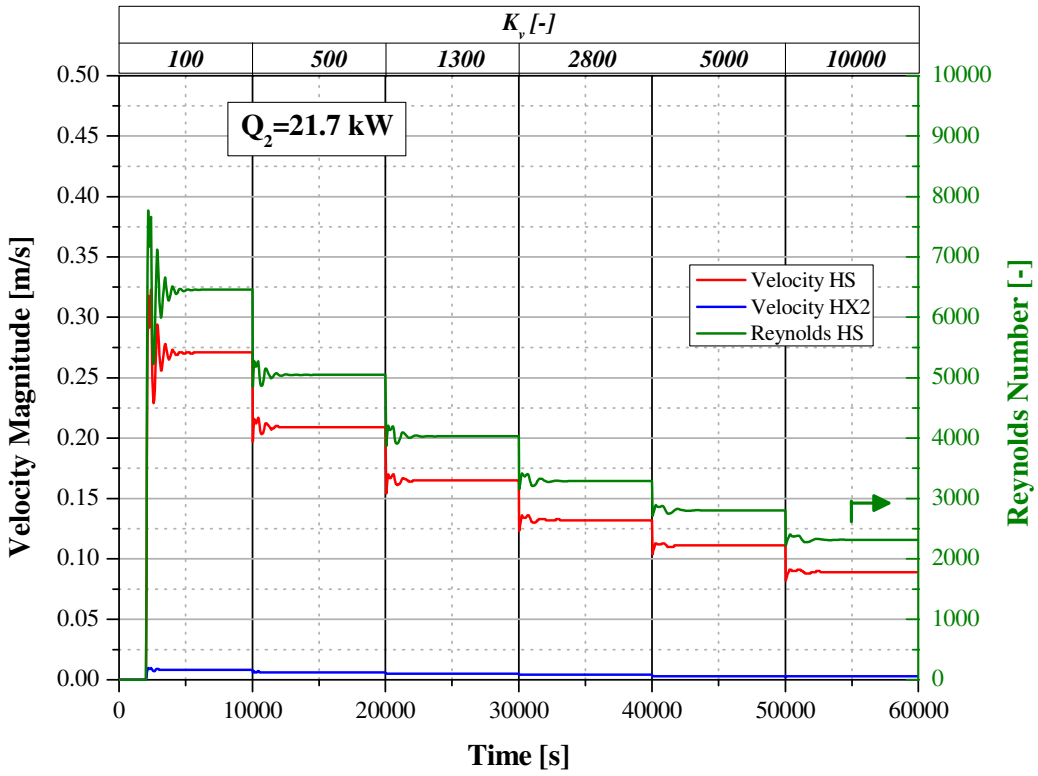

Figure 2.11.b: LBE Velocity along *HS* bundle, inside *HX-2* tubes and *HS* Reynolds number for the considered K_v (Test VAL-2).

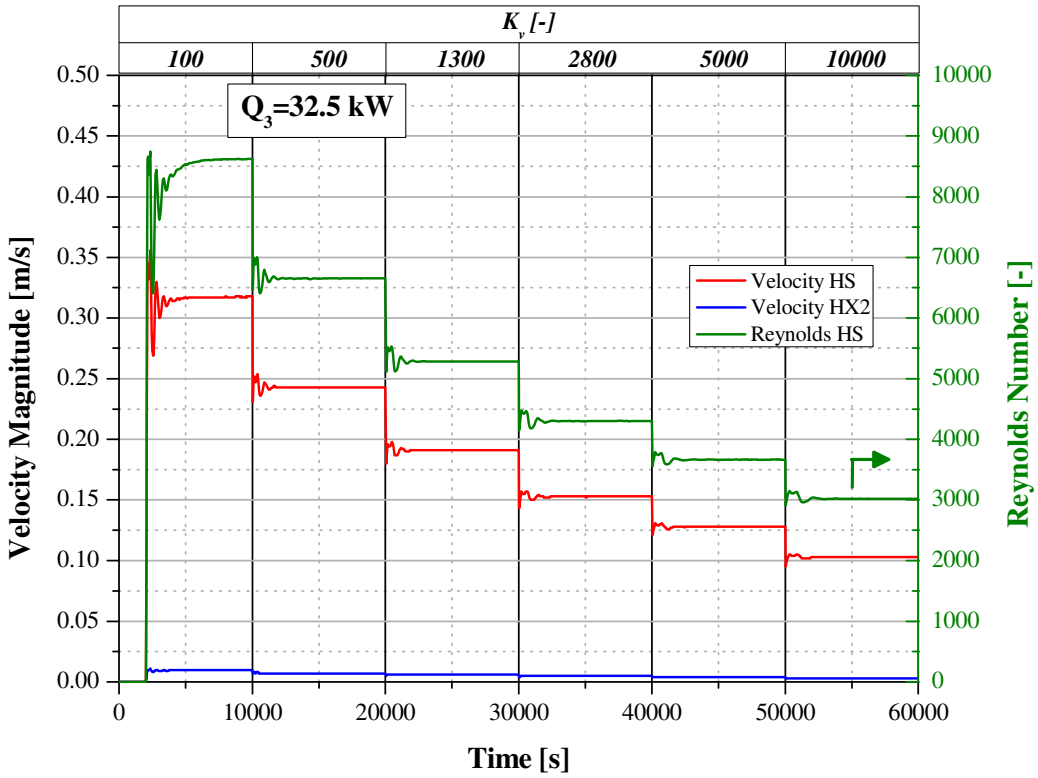

Figure 2.11.c: LBE Velocity along *HS* bundle, inside *HX-2* tubes and *HS* Reynolds number for the considered K_v (Test VAL-3).

The values of the bundle resistance coefficient, K_b, obtained by RELAP5, and the bundle pressure losses, ΔP_b, estimated by Eq. 2.5 are reported in Table 2.8.

Table 2.8: Resistance coefficient K_b and pressure drop ΔP_b [Pa] along the bundle.

Quantity	Valve resistance coefficient K_v [-]						Test name
	100	500	1300	2800	5000	10000	
K_b [-]	277	310	348	391	433	493	VAL-1
ΔP_b [Pa]	2848	1992	1436	1067	847	636	
K_b [-]	234	259	288	320	350	395	VAL-2
ΔP_b [Pa]	4121	2749	1918	1389	1081	803	
K_b [-]	212	234	257	283	308	345	VAL-3
ΔP_b [Pa]	5069	3290	2254	1608	1237	909	

Figures 2.12(a,b,c) report the trends of K_b and ΔP_b, for the considered valve resistance coefficient for test VAL-1, VAL-2 and VAL-3 (T_w=170°C).

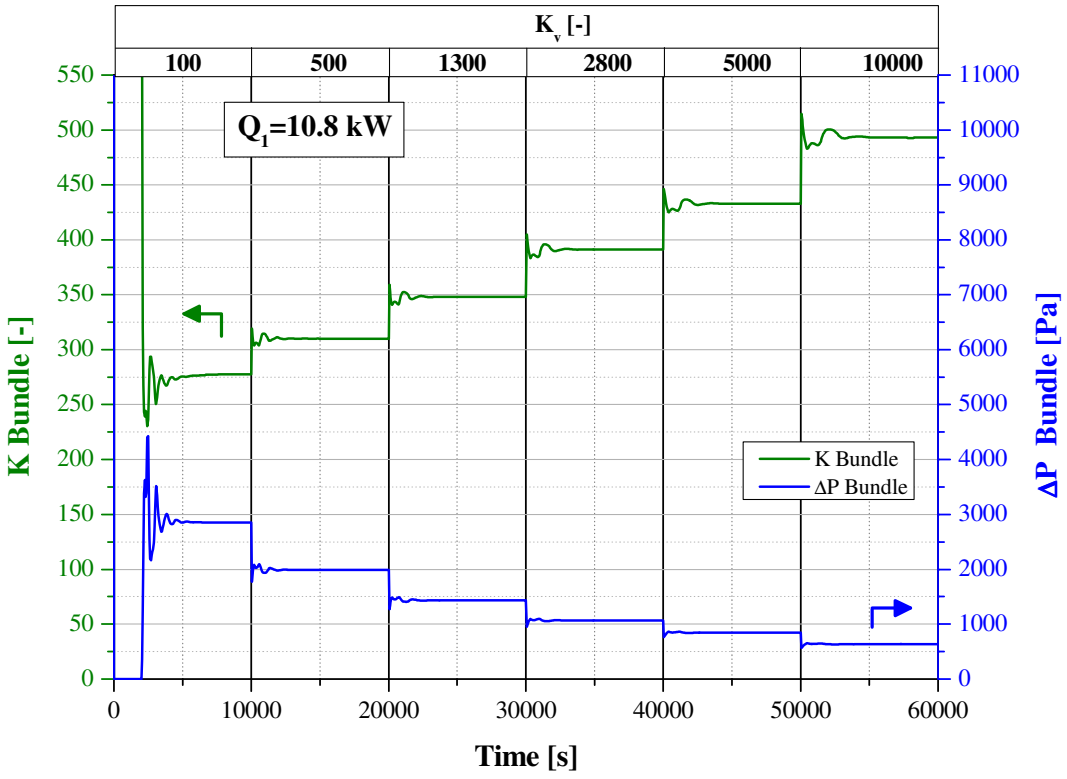

Figure 2.12.a. Bundle resistance coefficient and pressure drop (Test VAL-1).

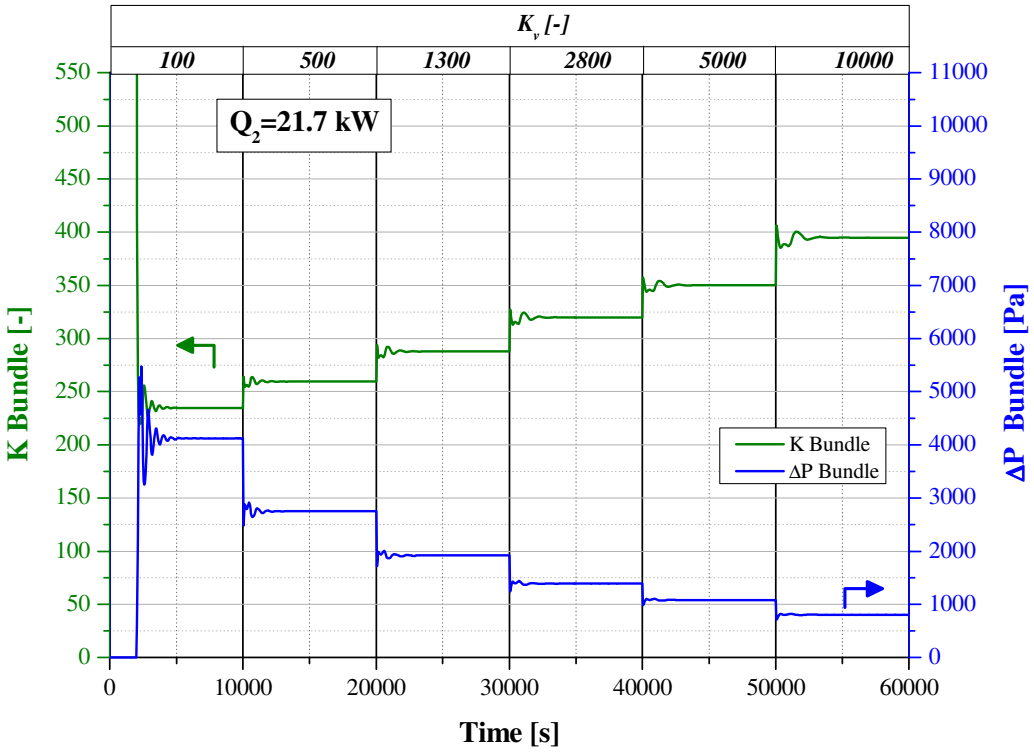

Figure 2.12.b: Bundle resistance coefficient and pressure drop (Test VAL-2).

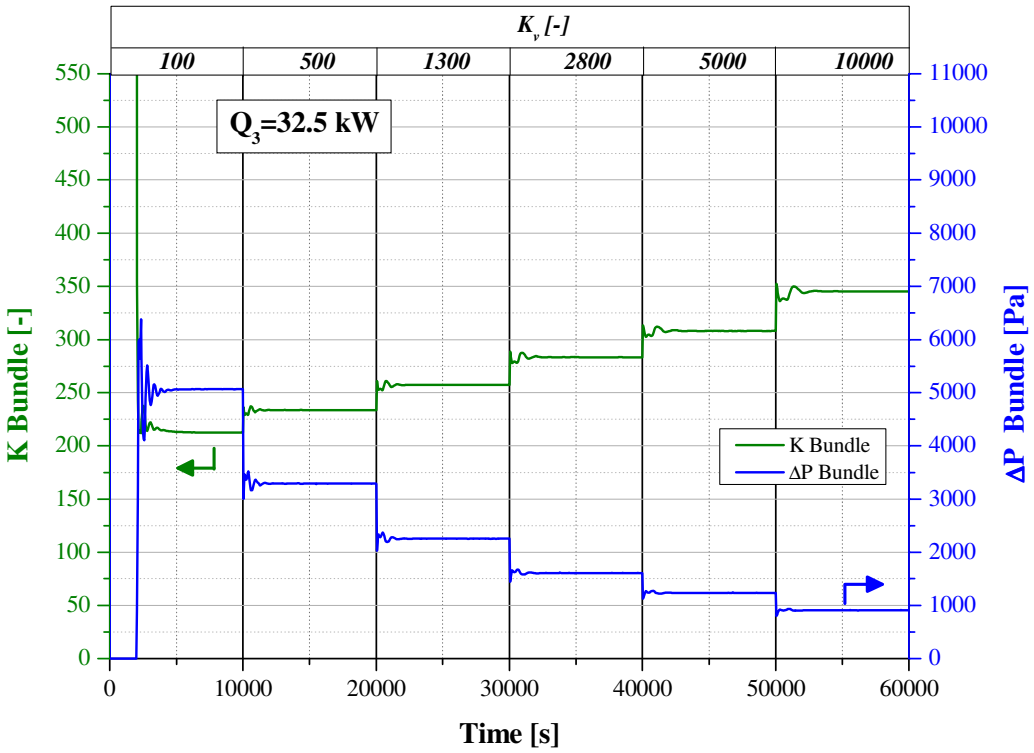

Figure 2.12.c: Bundle resistance coefficient and pressure drop (Test VAL-3).

3. Analysis performed by RELAP5-Fluent coupled codes

In this section the activity performed at the University of Pisa concerning the coupling between the RELAP5/Mod3.3 system code [3], modified to take into account the properties and heat transfer correlations to be used for the liquid lead and LBE [8-9], and the CFD Fluent code [10] is presented.
The set-up numerical model is based on a two-way semi-implicit coupling scheme and it has been preliminarily applied to NACIE facility in its new configuration (see section 1). In particular, the vertical part of the loop including the heater system and part of the piping before and after it has been simulated by the Fluent code in a simplified 2D axial-symmetric configuration, while the remaining part of the loop has been simulated by the RELAP5 code.
In the next part of the report the approach used to couple these two codes and the preliminary obtained results will be presented.

3.1 RELAP5 and Fluent models

To simplify the coupling with the CFD code, the RELAP5 nodalization of the whole NACIE primary circuit was firstly re-arranged in such a way to have the possibility of comparing the results obtained with RELAP5 stand-alone calculations with those of RELAP5-Fluent coupled simulations. First of all, the motor valve was substituted by a single junction and the non active *HX-1* has been removed from the nodalization. Then, the part of the loop of a length of 1.3 m, simulated by the Fluent code as a simple pipe, was firstly changed in RELAP5 in an equivalent way to the thermal power imposed on the external wall of the heater system, instead of the internal electrical pins. The "simplified" RELAP5 nodalization of the whole loop is reported in Figure 3.1. As can be seen in the figure, the length of the pipe section simulated by the Fluent code is 1.3 m and includes the *HS*, a short pipe of 0.05 m before it and pipes totalling 0.65 m after it. The tubing length of 0.65 m after the *HS* was considered sufficient in the CFD domain to reduce the possibility of occurrence of backflow conditions in the outlet section for the coupled code simulations.
In the following part of the report we will call "Heat Section (*HS*)" all the pipe section simulated by the Fluent code, taking into account that only a part of 0.6 m in height is the real heated portion.
In Figure 3.2 the RELAP5 nodalization used for the coupled simulations is reported. In the time dependent junction 115 and in time dependent volume 112, respectively, the boundary conditions of mass flow rate and temperature obtained from an inner reference section of the Fluent domain are applied, while the pressure imposed in the time dependent volume 110 is that obtained from the inlet section of the CFD domain (see Figure 3.3). To reduce the occurrence of the previously mentioned backflow conditions in the outlet section of the CFD domain, a very big value of the reverse form loss coefficient was set for the junction 215 and for the junction that connect the branch 125 with the pipe 130.
The axial symmetric CFD domain was discretized by a structured mesh composed by 7200 rectangular cells, uniformly distributed both in the axial and radial coordinates (see Figure 3.3). The boundary conditions of mass flux and temperature imposed in the inlet section of Fluent (mass-flow-inlet) are those obtained, respectively, from the time dependent junction 105 and the last cell of the vertical pipe 100 (see Figure 3.2). The pressure value imposed at the outlet section of the CFD domain (pressure outlet) is that obtained from the first cell of the vertical pipe 120. A special procedure has been considered when the pressure data are exchanged between RELAP5 and Fluent codes, because the first code work with absolute pressure while the CFD code, to reduce the round-off error, prefers to work with a pressure field reduced by the gravitational pressure contribute and by the "operative pressure", representing the average absolute pressure in the domain.

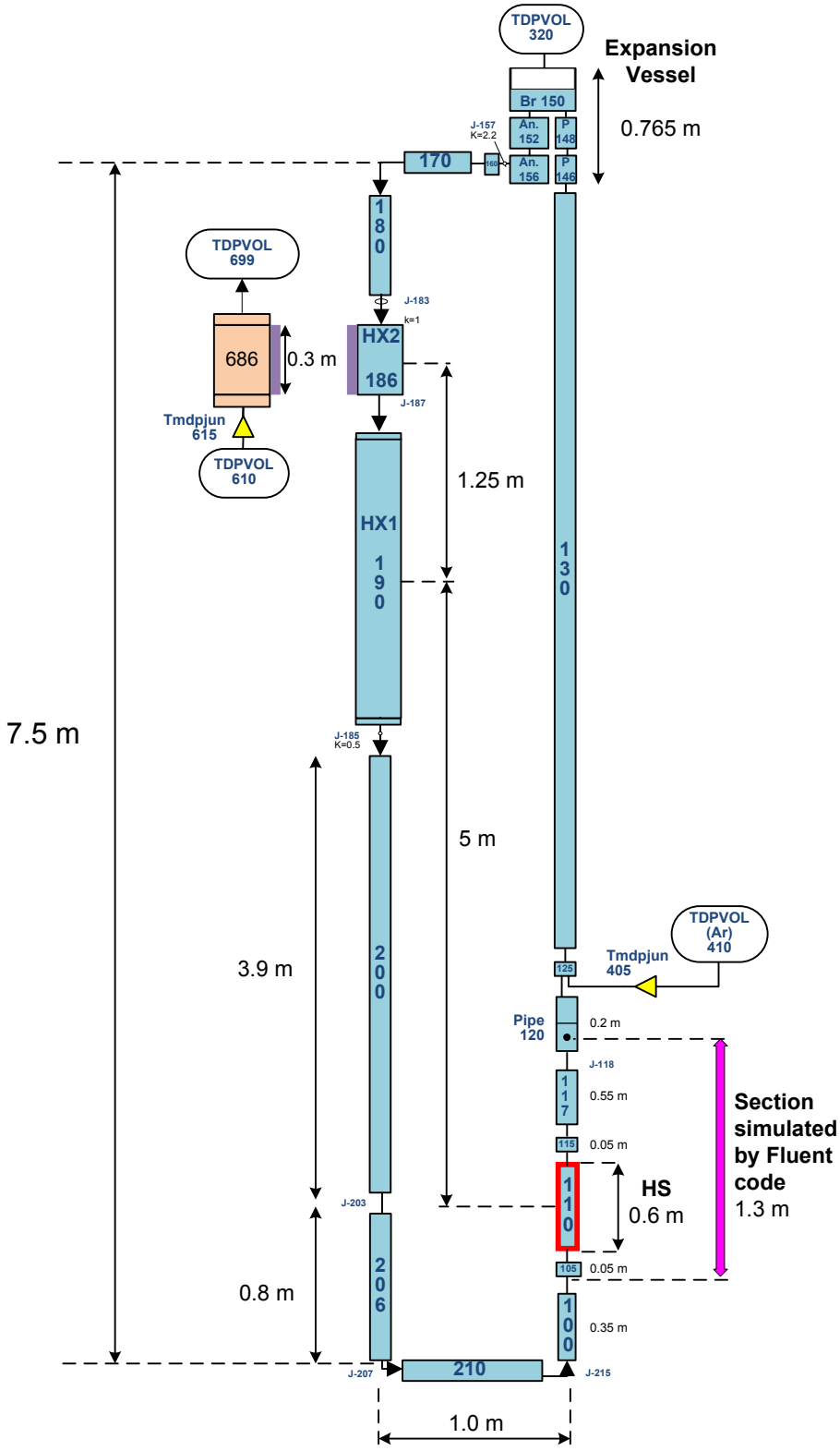

Figure 3.1: Simplified RELAP5 nodalization of the NACIE primary loop used for the stand-alone calculations.

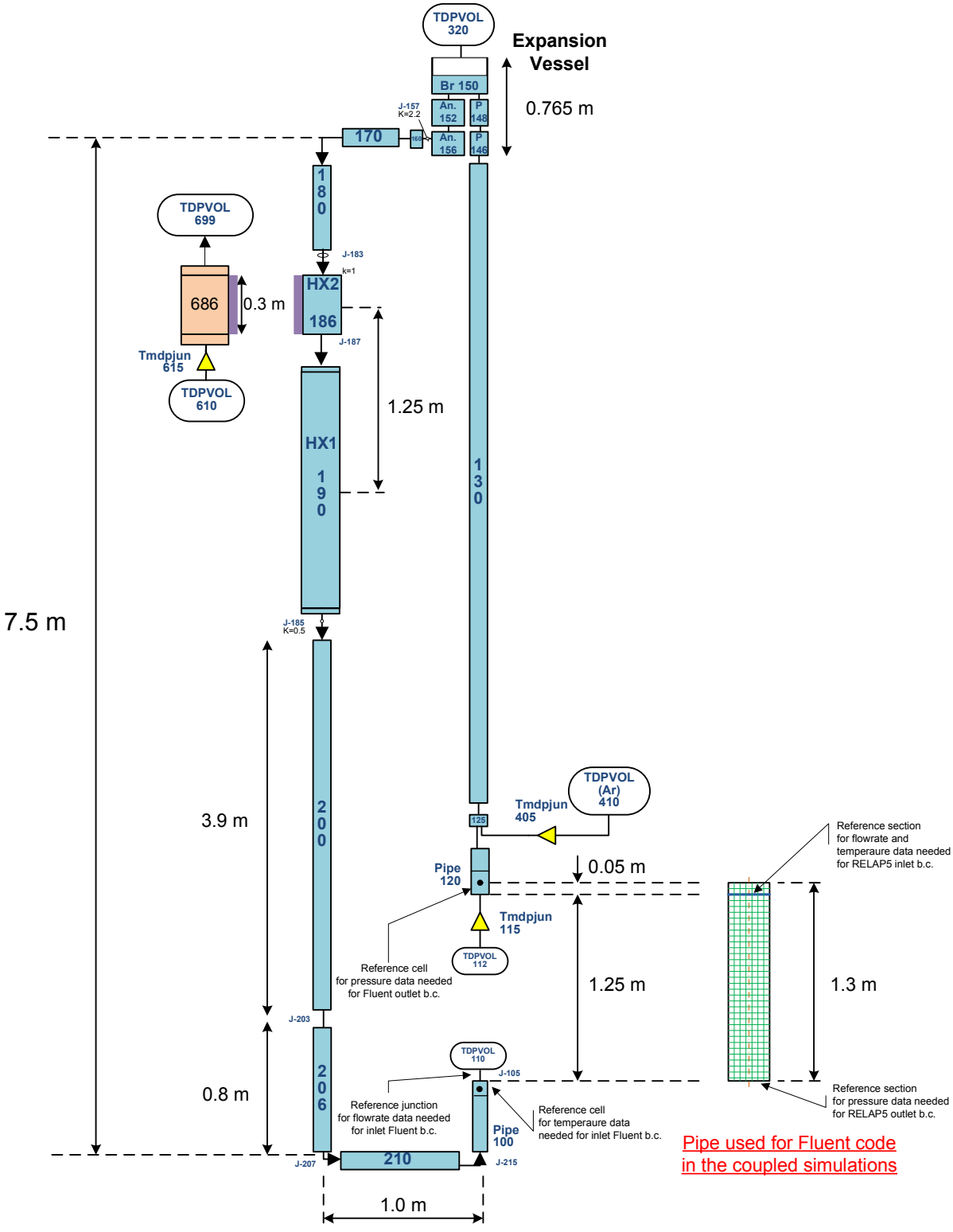

Figure 3.2: RELAP5 nodalization of the NACIE facility used for coupled simulations.

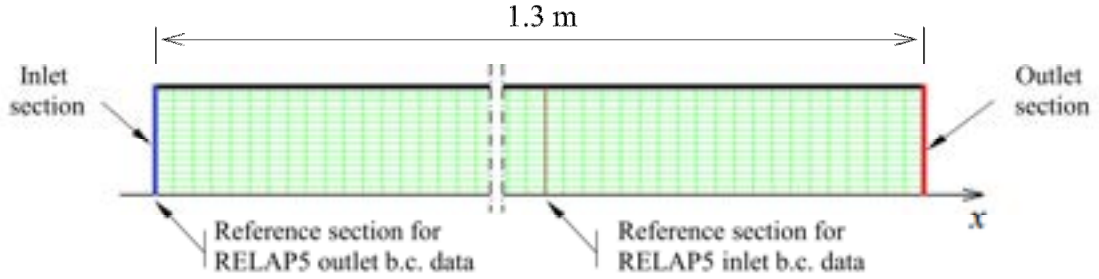

Figure 3.3: Axial-symmetric domain used in Fluent code for coupled simulations.

In the NACIE pipe section simulated by the Fluent code there are pressure drops, due to the presence of the electrical rods and of the helicoidal wire spacers, that can't be considered by the code itself without special measures. To simplify the coupling, on the base of the analysis performed in section 2, the form loss coefficient associated with the total pressure drop inside the real pipe section 1.3 m length has been considered constant and equal to 7. For this purpose seven different interior faces have been set as porous-jumps in the 2D domain and in each of it an equivalent constant coefficient of concentrate pressure drop equal to 1 was set. The same value of the form loss coefficient has been inserted in the *HS* of the RELAP5 nodalization used for stand-alone calculations.
In these first coupled simulations, uniform temperature and mass flux have been imposed at the inlet section of the 2D domain. In addition, for the same inlet section, a fixed turbulence intensity of 7% and a hydraulic diameter of 0.029 m are imposed as boundary conditions for the turbulence equations. The turbulence model adopted in the CFD calculations is the RNG k-ε, while the thermo-dynamic properties of the LBE are considered as a function of the temperature in agreement with Ref. [4].

3.2 Coupling procedure

The coupling procedure of RELAP5 and Fluent codes is based on the scheme shown in Figure 3.4. The execution of the RELAP5 code is operated by an appropriate MATLAB program, where a processing algorithm is also implemented allowing to receive boundary conditions (b.c.) data from Fluent, at the beginning of the RELAP5 time step, and to send b.c. data to Fluent code, at the end of the RELAP5 time step. In addition, a special User Defined Function (UDF) was realized for Fluent code to receive b.c. data from RELAP5 and to send b.c. data to RELAP5 for each CFD time step.
An initial RELAP5 transient of 1000 s will be executed to reach steady state conditions with a uniform temperature at 290°C and with fluid at rest. The end of this initial transient was considered time zero from which the coupled simulation started. After that, a sequential explicit coupling calculation is activated, where the Fluent code (master code) will be advanced firstly by one time step and then the RELAP5 code (slave code) will be advanced for the same time step period, using data received from the master code. In particular, for each of the three RELAP5 boundary condition data, a linear interpolation inside the time step period between the initial value (final value of the previous time step) and the final value of the current time step (obtained by the Fluent code calculation) is considered for RELAP5. After both the codes have terminated the current time step, the RELAP5 data needed to Fluent b.c. will be sent to it and the procedure for a new time step advancement will be repeated.

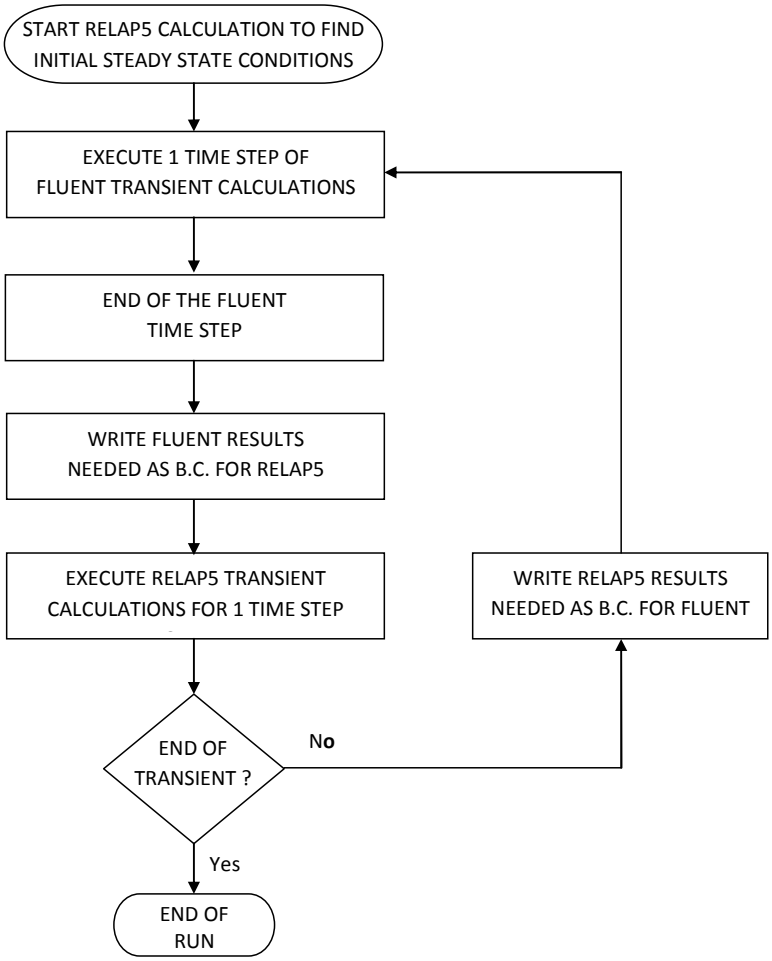

Figure 3.4: RELAP5-Fluent coupling procedure.

3.3 Matrix of simulations

The basic simulations considered in the present work are two in natural circulation conditions with a heating power of 10 and 20 kW and three in assisted circulation conditions with an injected gas flow rate of 5, 10 and 20 Nl/min. For the natural circulation test the heating power is increased linearly in the first 30 s of the transient and then is maintained constant in the remaining transient. For the assisted circulation test, instead, the mass flow rate of the argon injected in the riser is increased linearly in the first 30 s of the transient and then is maintained constant in the remaining transient.
A first sensitivity analysis has shown that for the assisted circulation tests a time step of one order of magnitude less than that for natural circulation tests was required. In particular, for the natural circulation tests a value of 0.1 s has been found sufficiently low to give results independent from the time step value itself, while a value of 0.01 s was found acceptable for the assisted circulation tests. Anyway, to verify the time step independence, three additional tests have been added in the matrix of simulations with higher and lower time step values compared to those used in the reference calculations.
A further simulation regarding the ULOF (Unprotected Loss Of Flow) accident with the breakdown of the gas injection into the riser during a condition with *HS* and *HX* activated was also performed.
The test matrix of the coupled simulations performed in this work is shown in Table 3.1, which summarises adopted boundary conditions and main variables that were monitored.

Table 3.1: Matrix of performed simulations.

Test name	Thermal power [kW]	Argon flow rate [Nl/min]	Time step [s]	Description	Monitoring variables
A	10	-	0.1	Natural circulation tests	• LBE flow rate • T_{in} and T_{out} in the *HS* • T_{in} and T_{out} in the *HX* primary side • P_{in} and P_{out} in the *HS* and pressure difference
B	20	-	0.1		
C	20	-	0.2		Check of the time step independence for the obtained results
D	-	5	0.01	Assisted circulation tests (gas injection)	• LBE flow rate • P_{in} and P_{out} in the *HS* and pressure difference
E	-	10	0.01		
F	-	20	0.01		
G	-	20	0.02		Check of the time step independence for the obtained results
H	-	20	0.005		
I	20	20	0.02	Unprotected loss of flow accident test	• LBE flow rate • T_{in} and T_{out} in the HS • T_{in} and T_{out} in the HX primary side

3.4 Obtained results

3.4.1 Natural circulation tests

The LBE mass flow rate time trends obtained from the two natural circulation tests simulated by the coupled codes are reported in Figure 3.5, where the results are compared with those obtained by corresponding simulations performed with the stand-alone RELAP5 code. The time interval of 4000 s, considered as the temporal window for the analysis of the natural circulation tests, is sufficient to reach steady state conditions for the LBE mass flow rate, obtaining an asymptotic value of about 1.5 kg/s for the test A (thermal power of 10 kW) and 1.9 kg/s for the test B (thermal power of 20 kW).

As can be seen, results obtained from the coupled codes are in very good agreement with the corresponding RELAP5 stand-alone calculations, even if an underestimation of about 2-3% can be observed. This underestimation is due to the greater distributed pressure losses predicted by the Fluent code, in respect to the RELAP5 stand-alone calculation, due to the simplifying assumption of uniform velocity at the inlet section of the 2D domain. This uniform inlet velocity produces a developing boundary layer that is responsible for the so called entrance effects which lead to a greater exchange in the momentum, heat transfer, etc.. A confirmation of this previous consideration can be obtained by observing the time trends of the pressure difference through the *HS*, reported in Figure 3.6. In fact, the pressure drop calculated by the coupled codes results greater than those obtained from the RELAP5 stand-alone simulations.

The temporal window of 4000 s is instead not sufficient for the test A to obtain steady state conditions for what concerns the temperature distribution along the loop. In fact, observing Figures 3.6 and 3.7 it can be seen that after about 3000 s, even if temperature oscillations are completely dumped, temperature trends show a constant temporal decrease.

For both *HS* and *HX* systems temperature time trends obtained by the coupled RELAP5-Fluent codes are in very good agreement with the data calculated by the RELAP5 stand-alone code (see Figures 3.6 and 3.7). For the test at higher thermal power (test B) the considered time interval is sufficient to obtain steady state conditions also for temperature distributions (see Figures 3.9 and 3.10).
The first temperature peak of 370°C for test A (see Figure 3.7) and of 414°C for test B (see Figure 3.9) is due to the mechanical inertia of the liquid metal combined with the heat flux imposed in the *HS*. The fluid requires a sufficient driving force due to the buoyancy effect to start moving and this creates in the first instant of the transient a heating of LBE that remains at rest inside the *HS* section.
In Figure 3.11 temperature distribution inside the 2D domain (Fluent domain for the *HS* section) is reported for test B and at 40 s from the beginning of the transient. This instant corresponds to where the maximum average temperature is reached at the outlet section of the *HS* domain (see Figure 3.9). The maximum temperature reached near the heated wall is in the order of 470°C. In Figure 3.12 the temperature profile in two different cross sections of the channel is reported. As it can be seen, at the end of the heated region of the channel results a temperature distribution with a minimum temperature of about 365°C near the axis and a maximum temperature near the wall of 460°C. The radial temperature profile on the outlet section instead appears approximately constant at 410°C.
For the same time instant, Figure 3.13 reports the radial profile of the axial velocity component for the two different cross sections. In the cross section at the end of the heated region velocity distribution appears with the maximum near the wall and with the minimum value in the center of the channel. This is coherent with the buoyancy effect connected with the temperature profile (see Figure 3.12). The velocity profile at the outlet section of the domain appears as a typically fully developed profile of a turbulent flow inside a cylindrical channel.
The LBE mass flow rate and the *HS* temperatures obtained for a time step equal to 0.1 s (Test B) were compared with those obtained with a time step equal to 0.2 s (Test C) to verify the time step independence of the results obtained with the coupled codes. The comparison is reported in Figure 3.14 for the mass flow rate and in Figure 3.15 for the inlet and outlet *HS* temperature. Perfect agreement between the corresponding time trends can be observed.

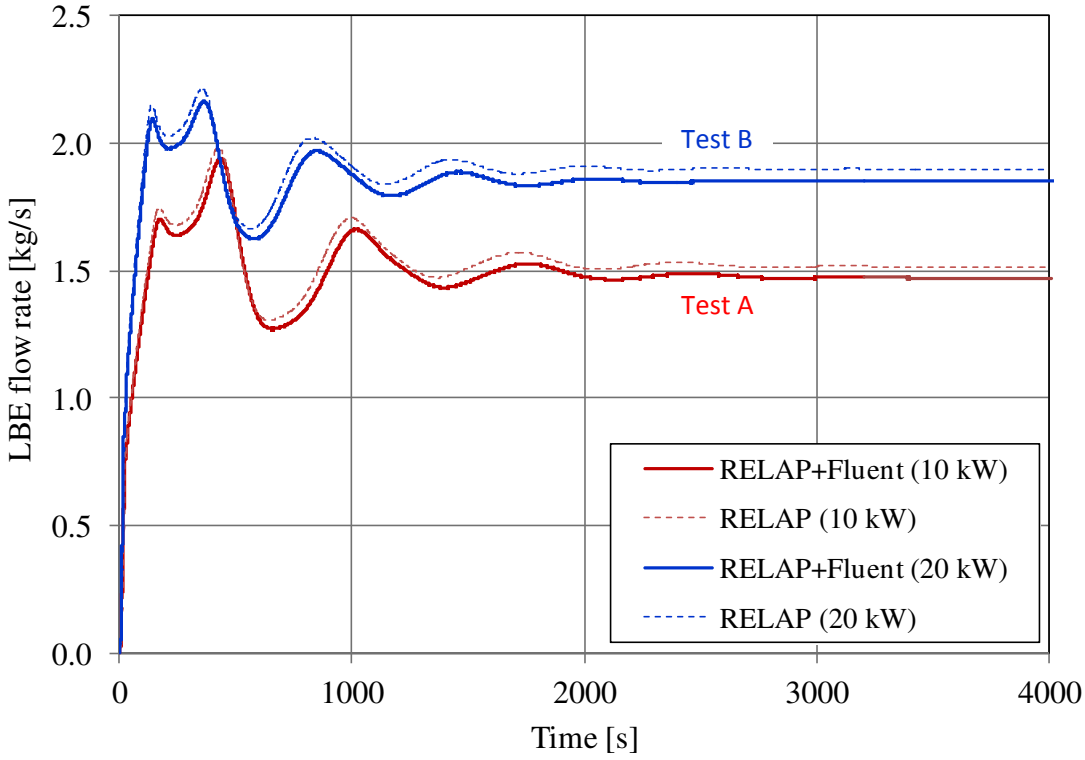

Figure 3.5: LBE mass flow rate time trend.

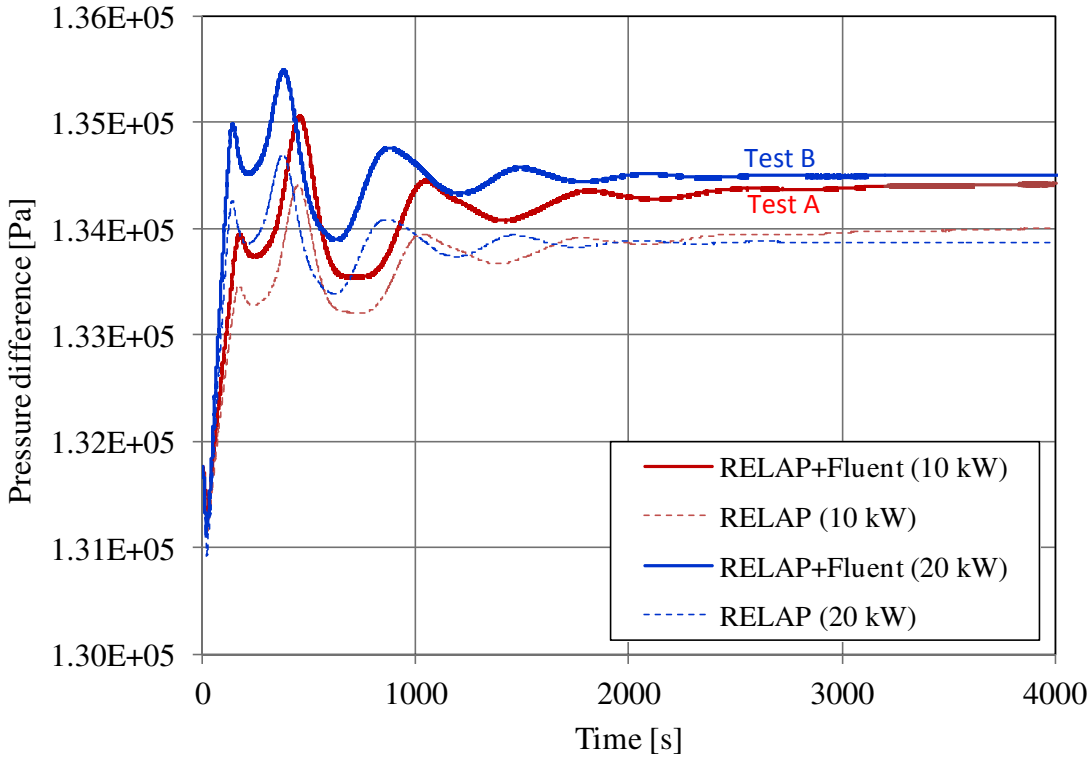

Figure 3.6: Pressure drop through the *HS*.

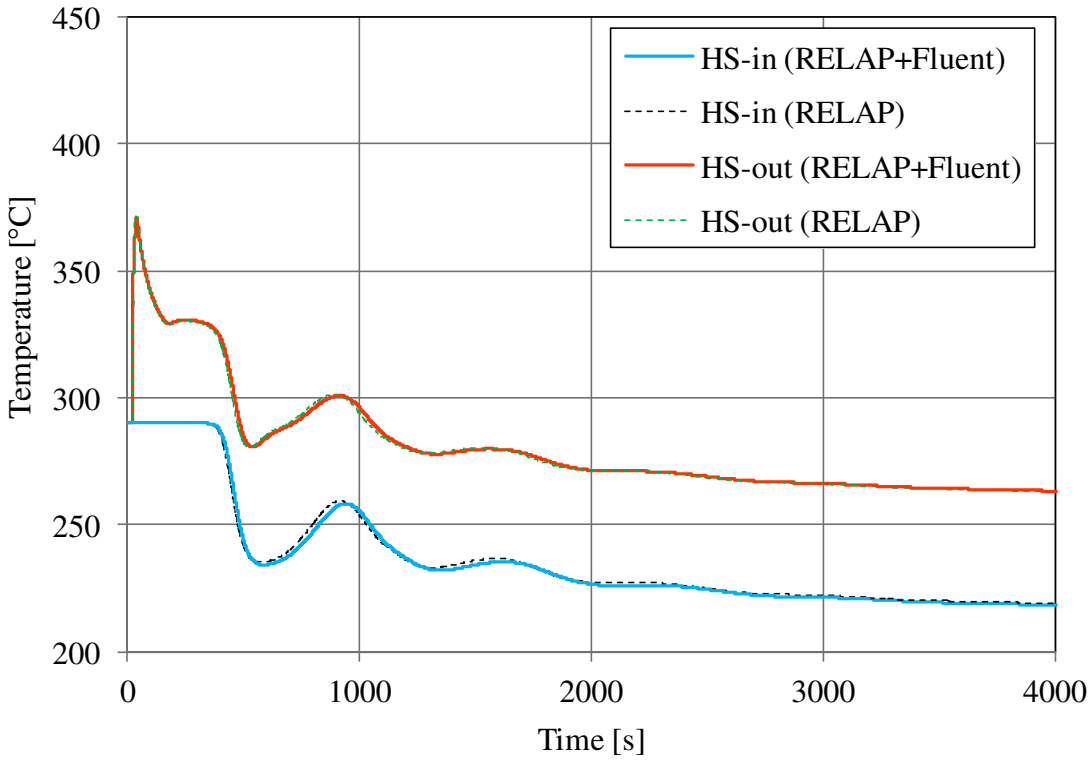

Figure 3.7: Inlet and outlet time trend temperature in the *HS* for test A (10 kW).

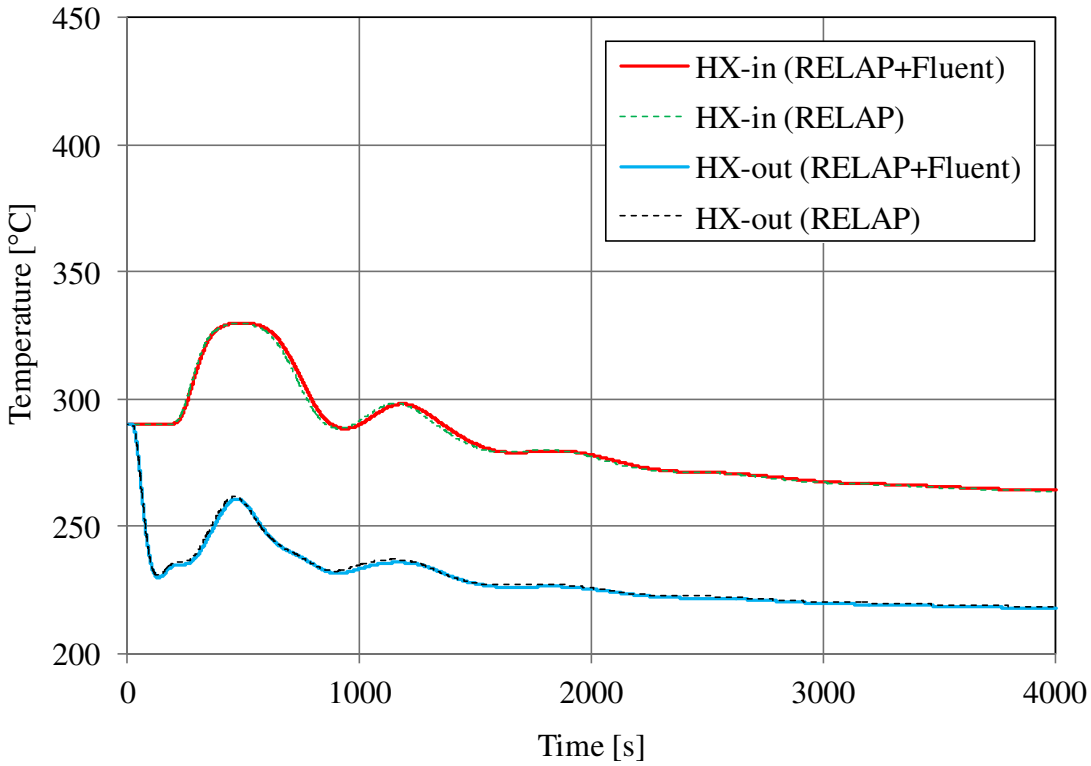

Figure 3.8: Inlet and outlet time trend temperature in the *HX* for test A (10 kW).

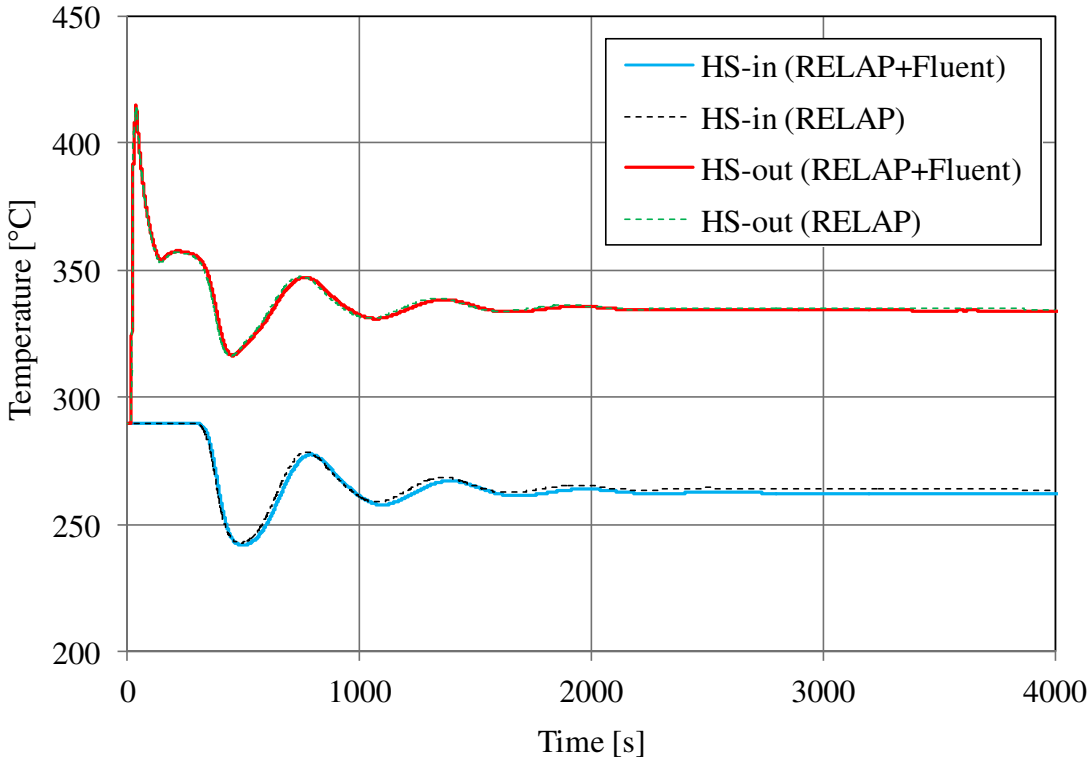

Figure 3.9: Inlet and outlet time trend temperature in the *HS* for test B (20 kW).

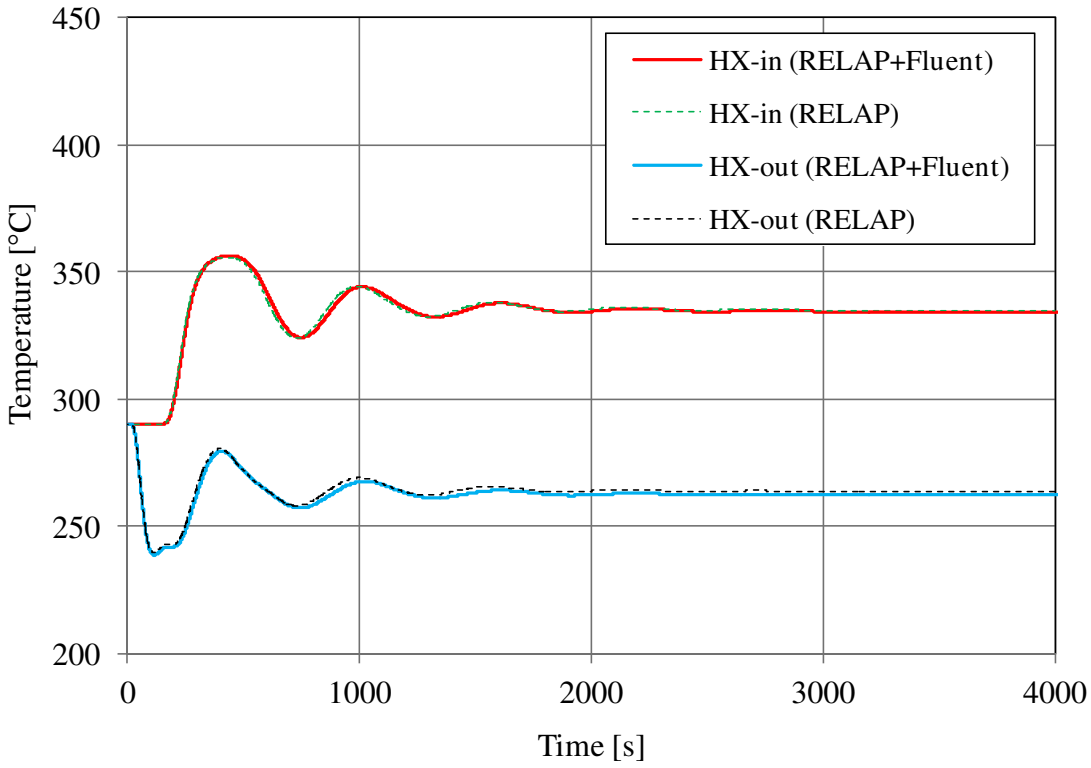

Figure 3.10: Inlet and outlet time trend temperature in the *HX* for test B (20 kW).

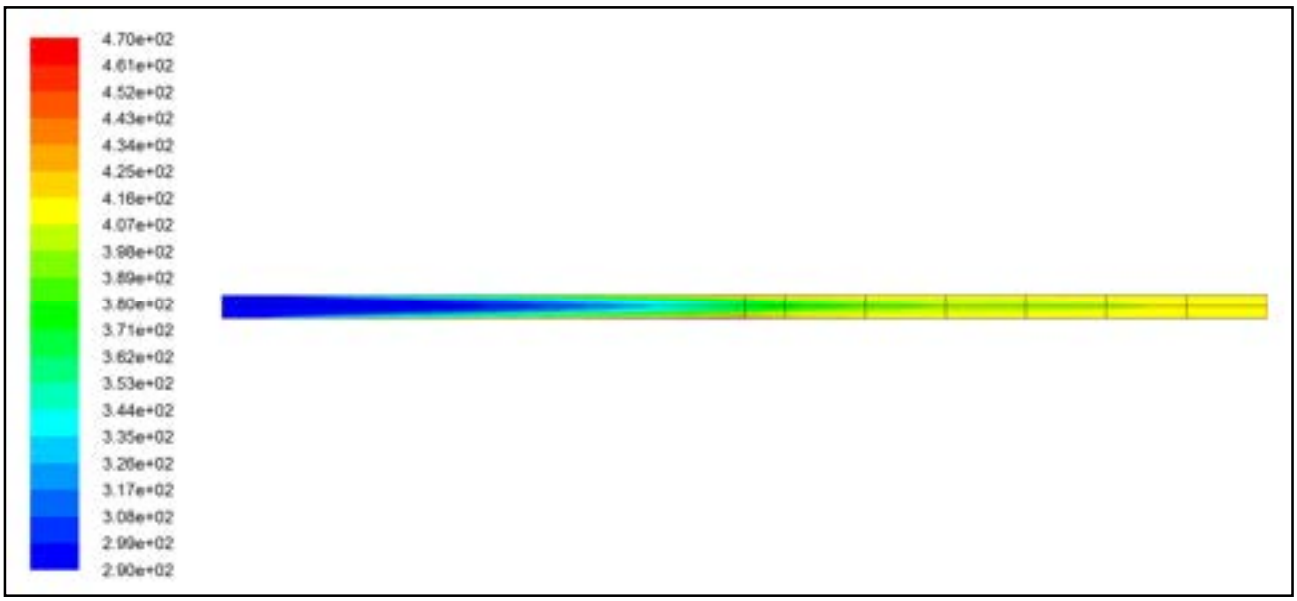

Figure 3.11: Temperature contour plot [°C] at 40 s of transient (Test B).

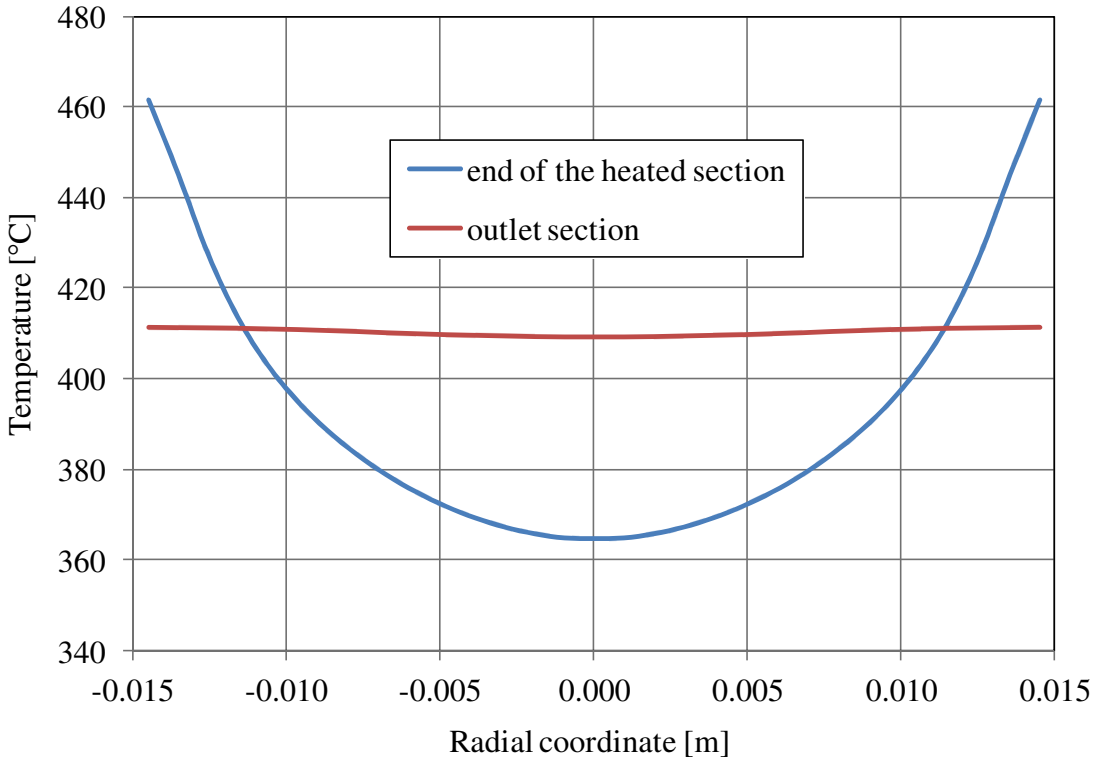

Figure 3.12: Temperature radial profile, at 40 s of transient (Test B).

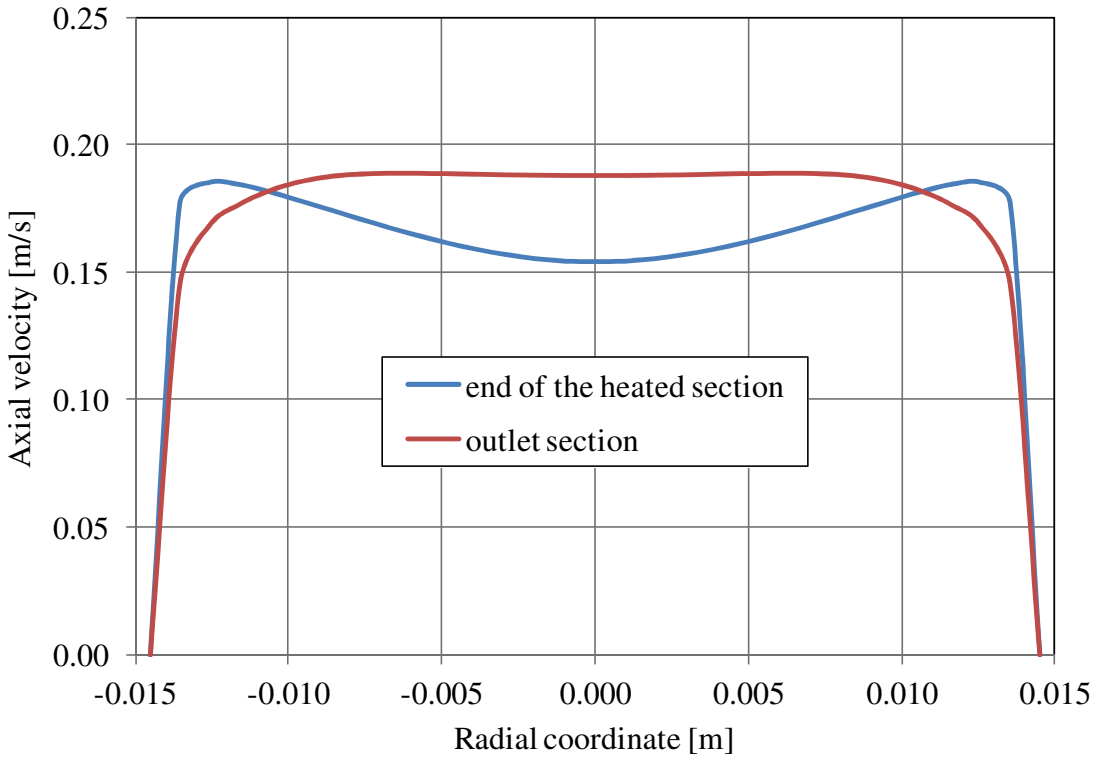

Figure 3.13: Axial-component velocity profile along the radial direction, at 40 s of transient (Test B).

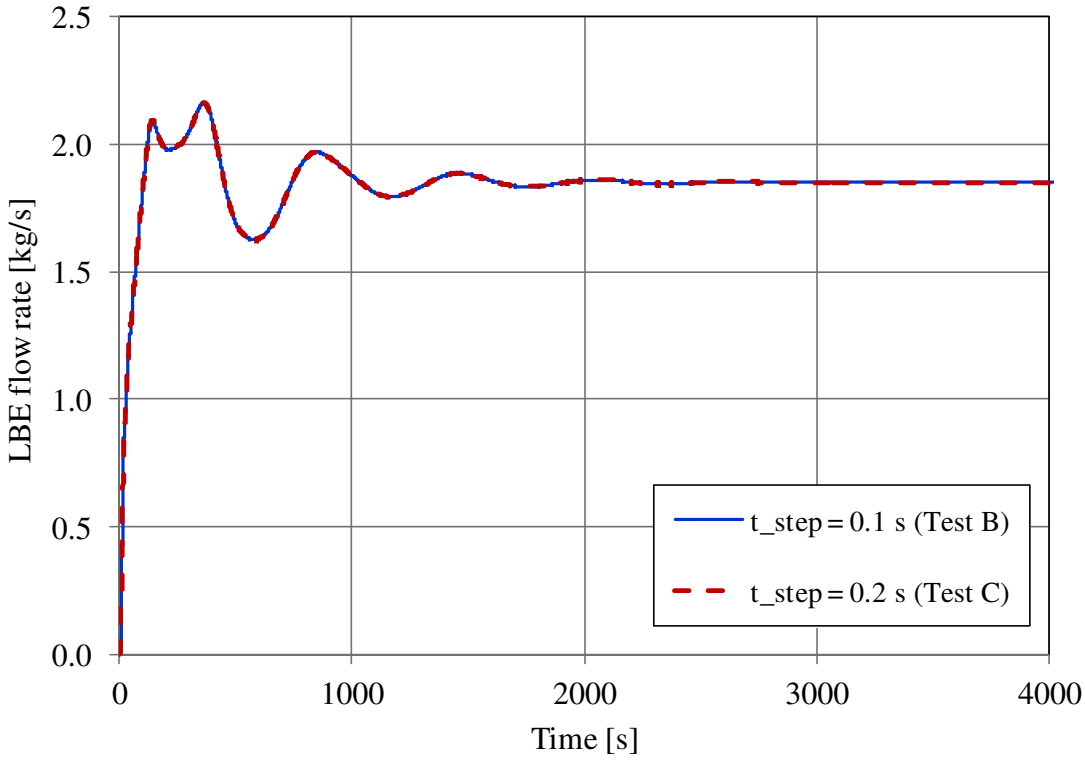

Figure 3.14: LBE mass flow rate time trend for two different time step calculations.

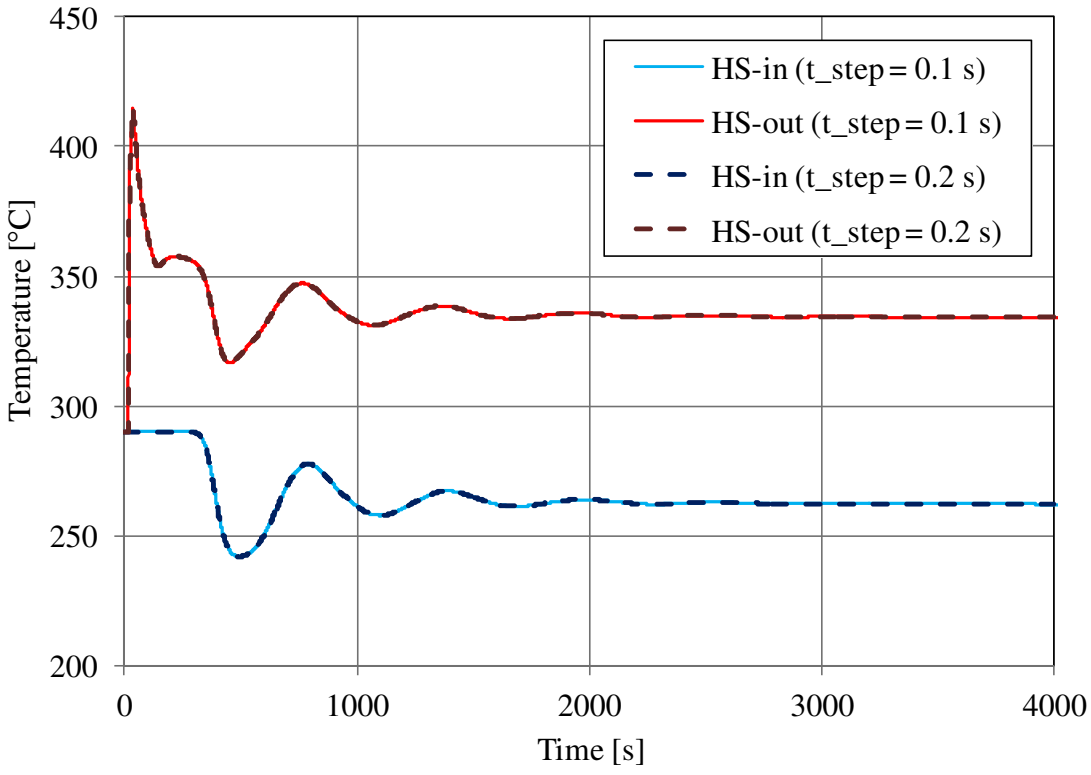

Figure 3.15: Inlet and outlet time trend temperature in the *HS* for two different time step calculations.

3.4.2 Assisted circulation tests

The LBE mass flow rate time trends obtained from the three gas-injection circulation tests simulated by the coupled codes are reported in Figure 3.16, where the results are compared with those obtained by corresponding simulations performed with the stand-alone RELAP5 code. Also in these tests we observe a little underestimation of the mass flow rate from the coupled code simulations. This is due, once again, to the greater pressure drop calculated by the CFD code for the *HS* 2D domain (see Figure 3.17). To better understand this behaviour, the *HS* pressure difference is reported for test D as a function of the LBE flow rate in the Figure 3.18. It can be seen that, for high flow rates, the pressure drop in the *HS* calculated by Fluent code in the coupled simulation is quite higher in respect to the correspondent one evaluated by the RELAP5 stand-alone calculation.

The cusp in the *HS* pressure difference, observed between 8 and 12 s (see Figure 3.17), can be due to a transition from laminar to turbulent flow conditions. This effect can be observed, even if with reduced entity, in the stand-alone calculation results.

Good agreement can be obtained comparing the pressure time trend for both the inlet and the outlet *HS* sections (see Figure 3.19). The pressure calculated by the coupled codes for test on the *HS* outlet section is practically the same as that evaluated by the stand-alone RELAP5 code. Instead, the coupled code simulation gives a higher pressure time trend for the *HS* inlet section. This is due to the previously mentioned higher pressure drops calculated by the Fluent code for the *HS* 2D domain.

It must be taken into account that the average velocity reached inside the *HS* channel in steady state conditions for test F is about 0.7 m/s. The velocity magnitude distribution inside the 2D domain at the end of the analysed transient is reported in Figures 3.20, 3.21 and 3.22. It can be seen as the maximum velocity predicted by the CFD code inside the channel of about 0.8 m/s and is reached at about half length of the domain. In Figure 3.23 the distribution of the turbulence kinetic energy is instead reported. From this figure it can be seen as turbulence, considered as uniform at the inlet section, developing along the channel.

The LBE mass flow rate and the *HS* pressure drop obtained for a time step equal to 0.01 s (Test F) were compared with those obtained with a time step equal to 0.02 s (Test G) and with a time step of 0.005 s (Test H) to verify the time step independence of the results obtained with the coupled codes. The comparison is reported in Figure 3.24 for the mass flow rate and in Figure 3.25 for the pressure drop. Perfect agreement between the corresponding time trends can be observed.

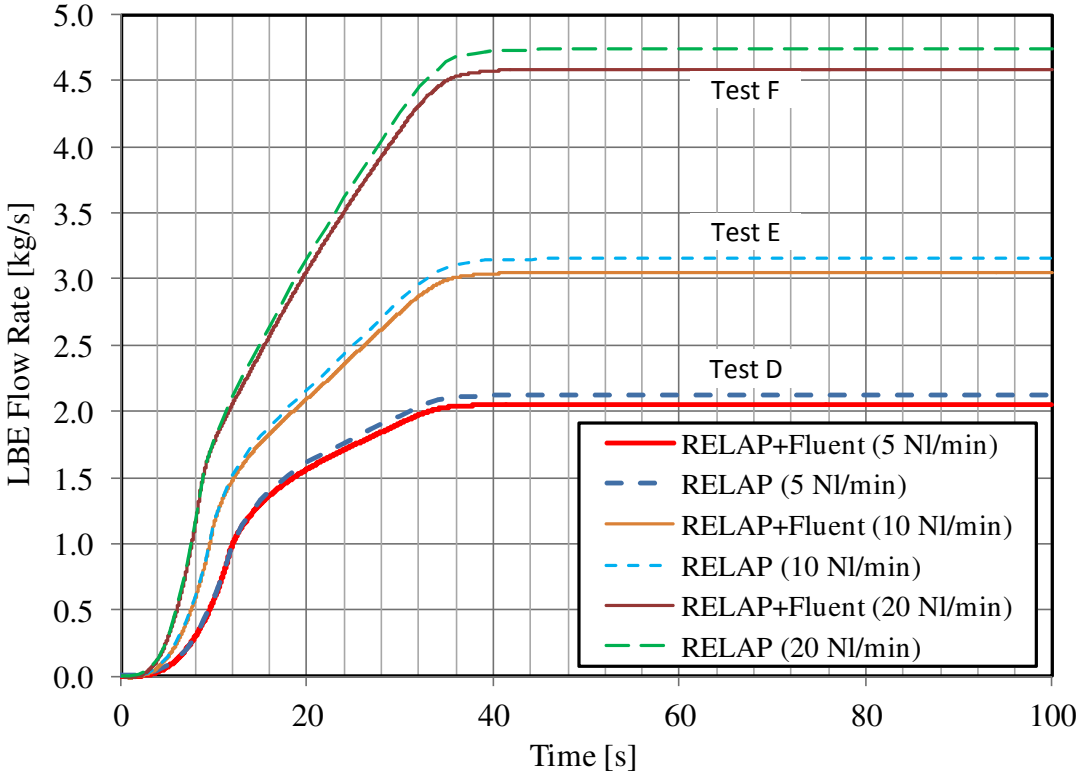

Figure 3.16: LBE mass flow rate time trend.

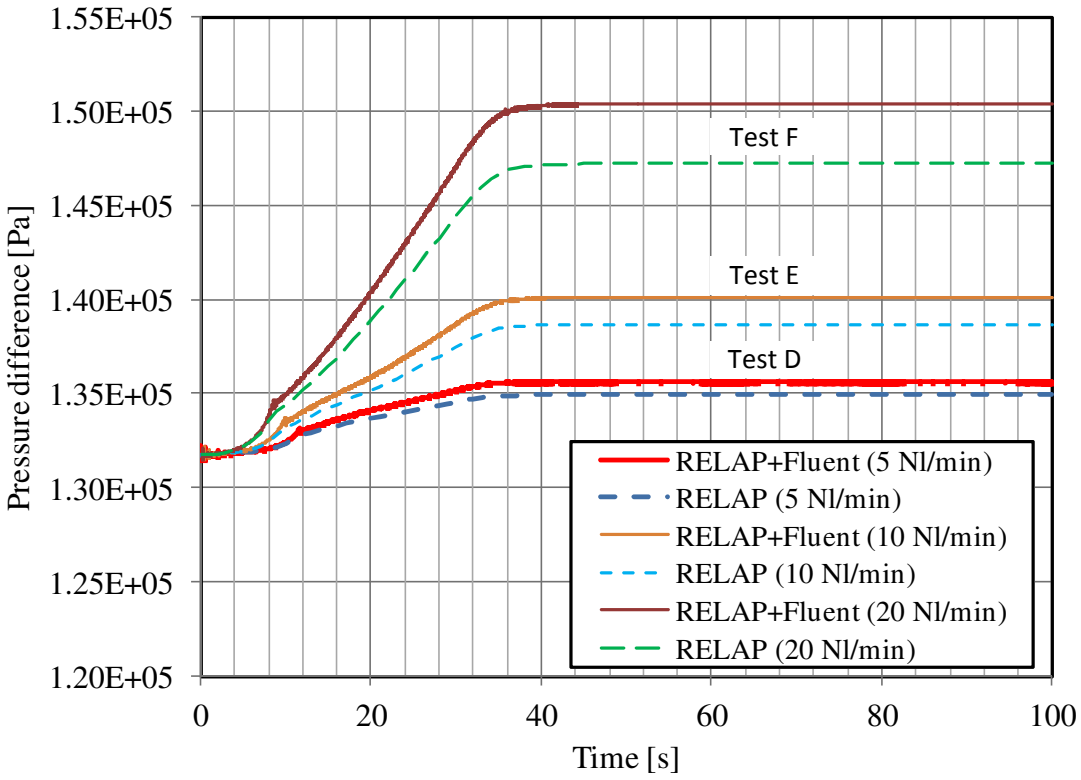

Figure 3.17: Pressure difference through the *HS*.

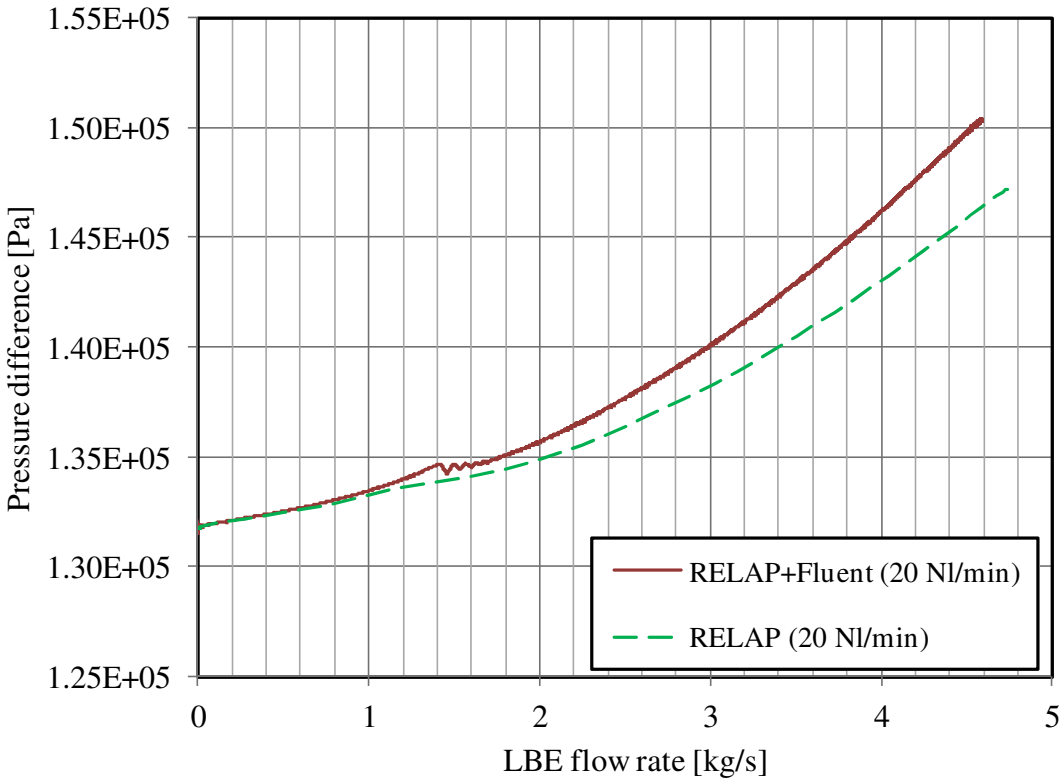

Figure 3.18: *HS* pressure difference vs. LBE flow rate (Test F).

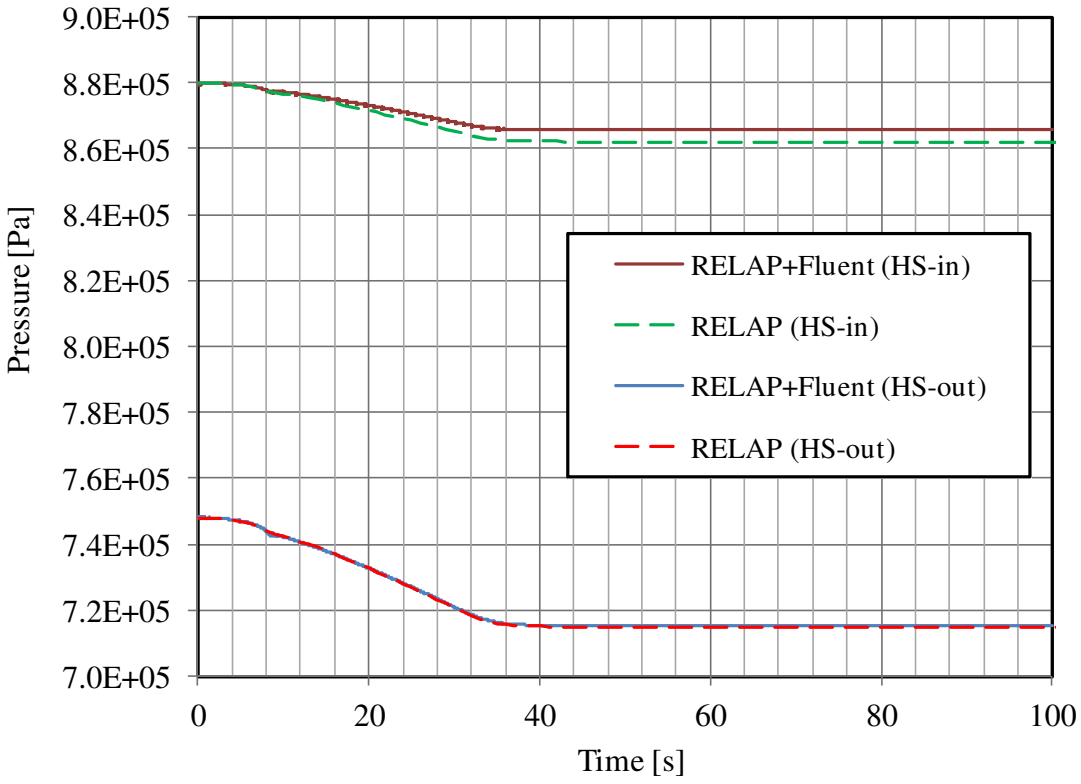

Figure 3.19: Inlet and outlet pressure time trend for the *HS* (Test F).

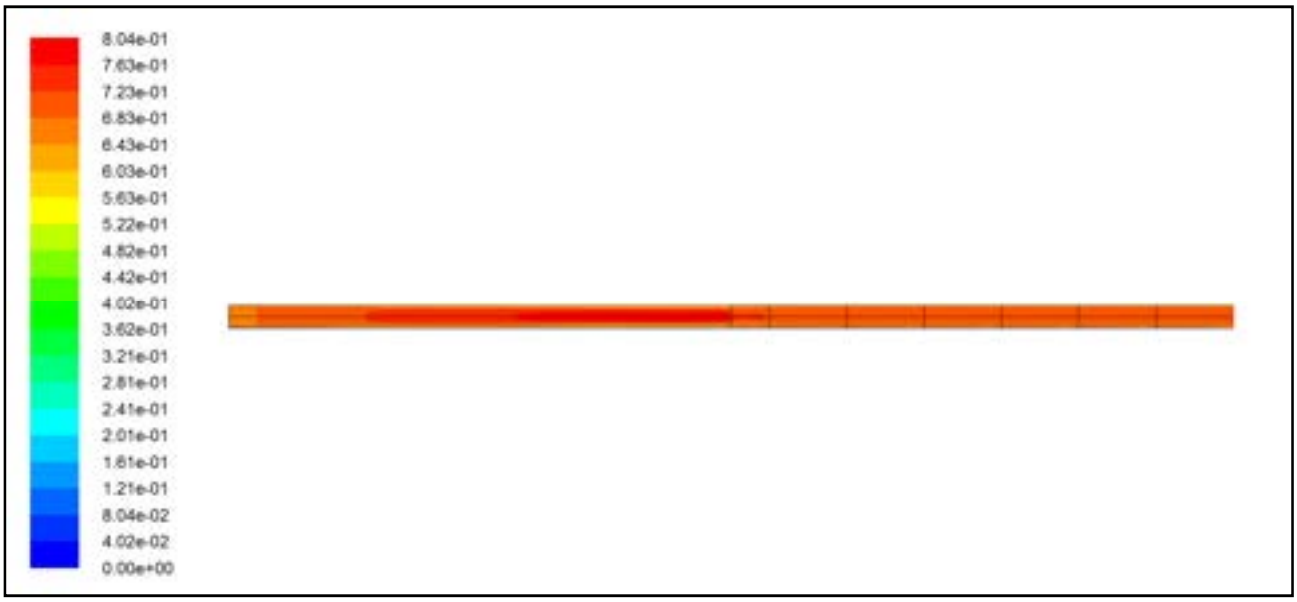

Figure 3.20: Velocity magnitude contour plot [m/s] at the end of the analysed transient (Test F).

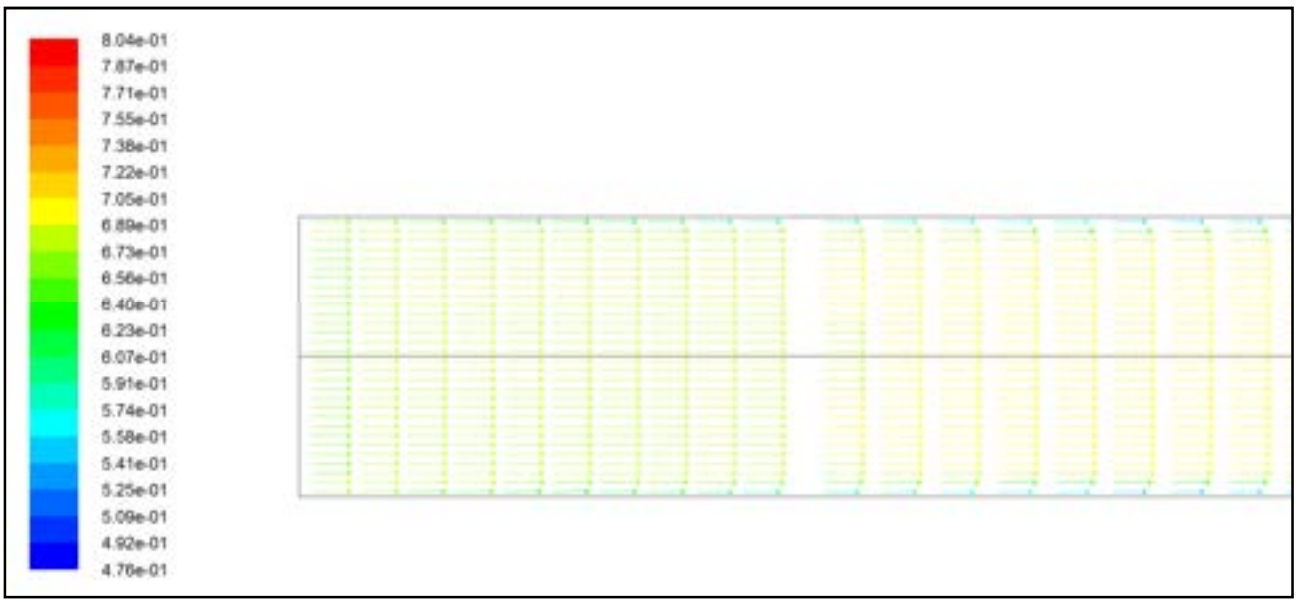

Figure 3.21: Velocity vector distribution near the inlet section, at the end of analysed transient (Test F).

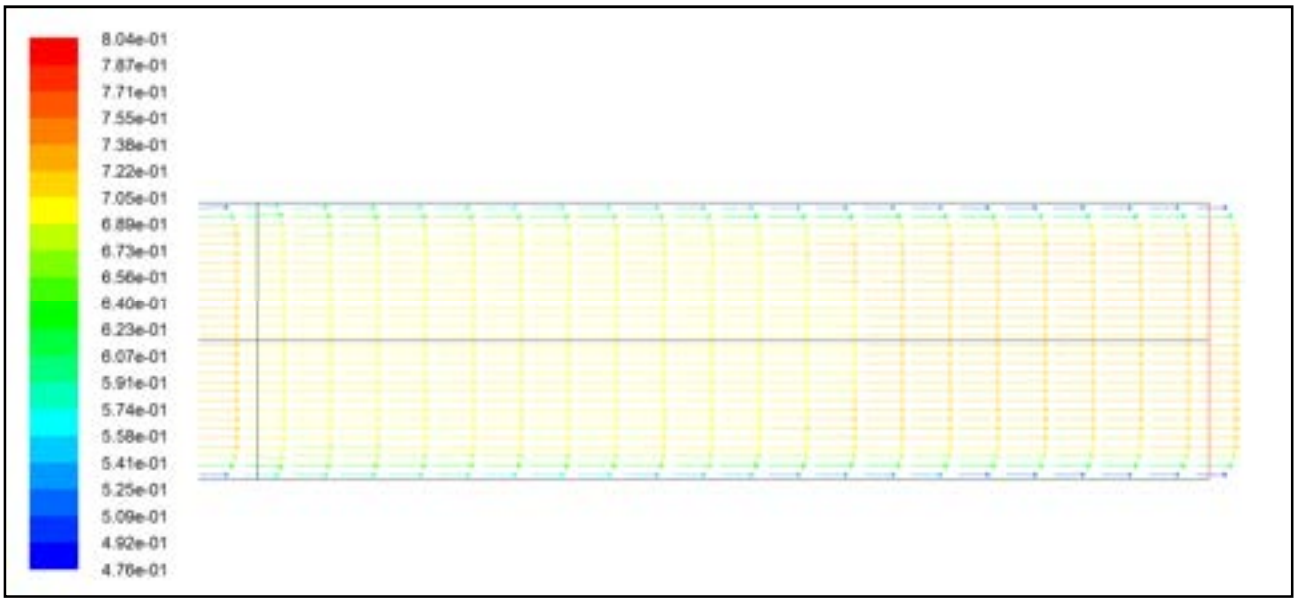

Figure 3.22: Velocity vector distribution near the outlet section, at the end of analysed transient (Test F).

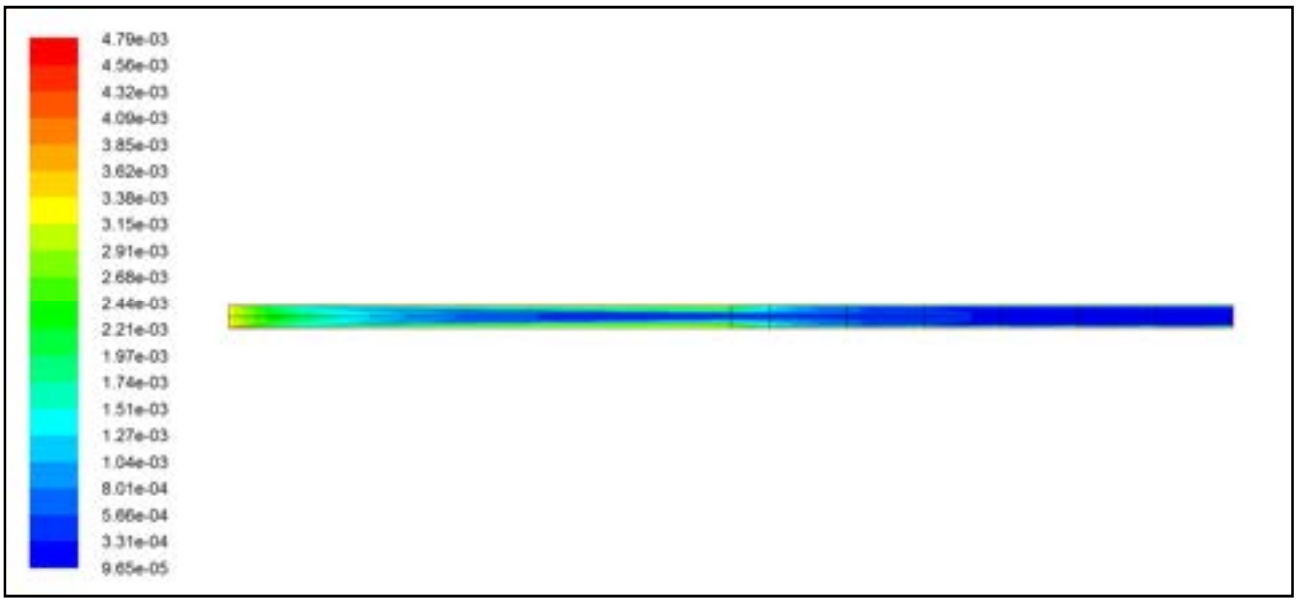

Figure 3.23: Turbulence kinetic energy [m^2/s^2] contour plot at the end of analysed transient (Test F).

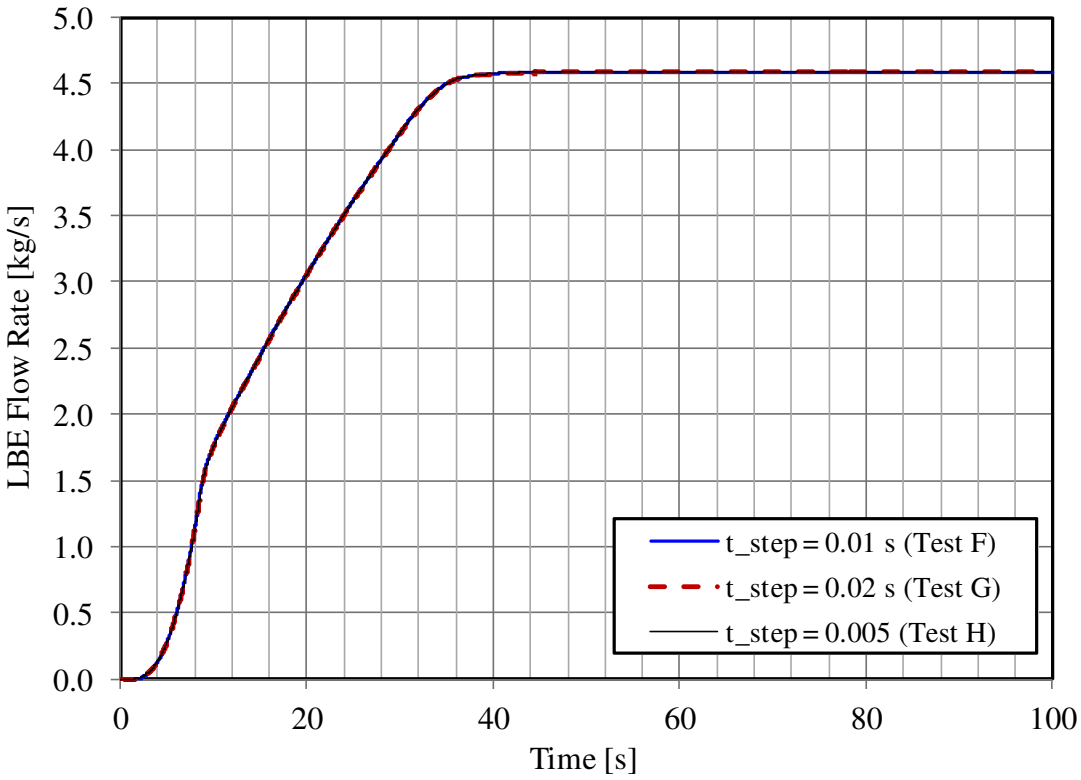

Figure 3.24: LBE mass flow rate time trend for three different time step calculations.

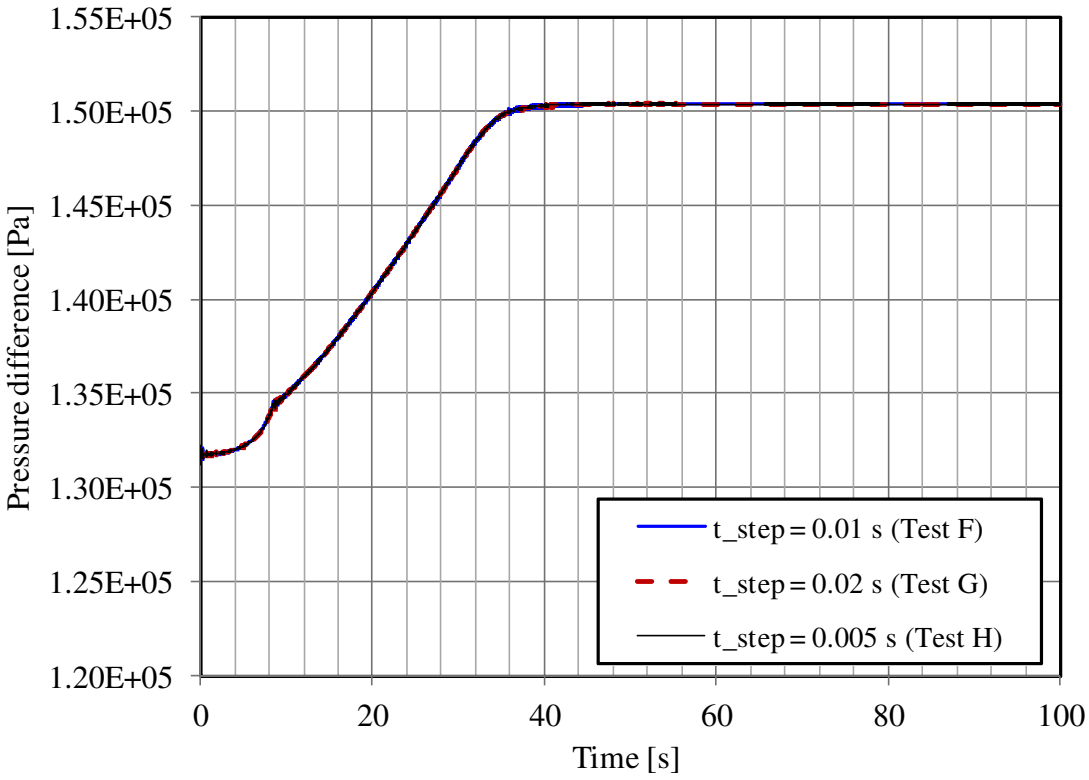

Figure 3.25: *HS* pressure drop for three different time step calculations.

3.4.3 ULOF test

The ULOF accident transient (Test I) is of fundamental interest for the safety of HLM reactors, because it represents the transition from forced to natural circulation conditions without the shutdown of the heater system.
In Table 3.2, boundary conditions imposed in this test are described with the associated RELAP5 actions. The time step used to simulate this test with the coupled codes was 0.02 s.

Table 3.2: Test I transient events.

Time [s]	Event	Description
0-30	The argon gas flow rate increase linearly from zero to 20 Nl/min and after 30 s its value remain constant up to ULOF event	***Starting phase**: achieving of the reference conditions*
50-80	The thermal power supplied through the *HS* increase linearly from zero to 20 kW and in the same time interval the water flow rate injected in the secondary side of the *HX* increase linearly to. From 80 s to the end of the analysed transient the value of the *HS* thermal power and of the *HX* water flow rate remain constant	
200-210	Gas flow injection system switched off decreasing linearly its value in a period of 10 s	***ULOF**: occurrence of initiating accidental event*
210-1000	The *HS* thermal power remain constant to 20 kW, while the *HX* remain at its operative set of conditions.	***ULOF**: accident evolution*

As shown in Figure 3.26, the induced LBE mass flow reach a value of about 4.6 kg/s for the asymptotic conditions with the only gas injection period and a value of about 5 kg/s in the phase of both gas injection and heating/cooling. After the argon injection shutdown the LBE mass flow rate (caused by natural circulation) reduces to a value of about 2 kg/s. This time trend agrees quite well with that obtained from the simulation performer by the RELAP5 stand alone code.
The LBE temperature results obtained with the coupled codes for both the heat section and heat exchanger present an adequate agreement with those obtained by the RELAP5 stand-alone code (see Figures 3.27 and 3.28), once again confirming the suitability of the set-up numerical scheme for coupled code calculations.

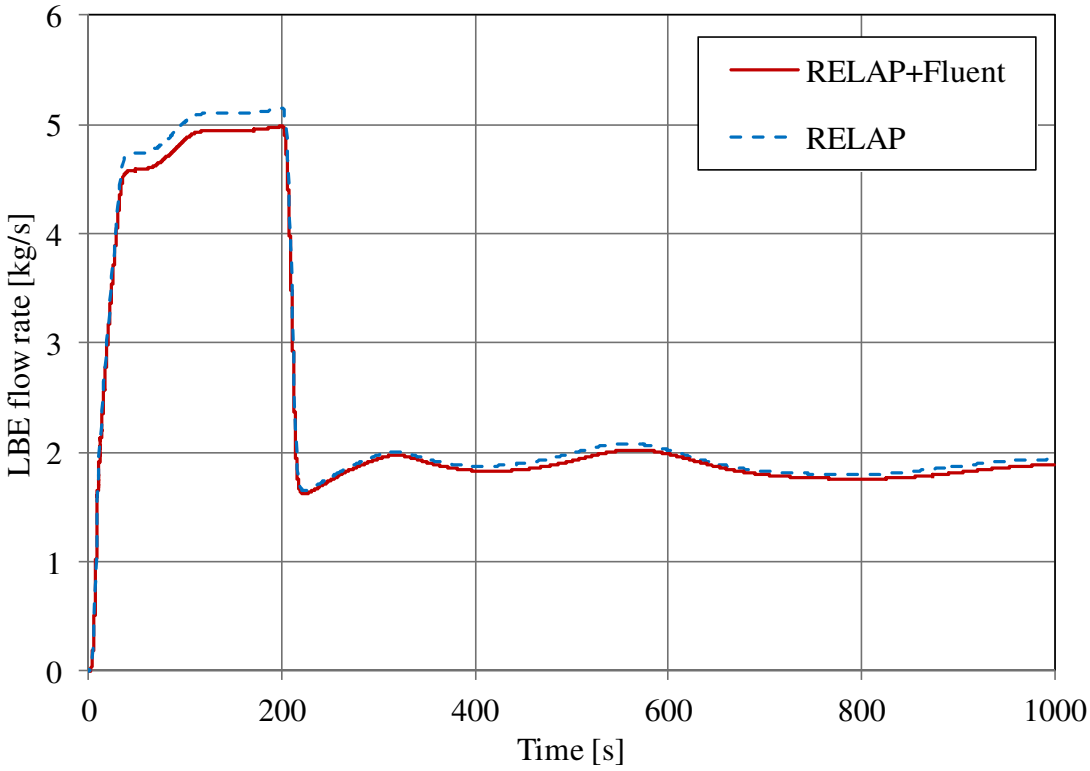

Figure 3.26: LBE mass flow rate time trend for Test I (ULOF).

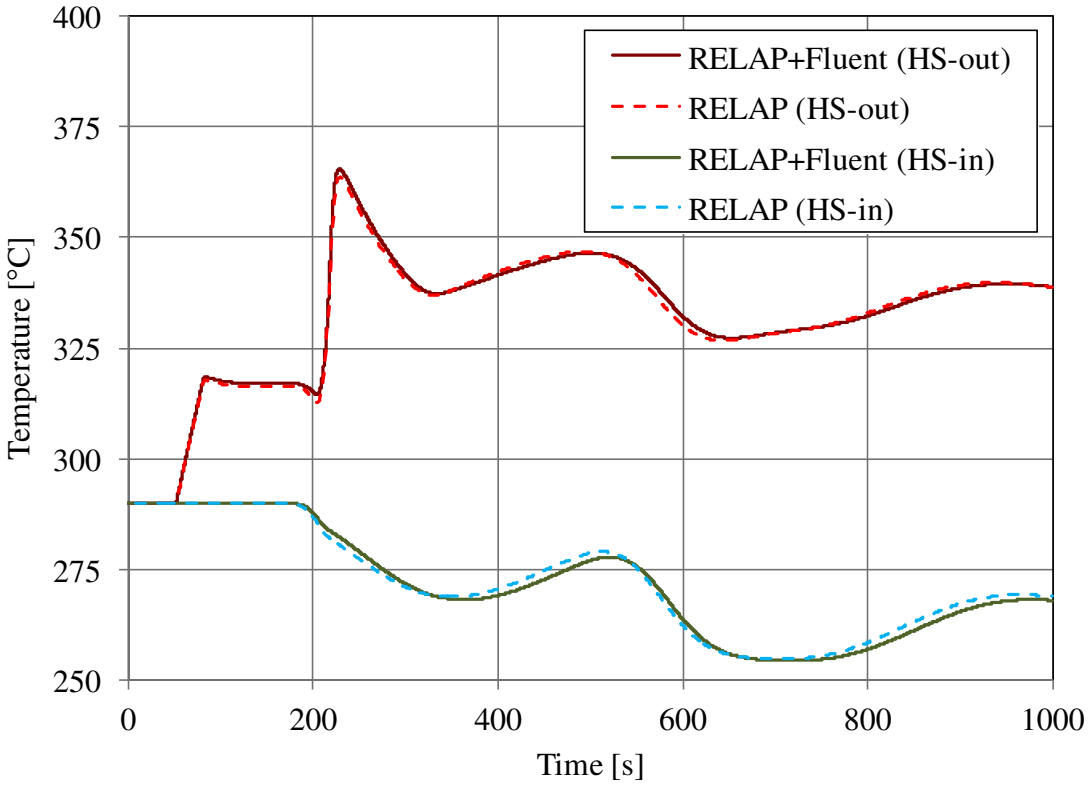

Figure 3.27: Inlet and outlet *HS* temperature time trends for Test I (ULOF).

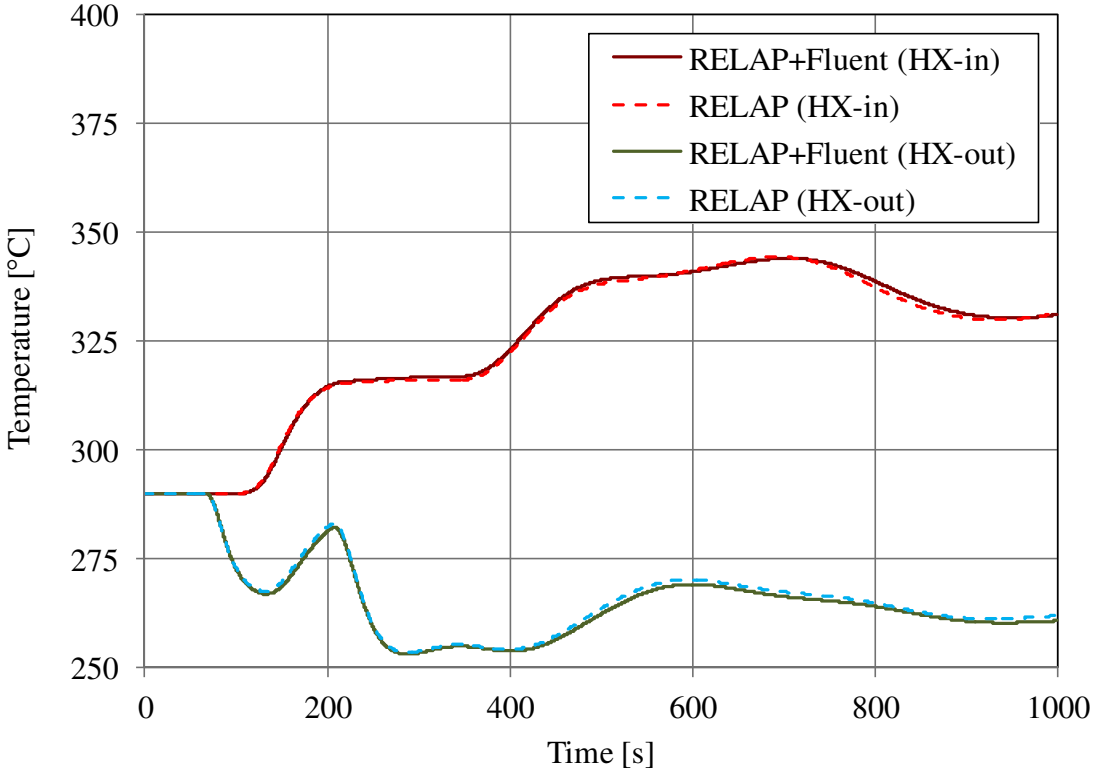

Figure 3.28: Inlet and outlet *HX* temperature time trends for test I (ULOF).

4. Conclusions

RELAP5 pre-test simulations on NACIE have been performed to analyze the thermal hydraulic behaviour of the facility and safety related parameters in natural circulation regime characteristic of a PLOFA scenario. Loop pressure losses, predominantly concentrated on the wire spaced fuel bundle, have been evaluated according to Rehme resistance coefficient correlation. Simulated bundle pressure losses are shown to be in good agreement with those obtained analytically using Rehme formulation. A first series of simulations (Test NAT) have been performed to predict the maximum LBE mass flow rate established in NACIE loop (given the thermal centers elevation of 6.25 m) for different values of *HS* power. The resulting LBE mass flow rates are around 1.5, 2 and 2.4 kg/s for heat power of 10.8, 21.7 and 32.5 kW respectively providing an adequate cooling of the heat bundle. NACIE loop simplified thermal-hydraulic analytical model provides a slight overestimation of the mass flow compared to RELAP5 results. Influence of secondary water inlet temperature has also been analyzed (from 120 to 170°C). The maximum clad temperature (430°C) is found for test NAT-3 (Q_3=32.5 kW) and a cooling water temperature of T_w= 170°C, while the LBE minimum temperature is found to be 176°C (about 50°C above freezing point), for test NAT-1 (Q_1=10.8 kW) and T_w=120°C. For the second series of simulation (Test VAL), performed at T_w=170°C, the flow rate in presence of an additional loop hydraulic resistance has been investigated at increasing values of resistance coefficient, K_v, (from 10^2 to 10^4). The established mass flow rates are found to be in good agreement with the results predicted by the simplified analytical model especially for higher values of K_v. The maximum clad temperature is found to be higher than 500°C only for Test VAL-3 (Q_3 = 32.5 kW) and K_v above 1300 (mass flow rate lower than 1.2 kg/s) which suggests the safety related limitation of the loop hydraulic properties for the considered simulation conditions. Future post-test analysis is foreseen to assess RELAP5 model simulation capability.

The performed simulations with coupled RELAP5-Fluent codes must be considered as a preliminary work that, despite the simplifications performed in set-up the model, proved its capability in the simulation of the thermal-hydraulic behaviour of an experimental facility like NACIE, in both natural and assisted circulation conditions. Further work must be done to optimize the numerical algorithm and to improve numerical stability. In particular, efforts must be carried out to develop an implicit scheme and to qualify it with the application to available experimental tests. In addition, thermo-dynamic properties for heavy liquid metals used by the RELAP5 code are not perfectly coincident with those considered for Fluent calculations and this can give some differences in the results that, anyway, can be considered as secondary order.

References

[1] M. Tarantino, S. De Grandis, G. Benamati, F. Oriolo, “Natural circulation in a liquid metal one-dimensional loop”, Journal of Nuclear Materials 376 (2008) 409–414.

[2] I. Di Piazza, P. Gaggini, M. Tarantino, M. Granieri, “The fuel rod bundle design for the NACIE facility”, ENEA SEARCH project, deliverable (D-N°2.1), 2012.

[3] Relap5/Mod.3.3 Code Manual, Volume II. Appendix A: Input Requirements, Nuclear Safety Analysis Division, January 2003.

[4] Handbook on Lead–bismuth Eutectic Alloy and Lead Properties, Materials Compatibility, Thermal-hydraulics and Technologies, 2007 edition, NEA No.6195.

[5] K. Rehme, “Pressure drop correlations for fuel elements spacers”, Nuclear Technology, 17, pp.15-23, 1973.

[6] P.A. Ushakov, A. V. Zhukov, N. M. Matyukhin, “Heat transfer to liquid metals in regular arrays of fuel elements”, High temperature, Vol.15, pp. 868-873, 1977.

[7] R. A. Seban and T. T. SHIMAZAKI, “Heat Transfer to a Fluid Flowing Turbulently in a Smooth Pipe with Walls at Constant Temperature” Trans. ASME, Vol. 73, pp. 803-809 (1951).

[8] F. Bianchi, P. Meloni, F. Mattioda, G. Forasassi, G. Fruttuoso, F. Oriolo, S. Bocci, “Implementation and preliminary verification of the RELAP5/PARCS code for Pb-Bi cooled subcritical systems”, AccApp’01 & ADTTA’01, Nuclear Application in the new Millenium, RENO (Nevada- USA), November 11-15, 2001.

[9] W. Ambrosini, N. Forgione, F. Oriolo Limiti di applicabilità dell’accoppiamento tra il codice RELAP5 Mod.3.3 e il codice PARCS multigruppo alla simulazione di sistemi sottocritici raffreddati a metalli liquidi pesanti, Parte I”, Università di Pisa, Dipartimento di Ingegneria Meccanica, Nucleare e della Produzione, Pisa, settembre 2007.

[10] Fluent Inc., Fluent 6.3, User's guide documentation 2006.

Nomenclature

Roman letters

A	area [m^2]
c_p	specific heat capacity at constant pressure [J/(kg K)]
d_{in}	pipe inner diameter [m]
d_{out}	pipe outer diameter [m]
d	pin diameter [m]
d_w	wire diameter [m]
D_h	hydraulic diameter [m]
g	gravity acceleration [m/s^2]
f_R	Rehme friction factor [-]
F	geometrical factor [-]
h	heat transfer coefficient [$W/(m^2 K)$]
h_i	height of RELAP5 sub-volumes [m]
H_w	wire pitch [m]
H	thermal centers elevation [m]
k	thermal conductivity [W/(m K)]
K	resistance coefficient [-]
L	length [m]
$\dot{m}$	mass flow rate [kg/s]
N_b	number of RELAP5 sub-volumes [-]
p	pitch [m]
P	pressure [Pa]
q''	heat flux [MW/m^2]
Q	heat source thermal power [kW]
Re	Reynolds number [-]
t	pipe thickness [m]
T	temperature [°C]
U	perimeter [m]
u	velocity magnitude [m/s]

Greek letters

β	volumetric thermal expansion coefficient [K^{-1}]
μ	dynamic viscosity [Pa s]
ρ	density [kg/m^3]
ε	area ratio [-]/pipe wall roughness [m]

Abbreviations and acronyms

CFD	Computational Fluid Dynamic
DIMNP	Dipartimento di Ingegneria Meccanica Nucleare e della Produzione
ENEA	Agenzia nazionale per le nuove tecnologie, l'energia e lo sviluppo sostenibile
HLM	Heavy liquid metal
HS	Heat Source
HTC	Heat transfer coefficient
HX	Heat Exchanger
LBE	Lead bismuth eutectic
MYRRHA	Multi-purpose hybrid research reactor for high-tech applications
NACIE	Natural Circulation Experiment
PLOFA	Protected Loss of Flow Accident

RELAP	Reactor Loss of Coolant Analysis Program
SEARCH	Safe ExploitAtion Related CHemistry for HLM reactors
TC	Thermocouple
ULOF	Unprotected Loss Of Flow

Appendix A

A.1 Pressure drop in wire wrapped rod bundles

For wire wrapped rod bundles the following correlation was proposed by Rehme for predicting the pressure drop in case of wire wrapped rod bundles

$$\Delta P_R = f_R \frac{L}{D_h} \frac{\rho u_b^2}{2} \tag{A.1}$$

where u_b is the average velocity in the rod bundle. The friction factor is calculated by means of the following correlation based on Rehme's experimental data.

$$f_R = \left[\frac{64}{\mathrm{Re}\sqrt{F}} + \frac{0.0816}{\left(\mathrm{Re}\sqrt{F}\right)^{0.133}} \right] F \frac{U_b}{U_{tot}} \tag{A.2}$$

and where,

$U_b=U_p+U_w$ is the bundle perimeter.
$U_{tot}=U_p+U_w+U_k$ is the total perimeter.

with U_k, U_p and U_w are the hexagonal wrapper perimeter, pin perimeter and wire perimeter respectively.

The geometrical factor F depends on the pitch to diameter ratio (p/d) and on the ratio between the mean diameter ($d_m=d+d_w$, d_w being the wire diameter) and the wire pitch (H_w).

$$F = \left(\frac{p}{d}\right)^{0.5} + \left[7.6 \frac{d_m}{H_w} \left(\frac{p}{d}\right)^2 \right]^{2.16} \tag{A.3}$$

Substituting the numerical values for NACIE fuel bundle we obtain: F=1.265 and U_b/U_{tot}=0.784. In Figure A.1 is shown the trend of the friction factor as a function of the Reynolds number for the NACIE wire-spaced pin bundle. It can be observed that, for Re~3000, increasing Reynolds (e.g. an LBE temperature increase) has an higher effects on friction factor (decreasing) than for Re~9000.

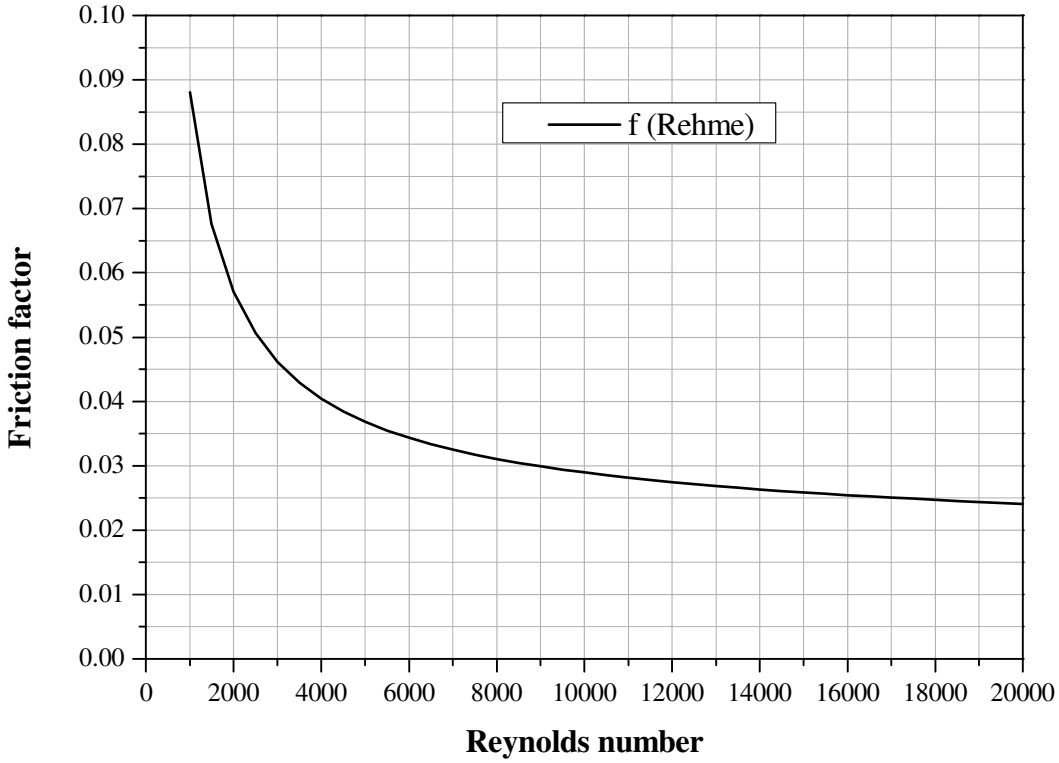

Figure A.1. Friction factor as a function of the Reynolds number
for the NACIE wire-spaced pin bundle (Rehme correlation).

Hence, for NACIE fuel bundle:

$$K_R = \left[f_{R,i} \frac{L_i}{D_h} + f_{R,a} \frac{L_a}{D_h} \right] \cdot \left(\frac{A_{ref}}{A_b} \right)^2 \tag{A.4}$$

where $f_{R,i}$ and $f_{R,a}$ are the Rehme friction factors for inactive and active pin length (L_i and L_a) respectively; D_h is the bundle hydraulic diameter, A_{ref} is the reference flow area (2.5'' downcomer pipe) and A_b is the bundle flow area. Thereby the bundle pressure loss is estimated by:

$$\Delta P_R = \frac{1}{2} \cdot K_R \rho_b u_{ref}^2 \tag{A.5}$$

with ρ_b mean LBE density within the bundle and u_{ref} is the reference velocity magnitude (LBE flowing in the downcomer).

A.2 Valve form loss coefficient: Abrupt area change with an Orifice.

Motor Valve (*Mtrvlv-203*) RELAP component could be considered as an orifice with variable flow area specified by the user. The general configuration is shown in Figure A.2. Conditions at the orifice throat will be designed by a subscript T.

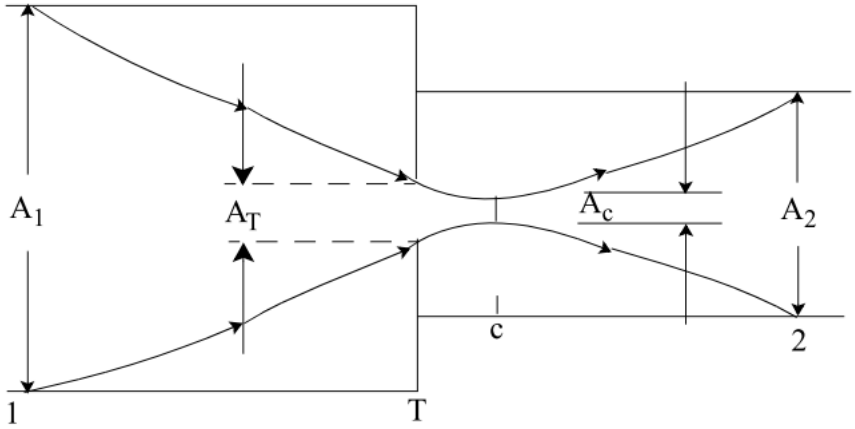

Figure A.2. Orifice at abrupt area change.

Three area ratios are used:

- area ratio of the vena contracta to the minimum physical area:

$$\varepsilon_c = \frac{A_c}{A_T} \tag{A.6}$$

- area ratio of the minimum physical area to the upstream flow area:

$$\varepsilon_T = \frac{A_T}{A_1} \tag{A.7}$$

- area ratio of the downstream to up upstream area:

$$\varepsilon = \frac{A_2}{A_1} \tag{A.8}$$

The loss associated with the contracting fluid stream from Station 1 to c (point of vena-contracta) is neglected in RELAP5. The dynamic pressure loss associated with the expansion from the vena-contracta to the downstream section is given by:

$$\Delta P = \frac{1}{2}\rho\left(1-\frac{A_c}{A_2}\right)^2 u_c^2 \tag{A.9}$$

The contraction ratio, $\varepsilon_c = \frac{A_c}{A_T}$, is a function of $\varepsilon_T = \frac{A_T}{A_1}$; the following function equation is used:

$$\varepsilon_c = 0.62 + 0.38 \cdot \varepsilon_T^{\,3} \tag{A.10}$$

Using the continuity equations, $u_c = \frac{A_T u_T}{A_c} = \frac{u_T}{\varepsilon_c}$ and $u_T = \frac{A_2 u_2}{A_T} = \frac{\varepsilon}{\varepsilon_T} u_2$. Equation (A.7) can be written as:

$$\Delta P = \frac{1}{2}\rho\left(1-\frac{\varepsilon}{\varepsilon_c \varepsilon_T}\right)^2 u_2^2 \tag{A.11}$$

where:

$$K_v = \left(1 - \frac{\varepsilon}{\varepsilon_c \varepsilon_T}\right)^2 \quad \text{(A.12)}$$

In the specific case of the Motor Valve in NACIE loop, we have ε=1 as A_1=A_2 (Downcomer flow area) and $\varepsilon_T = A_{valve}/A_1$. Therefore the code-calculated K_v, associated to the specific valve area is derived from:

$$K_v = \left(1 - \frac{1}{0.62\varepsilon_T + 0.38 \cdot \varepsilon_T^{\,4}}\right)^2 \quad \text{(A.13)}$$

Breve CV del gruppo di lavoro

Gianluca Barone

Si è laureato in Ingegnere Nucleare all'Università di Roma nel 2004 ed ha conseguito il Master di II livello in "Tecnologie degli Impianti Nucleari" presso l'Università di Pisa nel 2011. Attualmente borsista presso il DIMNP dell'Università di Pisa. Esperto di codici di sistema, con particolare riguardo al codice di termoidraulica nucleare RELAP5.

Nicola Forgione

Ricercatore in Impianti Nucleari presso il Dipartimento di ingegneria Meccanica, Nucleare e della Produzione (DIMNP) dell'Università di Pisa dal 20 dicembre 2007. Laureato in Ingegneria Nucleare nel 1996 presso l'Università di Pisa ed in possesso del titolo di Dottore di Ricerca in Sicurezza degli Impianti Nucleari conseguito all'Università di Pisa nel 2000. La sua attività di ricerca è incentrata principalmente sulla termofluidodinamica degli impianti nucleari innovativi, con particolare riguardo ai reattori nucleari di quarta generazione. Autore di oltre 20 articoli su rivista internazionale e di numerosi articoli a conferenze internazionali.

Daniele Martelli

Ha conseguito la laurea in Ingegneria Aerospaziale presso l'Università di Pisa nel 2009. A partire dallo stesso anno ha iniziato a collaborare, attraverso la società spin-off ACTA, con il DIMNP per analisi di fluidodinamica computazionale nell'ambito dell'ingegneria nucleare. Nel biennio 2010-2011 ha usufruito di una borsa di ricerca presso il DIMNP riguardante l'analisi del comportamento termoidraulico dei sistemi di refrigerazione dei reattori nucleari refrigerati a metallo liquido. Da gennaio 2012 è inscritto al corso di dottorato in "Ingegneria Nucleare e Sicurezza Industriale" in svolgimento presso il DIMNP dell'Università di Pisa. La sua attività di ricerca è principalmente incentrata sullo studio dei fenomeni di scambio termico in regime di convezione naturale e mista per reattori nucleari refrigerati a metallo liquido pesante.